

NISTIR 6819

**Comparison of concrete rheometers:
International tests at LCPC
(Nantes, France)
in October, 2000**

Editors:

Chiara F. Ferraris, Lynn E. Brower

Authors (alphabetical order):

**Phil Banfill, Denis Beaupré,
Frédéric Chapdelaine, François de Larrard,
Peter Domone, Laurent Nachbaur,
Thierry Sedran, Olaf Wallevik,
Jon E. Wallevik**



NIST

National Institute of Standards and Technology
Technology Administration, U.S. Department of Commerce

Comparison of concrete rheometers: International tests at LCPC (Nantes, France) in October, 2000

Editors:

Chiara F. Ferraris, National Institute of Standards and Technology (USA)
Lynn E. Brower, Master Builders Technologies (USA)

Authors (in alphabetical order):

Phil Banfill, Heriot-Watt Univ., (UK)
Denis Beaupré, Laval Univ., (Canada)
Frédéric Chapdelaine, Laval Univ (Canada)
François de Larrard, Laboratoire Central des Ponts et Chaussées, (France)
Peter Domone, University College London (UK)
Laurent Nachbaur, Laboratoire Central des Ponts et Chaussées, (France)
Thierry Sedran, Laboratoire Central des Ponts et Chaussées, (France)
Olaf Wallevik, The Icelandic Building Research Institute, (Iceland)
Jon E. Wallevik, Norwegian Univ. of Science and Technology, (Norway)

September 2001



U.S. Department of Commerce
Donald L. Evans, Secretary

National Institute of Standards and Technology
Karen H. Brown, Acting Director

Disclaimer

Commercial equipment, instruments, and materials mentioned in this paper are identified to foster understanding. Such identification does not imply recommendation or endorsement by the National Institute of Standards and Technology (NIST), nor does it imply that the materials or equipment identified are necessarily the best available for the purpose.

During the trial in France, on October 2000, to ensure proper use, each designer operated his instrument and described its operation in this report. All data were immediately, after each test, collected in electronic form on specially labeled diskettes for later analysis.

The role of NIST was to coordinate and foster the rheometer study. Dr. Chiara Ferraris is the chair of ACI 236A, “Workability of Fresh Concrete”, and in this role she organized the tests and edited the report. She is not one of the authors, but only an editor. Lynn Brower, co-editor, is the secretary of ACI 236A.

The opinions expressed in this report are not endorsed by NIST and they reflect only the opinion of the authors.

Preparation of the report

Editors

Chiara F. Ferraris, National Institute of Standards and Technology, Gaithersburg (USA)

Lynn Brower, Master Builders, Inc., Cleveland OH (USA)

Authors (alphabetical order)

Phil Banfill, Heriot-Watt Univ., Edinburgh (UK)

Denis Beaupré, Laval Univ., Quebec (Canada)

Frédéric Chapdelaine, Laval Univ., Quebec (Canada)

François de Larrard, Laboratoire Central des Ponts et Chaussées, Nantes (France)

Peter Domone, University College London (UK)

Laurent Nachbaur, Laboratoire Central des Ponts et Chaussées, Paris (France)

Thierry Sedran, Laboratoire Central des Ponts et Chaussées, Nantes (France)

Olaf Wallevik, The Icelandic Building Research Institute, Reykjavik (Iceland)

Jon E. Wallevik, Norwegian Univ. of Science and Technology, Trondheim (Norway)

Contact

Chiara F. Ferraris

NIST

100 Bureau drive, MS 8621, Gaithersburg MD 20899 (USA)

Phone: +301-975 6711

Fax: +301-990 6891

E-mail: clarissa@nist.gov

Participants in the tests at LCPC, Nantes (France)



1st row: left to right

Jean-Yves Petit, Jinhua Jin, Jon Wallevik, Daniel Michel, Francois de Larrard, Chiara Ferraris, Olafur Wallevik, Marie-Andrée Gilbert, Thierry Sedran, Frederic Chapdelaine, Mohammed Sonebi, Joseph Daczko

2nd Row: left to right

Alain Doucet, Michel Dauvergne, Pierre Chelet (behind Michel), Bernard Dehousse, Phil Banfill, Peter Domone, Andreas Griesser, Laurent Nachbaur, Erik Nordenswan

On top of the CEMAGREF-IMG:

Denis Beaupré

Affiliations of participants (in alphabetical order):

Addtek, Parainen (Finland): Erik Nordenswan

Advanced Concrete and Masonry Centre, Paisley (UK): Mohammed Sonebi

Heriot-Watt Univ., Edinburgh (UK): Phil Banfill, Jinhua Jin

The Icelandic Building Research Institute, Reykjavik (Iceland): Olaf Wallevik

Laboratoire Central des Ponts et Chaussées, Nantes (France): François de Larrard, Thierry Sedran, Alain Doucet, Michel Dauvergne, Pierre Chelet, Bernard Dehousse, Daniel Michel

Laboratoire Central des Ponts et Chaussées, Paris (France): Laurent Nachbaur

Laval Univ., Quebec (Canada): Denis Beaupré, Frédéric Chapdelaine, Marie-Andrée Gilbert

National Institute of Standards and Technology, Gaithersburg (USA): Chiara F. Ferraris

Norwegian Univ. of Science and Technology, Trondheim (Norway): Jon E. Wallevik

Univ. d'Artois, Bethune (France): Jean-Yves Petit

University College London (UK): Peter Domone

Master Builders, Inc., Cleveland OH (USA): Joseph Daczko

Swiss Federal Institute of Technology, Zürich (Switzerland): Andreas Griesser

Foreword

The American Concrete Institute (ACI) sub-committee 236A, “Workability of Fresh Concrete,” immediately was faced, upon its creation in fall 1999, with how to determine appropriate methods to measure concrete workability. The material science-based approach to measure workability would be to use a concrete rheometer. There are several rheometers used around the world that have significant design differences, but no standard method with which to compare their results. ACI 236A members determined that, as no reference material was available, one method to compare the rheometers would be to test them under the same conditions using the same concretes. Some tentative analysis made to compare two rheometers was performed in the past [1, 2] but did not involve most of the available rheometer designs.

ACI 236A drafted a plan for comparing the five types of rheometers available and requested funds from the Concrete Research Council (CRC) of ACI and from industry to support this work. CRC granted funds in 2000 and the first trial was scheduled for October, 2000. It was held at the Laboratoire Central des Ponts et Chaussées (LCPC) facility in Nantes, France on October 23-27, 2000. The rheometers selected included all commercially available concrete rheometers (four), to the best knowledge of the ACI 236A committee members, and one coaxial concrete rheometer developed for research.

The authors of this report are principal investigators who participated in the first trial and contributed to the report. This report describes the tests performed and the results obtained. It was not published as an ACI document and therefore was not submitted to the Technical Activities Committee (TAC) for approval. There are two reasons for this not being an ACI document: 1) ACI documents are guidelines and practice recommendations, not research reports; 2) all ACI reports are consensus documents balloted and approved by the members of a committee, while this report only reflects the views and opinions of the authors. All members of ACI 236A were invited to review the document prior to publication (as shown in the acknowledgements). It was also discussed during the regular meetings of ACI 236A at the ACI spring 2001 convention in Philadelphia (PA).

Acknowledgements

This project could not have been possible without the financial support of the ACI Concrete Research Council. Its support offset the cost of the transportation of the rheometers from Canada, Switzerland, UK, and Grenoble (France) to the test site at Laboratoire Central des Ponts et Chaussées (LCPC) in Nantes (France). We are thankful for the hospitality and the professionalism of the staff of LCPC, who welcomed the international team for the week-long tests. We would like to acknowledge the participation of LCPC staff, in particular: Michel Dauvergne, Daniel Michel, Alain Doucet, Pierre Chelet, Bernard Dehousse, David Chopin and Bernard Guieysse. They prepared and tested all the concrete used for this project, and conducted all the concrete quality control measurements.

We would also like to thank all the participants and their organizations for their involvement in the planning and execution of this comparison. Their names are listed in the participants list placed before the foreword. Also, Master Builders Technology (MBT) should be thanked for providing their expertise to administer the funds provided by CRC.

The authors would also like to **thank all the reviewers** for their efforts in reading this rather large report (in alphabetical order): Emmanuel Attiogbe (MBT), Samir Chidiac (McMaster Univ.), Geoffrey Fronhsdorff (NIST), Edward Garboczi (NIST), Aulis Kappi (Addtek R&D), Nicos Martys (NIST), Abdelbaki Mekhatria (CRIB, Laval Univ.), Della Roy (Penn State Univ.), Leslie Struble (ACBM, Univ. of Illinois), Kejin Wang (Iowa State Univ.), and Walter Rossiter (NIST). We would also like to thank the members of ACI 236A for their lively discussion during the Spring 2001 meeting and their support of this study.

Table of Contents

1. INTRODUCTION.....	1
2. CONCRETE MIXTURES USED IN TESTS AT NANTES	3
2.1. CONSTITUENTS.....	3
2.2. MIXTURE PROPORTIONS	4
2.3. CONCRETE PRODUCTION.....	4
2.4. FRESH CONCRETE ANALYSES.....	7
3. CONCRETE RHEOMETERS	11
3.1. THE BML RHEOMETER.....	11
3.1.1. <i>Description of apparatus.....</i>	<i>11</i>
3.1.2. <i>Test procedures</i>	<i>14</i>
3.1.3. <i>Calibration</i>	<i>17</i>
3.2. THE BTRHEOM RHEOMETER.....	19
3.2.1. <i>Description of the apparatus.....</i>	<i>19</i>
3.2.2. <i>Test procedure.....</i>	<i>19</i>
3.2.3. <i>Analysis of the data</i>	<i>20</i>
3.3. THE CEMAGREF-IMG RHEOMETER.....	22
3.3.1. <i>Description of the apparatus.....</i>	<i>22</i>
3.3.2. <i>Test procedure.....</i>	<i>25</i>
3.3.3. <i>Analysis of the data</i>	<i>25</i>
3.4. THE IBB RHEOMETER.....	30
3.4.1. <i>Description of the apparatus.....</i>	<i>30</i>
3.4.2. <i>Analysis of the data</i>	<i>31</i>
3.5. THE TWO-POINT RHEOMETER.....	33
3.5.1. <i>Description of the apparatus.....</i>	<i>33</i>
3.5.2. <i>Test procedure.....</i>	<i>34</i>
3.5.3. <i>Analysis of the data</i>	<i>36</i>
4. RESULTS.....	37
4.1. QUALITY CONTROL MEASUREMENTS: SLUMP, MODIFIED SLUMP, DENSITY.....	37
4.2. COMPARISON BETWEEN RHEOMETERS	39
4.2.1. <i>Comparison with the slump and modified slump test</i>	<i>39</i>
4.2.2. <i>Variation of the values by concrete composition</i>	<i>41</i>
4.2.2.1. <i>Analysis of variation of the yield stress and plastic viscosity by mixture</i>	<i>41</i>
4.2.3. <i>Relative rank of the data by each rheometer.....</i>	<i>43</i>
4.2.4. <i>Graphical comparison of pairs of rheometer results.....</i>	<i>44</i>
4.2.5. <i>Correlation functions and coefficients between pairs of rheometers.....</i>	<i>45</i>
5. DISCUSSION.....	60
5.1. COMMENTS ON CORRELATIONS BETWEEN PAIRS OF RHEOMETERS.....	60
5.1.1. <i>Linear regression or not?</i>	<i>60</i>
5.1.2. <i>Critical review of R.....</i>	<i>60</i>
5.2. DISCUSSION ON DISCREPANCIES ON ABSOLUTE VALUES	61
5.3. CORRELATION BETWEEN THE SLUMP AND THE YIELD STRESS	62
6. SUMMARY OF FINDINGS	64
7. FUTURE WORK.....	65
8. REFERENCES	66
APPENDIXES	A-69

List of Figures

Figure 1: Size distributions of the aggregates used	3
Figure 2: The ConTec viscometers: a) Version 3; b) Version 4.....	11
Figure 3: Output from the FreshWin software: A) The menu-driven window used to change relevant parameters; B) The basic output of a test result.....	12
Figure 4: The inner and outer cylinder of the BML Viscometer 3 (or BML rheometer hereafter).	12
Figure 5: The assembly of inner cylinder of the BML viscometer 3. This figure shows the sequence for installing the inner cylinder.	13
Figure 6: A top view of a coaxial cylinder rheometer. The outer cylinder (radius r_o) rotates at angular velocity ω_o , while the inner cylinder (radius r_i) is stationary and registers the torque transferred through the fluid material.....	15
Figure 7: The relation between torque measured by the rheometer and shear stress.....	17
Figure 8: Output from the software during calibration of the BML rheometer.....	18
Figure 9: Principle of the BTRHEOM rheometer.....	19
Figure 10: The BTRHEOM rheometer showing the blades at the top and bottom of the bucket containing the concrete.....	21
Figure 11: Schematic of the CEMAGREF-IMG rheometer.....	22
Figure 12: Picture of the CEMAGREF-IMG rheometer.....	23
Figure 13: Top view of the CEMAGREF-IMG rheometer with grid on the inner cylinder and blades on the outer one.	23
Figure 14: Sketch showing set-up of the calibrated load cells to measure the torque.....	24
Figure 15: Description of the speed-meter.....	25
Figure 16: Diagram of plug flow phenomenon	26
Figure 17: Typical curves versus time obtained during a test.....	29
Figure 18: Torque-rotation speed curve for the same test as in Figure 17.	29
Figure 19: The IBB Rheometer.....	30
Figure 20: Details of the H-shaped impellers, bowls and planetary motion for IBB rheometer for concrete (a) and mortar (b) . Dimension in mm.....	31
Figure 21: Example of calculation with indication of the meaning of the parameters. Y= speed; x = Torque	32
Figure 22: Impeller and bowl dimensions (in mm).....	33
Figure 23: The overall arrangement of the Two-Point test apparatus	34
Figure 24: Comparison of the slumps measured by the standard method and the modified method. The dotted line represents the 45 ° line.	37
Figure 25: Comparison of standard slump and yield stress as measured with the five rheometers. The second axis in N·m gives the results obtained with the IBB.	40
Figure 26: Comparison of plastic viscosity calculated from the modified slump test and plastic viscosity as measured with the five rheometers. The second axis in N·m·s gives the results obtained with the IBB.	41
Figure 27: Comparison of the yield stresses as measured with the rheometers	42
Figure 28: Comparison of the plastic viscosities as measured with the rheometers	42
Figure 29: Comparison between BML and BTRHEOM.....	48
Figure 30: Comparison between BML and CEMAGREF-IMG.....	49
Figure 31: Comparison between BML and IBB.....	50
Figure 32: Comparison between BML and Two-Point test.....	51
Figure 33: Comparison between BTRHEOM and CEMAGREF-IMG.....	52
Figure 34: Comparison between BTHEOM and IBB.....	53
Figure 35: Comparison between BTRHEOM and Two-Point test.....	54
Figure 36: Comparison between IBB and CEMAGREF-IMG.....	55
Figure 37: Comparison between CEMAGREF-IMG and Two-Point test.....	56
Figure 38: Comparison between IBB and Two-Point test.....	57
Figure 39: Comparison of plastic viscosities between BML, BTRHEOM and Two-Point test when the data points from Mixture #4 were omitted.....	58

Figure 40: Comparison of plastic viscosities between IBB and Two-Point test. The data from Mixture #4 were omitted.....	59
Figure 41: Comparison of measured and predicted yield stress according to equations developed by Hu and Kurakawa	63

List of Tables

Table 1: Compositions of mixtures (in kg/m ³) produced with crushed 5/16 mm coarse aggregate in the mixing plant during the rheology week.....	6
Table 2: Compositions of mixtures (in kg/m ³) produced with rounded 4/20 mm coarse aggregate on the mixing plant during the rheology week.....	6
Table 3: Composition of a mixture (in kg/m ³) produced with crushed 0/6.3 mm coarse aggregate in the mixing plant during the rheology week.....	7
Table 4: Fresh concrete analyses. Mixtures # 1-4.	8
Table 5: Fresh concrete analyses. Mixtures # 5-7 & 12.....	9
Table 6: Fresh concrete analyses. Mixtures # 8-11.....	10
Table 7: Dimensions of the inner and outer cylinders of the five standard measuring systems. The configuration used in the tests presented here is highlighted in gray.....	12
Table 8: Slump Measurements	38
Table 9: Yield stress and viscosities calculated from the measurements.....	39
Table 10: Ranking of the yield stresses of the mixtures as determined by the rheometers and the slump. The mixtures are ranked in decreasing order of yield stress from 1 to 12. The higher the slump, the lower the yield stress.	44
Table 11: Ranking of the plastic viscosity of the mixtures as determined by the rheometers. The mixtures are ranked in decreasing order of plastic viscosities from 1 to 12.....	44
Table 12: Correlation coefficients for yield stress	46
Table 13: Correlation coefficients for plastic viscosity	46
Table 14: Correlation coefficients for plastic viscosity if Mixture #4 for Two-Point test is not considered (see text for rationale).	46
Table 15: Between-rheometer linear correlation functions for the yield stress. The rheometers in the column head are Y and those in the row head are X. In each cell the coefficients of the equation $Y=AX +B$ are shown. The rheometers are listed in alphabetical order.....	47
Table 16: Between-rheometer linear correlation functions for the plastic viscosity (all data available are used). The rheometers in the column head are Y and those in the row head are X. In each cell the coefficients of the equation $Y=AX +B$ are shown. The rheometers are listed in alphabetical order.....	47
Table 17 Critical values for the correlation coefficient R of a sample extracted from a normal distributed population. α is the probability, and $v = n-2$, n being the number of points. If the calculated value of R is higher than the reference value shown in the table, there is a probability α that X and Y are dependent.	61

1. Introduction

Concrete is a complex material and its properties in the fresh state can have a large effect on hardened properties. Unfortunately, the technology to measure the properties of fresh concrete has not changed significantly in the last century. The main fresh concrete property, workability, is still measured using the slump test (ASTM C 143). In fact, concretes with the same slump may flow differently and have different workability [3, 4].

The reason two concretes with the same slump behave differently during placement is that concrete flow cannot be defined by a single parameter. Most researchers agree that the flow of concrete can be described reasonably well using a Bingham equation. This equation is a linear function of the shear stress (the concrete response) versus shear rate. Two parameters provided by the Bingham equation are the yield stress and the plastic viscosity. The yield stress correlates reasonably well with the slump value, but the plastic viscosity is not measured at all using the slump test. Plastic viscosity governs concrete flow behavior after flow has started, i.e., after the yield stress is overcome. The existence of the plastic viscosity helps explain why concretes with the same slump may behave differently during placement.

It is critical to completely define concrete flow when special concretes, demanding major control of workability, such as a self-compacting concrete (SCC) or high performance concrete (HPC), are used or when concrete is placed in highly-reinforced structures [5]. This is critical because a single parameter such as the slump does not adequately describe their behavior during placement. More sophisticated and precise tools are needed to determine the workability or flow properties of such concretes. Several instruments have been designed to address this problem [6], some in an empirical manner, and some attempting to apply absolute physical measurements to concrete rheology, i.e., fluid rheology. The devices attempting to use fluid rheology methods to measure the flow of concrete, i.e., measuring shear stress at varying shear rates, are called rheometers [7]. They all measure the resistance to flow of concrete at varying shear rate conditions. Rheometers designed for polymers or neat fluids with no solid particles are not suitable for measuring concrete due to the presence and size of the solid aggregates. This situation has led to a wide variety of designs for concrete rheometers, making it difficult if not impossible to compare the results of the rheometers on a common basis. One obvious solution would be to have a standard reference material to calibrate the rheometers. No such standard material has been developed to simulate fresh concrete behavior. Therefore, the best alternative was to conduct measurements using the rheometers on the same concrete mixtures. The first project goal was to compare the data measured by the various devices. If these measurements differed significantly, the second goal was to establish correlation functions between the rheometer results to make possible reasonable comparisons of data obtained with different rheometers.

The concrete rheometers that are available today and were used in this study are:

- BML (Iceland) [8, 9]
- BTRHEOM (France) [10, 11]
- CEMAGREF-IMG coaxial rheometer (France) [1]

- IBB (Canada) [12]
- Two-Point (UK) [13]

The IBB and Two-Point rheometers are based on rotating an impeller in fresh concrete contained within a cylindrical vessel. The shape of the vane varies with the rheometer. The speed of rotation of the blade is increased and then decreased while the concrete resistance or torque is measured. The BTRHEOM is a parallel plate rheometer. The concrete is placed in a cylindrical container with a fixed bottom plate. A top plate embedded in the concrete is rotated at increasing and then decreasing speeds and the torque is measured. The CEMAGREF-IMG and the BML are coaxial cylinder rheometers in which one cylinder (inner cylinder for the CEMAGREF-IMG and outer for the BML) is rotated at increasing and decreasing speed and the torque induced by the concrete on the inner cylinder is measured. The flow pattern of the concrete in the IBB and Two-Point rheometers cannot be easily assessed or modeled, while the flow can be mathematically modeled for the coaxial rheometers (BML, CEMAGREF-IMG) and for the parallel-plate rheometer (BTRHEOM). For these three rheometers (BML, BTRHEOM, CEMAGREF-IMG), rheological characteristics in fundamental units can be calculated. The Two-Point test rheometer requires indirect methods using calibrating fluids of known viscosity to convert quantitative data into the fundamental units needed. On the other hand, the IBB is not calibrated with a fluid and therefore, the results are not reported in fundamental units. The aim of the present project was to compare measurements from these five rheometers to provide data to establish correlations among them. Differences between the various rheometers were expected, due to the complex granular structure of concrete. Slip at the rheometer surfaces and coarse particle segregation are just two examples of such granular aspects of fresh concrete behavior. They are not accounted for in rheometer analyses, that are based upon classical fluid mechanics of homogeneous fluids.

Comparison and correlation functions, which can relate the results obtained with the various rheometers, are essential to advance the science of concrete rheology and therefore provide a better characterization of concrete “workability”.

Under the auspices of ACI sub-Committee 236A, “Workability of Fresh Concrete,” a group of researchers obtained a grant from ACI’s Concrete Research Council (CRC) to conduct a series of comparison tests on concrete rheometers. The first test was conducted on October 23-27, 2000 in the facilities of the Laboratoire Central des Ponts et Chaussées (LCPC) located in Nantes (France).

This report describes the rheometers used and their operation, the concrete compositions and preparation procedure, and all the data obtained as well as some data interpretation of this. All the data are presented as measured. This will provide a valuable database for use by researchers in this field. Summaries of the different aspects of this research along with further analysis, will be presented in ACI journals and other publications.

2. Concrete Mixtures Used in Tests at Nantes

2.1. Constituents

Twelve mixtures were produced with local materials from the Nantes area.

The cement was a CPA CEM I 52.5 from Saint-Pierre la Cour (equivalent to an ASTM type I). For the self-compacting mixtures, a “Piketty” limestone filler was added. A densified silica fume from Anglefort was used in some concretes for which both low yield stress and low plastic viscosity was required. Most mixtures used a high-range water reducer (HRWRA), which was either a polycarboxylate (commercial name: “MBT Glenium 27”) or a sulphonated melamine (Commercial name: “Chryso Résine GT”). A viscosity agent (Commercial name: “ MBT Meyco MS685”, a suspension of amorphous precipitated nanosilica) was added to the self-compacting mixtures. Tap water was used for all mixtures.

Up to four different aggregate fractions were used for each concrete, to obtain the best possible control of the aggregate size distribution. All concretes contained the same sand, a 0/4 (from 0 mm to 4 mm) Estuaire sand (from the Loire river). In addition, some mixtures also used a very fine (correcting) sand called 0/0.4 from Palvado, to maintain a continuous distribution between the cement and the aggregate size ranges.

Mixtures #1-7 were made with two fractions of crushed coarse aggregate (gneiss from the Pontreaux quarry, with a maximum size of 16 mm). Mixtures # 8-11 contained a rounded silico-calcareous river gravel (also in two fractions) from Longué (Vienne river), with a maximum size of 20 mm. Finally, the last mixture #12 only contained a “small” crushed aggregate from Pontreaux with a maximum size of 6.3 mm. Size distributions of all aggregates are displayed in Figure 1.

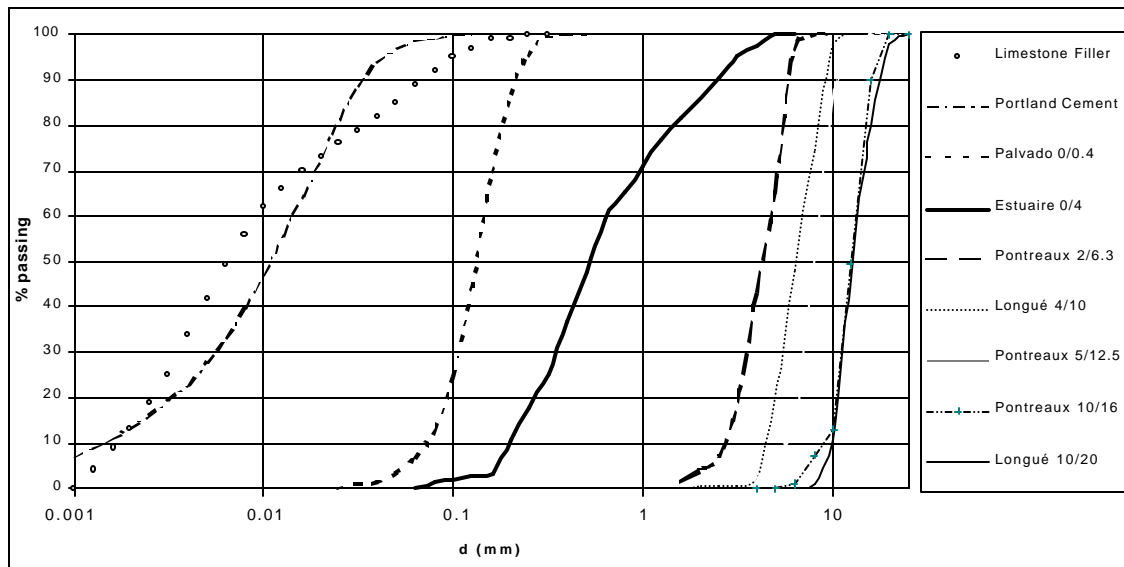


Figure 1: Size distributions of the aggregates used

2.2. Mixture proportions

The mixtures were designed with the help of LCPC mixture-design software BétonlabPro 2 [14]. The objective was to obtain a broad range of combinations of yield stress and plastic viscosity, while minimizing the tendency to segregation. This strategy was followed for #1-4 and #8-11 mixtures. The main difference between these two series was the nature of the coarse aggregate. Since the goal of this rheology project was to test the correlation between a variety of devices, it was useful to see whether such correlations would hold for different types of aggregate. Repetitions of mixtures were planned if time allowed.

Mixture #5 was a gap-graded mixture, with the high coarse/fine aggregate ratio slightly higher than most mix-design method recommendations. The idea was to generate a concrete in which mortar and coarse aggregate would have a tendency to separate from each other, but would not display any obvious segregation in the normal operations of mixing, discharging and casting.

Mixtures #6-7 were planned to be self-compacting mixtures, with very low yield stress, moderate plastic viscosity and high stability at rest and during casting in congested areas. Both mixtures had the same “dry” composition, differing only in the water and superplasticizer dosages.

Finally, mixture # 12 was a high-performance micro-concrete made with a very small aggregate (having a maximum size of 6.3 mm), with a high amount of fines, a low yield stress and a moderate plastic viscosity. Although the test of this concrete was not originally intended, it was considered interesting to include it, because this mixture was designed to minimize the wall effects and segregation in the various rheometers.

Before the testing date, all mixtures were prepared and adjusted in the laboratory, on the basis of 40 L batches produced with a 120 L pan mixer.

2.3. Concrete production

Between development of the mixtures in the laboratory and production at the concrete plant, the cement silo was filled with a new delivery of portland cement (from the same manufacturer). Also, the various aggregate fractions were stored outside, so that aggregate water content varied widely during the project.

Concretes were produced at the Mixing Study Station of LCPC, Nantes (see figure in Appendix A). This station is devoted to research on the production of granular cold material (like concrete and various road base materials) on an industrial scale. A variety of mixers can be mounted on the station, which incorporates all ordinary facilities for storing, weighing and batching materials with suitable automation. For this project, a 1 m³ pan-mixer was used.

In order to control the water content of the concretes, the sand fractions were first weighed and batched into the mixer. The sand fractions could contribute the largest error

in the water content of the concrete. After some minutes of mixing, a sample of the sand was taken to measure the water content. Then, the masses to be added in order to control the proportions of the mixture were calculated, and all the other materials were batched, including coarse aggregate fractions, cement and other binders if any, and finally the rest of water incorporating one third of the total superplasticizer amount. The rest of the superplasticizer was added later as needed.

Due to changes in material batches, sand water content, and batch size, the workability of the concretes often differed from that originally obtained in the lab. In order to avoid production of unsuitable mixtures, the mixing process was systematically interrupted, and the concrete sampled to make a slump test. Based on this slump indication, supplementary additions of water and/or superplasticizer were made as needed. Then mixing was restarted and stopped after a while to check whether the slump was acceptable or not. Concretes were generally accepted after a number of corrections ranging from 0 to 3 (depending on the mixture) but, as the scope of the program was to compare the different rheometers on the same mixtures whatever they were, the variety of mixing procedures was not a problem.

Each concrete mixture was then discharged on a conveyor belt and first poured into a 500 L bucket used to feed the CEMAGREF-IMG rheometer (see picture in Appendix A), and then into a smaller bucket for the other rheometers. During the operation of the conveyor belt, automatic sampling of fresh concrete was performed with a mechanical sampler [15]. The aim of this sampling was to check that no segregation took place during discharge, which would have created an artifact by leading to different mean compositions in the various rheometers (see Section 0 for a description of the methodology and the results).

Then the buckets were transported to the laboratory. The larger bucket was discharged into the CEMAGREF-IMG rheometer, and the small one was offered to the participants. Each team filled its rheometer by hand scooping from the small bucket. During this stage, an operator was continuously agitating the mixture to avoid any significant segregation in the small bucket. The specific gravity of the fresh concrete was determined with a 5 L specimen. Based upon this measurement, the real composition of mixtures per unit volume could be calculated. Mixture compositions appear in Table 1, Table 2 and Table 3.

Table 1: Compositions of mixtures (in kg/m³) produced with crushed 5/16 mm coarse aggregate in the mixing plant during the rheology week.

Mixture No.	1	2	3	4	5*	6**	7**
Pontreaux 10/16	368	482	620	456	1161	780	768
Pontreaux 5/12.5	588	405	356	458	-	175	173
Estuaire 0/4	763	804	440	783	661	773	762
Palvado 0/0.4	-	-	-	56	-	52	52
Cement from St Pierre la Cour	494	426	723	419	391	314	310
Piketty limestone filler	-	-	-	-	-	135	133
Anglefort silica fume	-	21.3	-	-	-	-	-
Glenium 27 SP (in bold: Chryso GT SP)	6.294	6.722	11.403	0.000	1.590	13.837	10.175
Viscosifier agent	-	-	-	-	-	8.171	8.059
Water	188	216	222	201	194	175	184
Target yield stress	high	low	low	high	mod.	very low	very low
Target plastic viscosity	high	low	high	low	mod.	low	low

Notes: *: gap-graded mixture. **: attempt to a self-compacting mixtures

Table 2: Compositions of mixtures (in kg/m³) produced with rounded 4/20 mm coarse aggregate on the mixing plant during the rheology week.

Mixture No.	8	9	10	11
Longué 10/20	563	461	600	550
Longué 4/10	363	394	349	317
Estuaire 0/4	739	797	438	743
Palvado 0/0.04	-	-	-	53
OPC from St Pierre la Cour	480	422	725	398
Anglefort Silica fume	-	21.1	-	-
Glenium 27 Superplasticizer	6.414	5.316	7.608	1.164
Water	205	218	225	213
Target yield stress	high	low	low	high
Target plastic viscosity	high	low	high	low

Table 3: Composition of a mixture (in kg/m³) produced with crushed 0/6.3 mm coarse aggregate in the mixing plant during the rheology week

Mixture No.	12
Pontreaux 2/6.3	825
Estuaire 0/4	564
Cement from St Pierre la Cour	613
Piketty limestone filler	107
Glenium 27 superplasticizer	10.215
Water	230
Target yield stress	Low
Target plastic viscosity	Moderate

2.4. Fresh concrete analyses

The results of the fresh concrete analyses are given in Table 4, Table 5, and Table 6. For each mixture, eight samples were taken. Five corresponded with the concrete discharged into the large bucket for the CEMAGREF-IMG rheometer and the remaining three corresponded to the small bucket reserved for the laboratory rheometers. For each sample, the paste content was determined by weighing the raw sample, then subtracting the mass of dry aggregate obtained after washing on a 80 μm sieve and drying in a microwave oven. The size distribution was then determined by sieving the particles less than 2 mm and with a dedicated optical apparatus [15] for coarser particles. The results in terms of the percentages of the various fractions are displayed in the tables.

For each concrete and each size fraction, the mean value and standard deviation were calculated on the 8-sample series on one hand, and on the 5-sample and 3-sample sub-populations on the other hand. Looking at the overall standard deviations, it can be noted that the concretes were quite homogeneous. The highest standard deviation on paste percentage for any concrete was 0.98 % for Mixture # 10. In absolute terms, it appears that the cement content variation of the samples was 18 kg/m³, a quite limited value.

It is important to judge whether differences in composition found between the concrete for the large rheometer and the rest of the batch were significant. From the results of statistical tests, it seems that a significant difference was found for four mixtures. However, still focusing on the paste content, the highest difference found between the mean values of the two populations is for Mixture # 8. Here, the mean paste contents for the large rheometer concrete and for the rest of the batch were 28.7 % and 29.4 %, respectively. The corresponding cement contents were from 480 kg/m³ to 492 kg/m³. By performing a simulation with the BétonlabPro 2 software [14], and assuming a constant water/cement ratio, it appears that the corresponding variation in slump was about 7 mm, which is not significant. It can be concluded, therefore, that the mixtures were essentially homogeneous. No significant segregation occurred during the discharge of concrete batches, which could have created a bias in the rheometer comparison.

Table 4: Fresh concrete analyses. Mixtures # 1-4.

The unshaded rows give the results of the concrete used for the CEMAGREF-IMG rheometer, while the shaded areas are for the other rheometers.

Nominal Values	% of paste by mass fraction				% of 0.08/2 fraction				% of 2/10 fraction				% of 10/D fraction			
	28.6	28.4	40.3	26.2												
Mixtures	# 1	# 2	# 3	# 4	# 1	# 2	# 3	# 4	# 1	# 2	# 3	# 4	# 1	# 2	# 3	# 4
1	28.8	25.1	38.1	26.9	35.3	31.2	22.7	38.6	32.5	25.9	21.9	27.0	32.2	42.9	55.4	34.4
2	29.2	25.7	38.0	26.4	35.7	32.0	22.5	36.9	30.9	26.5	23.9	25.8	33.3	41.5	53.6	37.2
3	29.2	26.2	39.0	26.4	35.3	31.6	23.8	37.9	30.1	24.3	25.1	26.4	34.5	44.1	51.2	35.7
4	28.9	25.2	38.6	27.2	34.5	30.2	23.0	38.1	27.9	25.4	25.1	26.7	37.5	44.4	51.9	35.2
5	29.5	25.4	38.6	26.5	36.1	31.1	23.1	37.4	33.5	24.3	26.0	25.7	30.4	44.6	50.9	36.9
Mean value	29.1	25.5	38.5	26.7	35.4	31.2	23.0	37.8	31.0	25.3	24.4	26.3	33.6	43.5	52.6	35.9
Standard deviation	0.26	0.44	0.41	0.36	0.60	0.69	0.51	0.65	2.14	0.98	1.58	0.57	2.67	1.28	1.91	1.20
6	28.3	25.9	39.0	26.4	34.3	32.0	23.7	37.5	33.3	28.6	25.4	27.8	32.4	39.3	50.8	34.7
7	29.3	25.8	38.3	26.2	36.0	32.0	22.9	36.7	31.4	26.0	25.4	26.0	32.6	42.0	51.7	37.3
8	29.3	25.4	37.9	26	33.9	30.6	22.7	36.1	31.9	27.9	23.64	24.1	34.2	41.4	53.68	39.8
											3				6	
Mean value	29.0	25.7	38.4	26.2	34.7	31.6	23.1	36.8	32.2	27.5	24.8	26.0	33.1	40.9	52.1	37.3
Standard deviation	0.56	0.26	0.56	0.20	1.10	0.78	0.56	0.69	0.98	1.34	1.03	1.83	0.97	1.38	1.47	2.52
ALL SAMPLES																
Mean value	29.1	25.6	38.4	26.5	35.2	31.4	23.0	37.4	31.4	26.1	24.5	26.2	33.4	42.5	52.4	36.4
Standard deviation	0.37	0.38	0.43	0.38	0.82	0.69	0.49	0.81	1.80	1.55	1.34	1.09	2.10	1.81	1.67	1.77

Table 5: Fresh concrete analyses. Mixtures # 5-7 & 12.

The unshaded rows give the results of the concrete used for the CEMAGREF-IMG rheometer, while the shaded areas are for the other rheometers.

Nominal values	% of paste by mass fraction				% of 0.08/2 fraction				% of 2/10 fraction				% of 10/D fraction		
	24.3	26.5	26.7	40.7											
Mixtures	# 5	# 6	# 7	# 12	# 5	# 6	# 7	# 12	# 5	# 6	# 7	# 12	# 5	# 6	# 7
1	25.1	26.2	25.3	40.8	26.8	34.3	32.9	34.7	9.5	16.6	13.4	65.3	63.8	49.1	53.6
2	25.5	26	26.3	40.5	26.3	33.4	34.5	34.1	9.8	14.7	16.1	65.9	63.9	51.9	49.4
3	25.0	26.7	26.3	40.1	26.3	35.1	34.8	34.3	9.8	14.7	14.7	65.7	63.9	50.2	50.5
4	25.2	26.3	26.1	41	26.3	33.6	34.0	34.1	10.9	15.8	13.6	65.9	62.7	50.7	52.5
5	25.3	27	25.6	40.2	26.8	35.2	33.4	33.6	10.0	16.6	13.1	66.4	63.1	48.2	53.5
Mean value	25.2	26.4	25.9	40.5	26.5	34.3	33.9	34.1	10.0	15.7	14.2	65.8	63.5	50.0	51.9
Standard deviation	0.19	0.40	0.45	0.38	0.27	0.82	0.77	0.41	0.56	0.95	1.23	0.40	0.54	1.43	1.88
6	24.6	26.9	26.2	41.2	25.2	34.8	34.0	35.1	9.4	15.5	16.8	64.9	65.3	49.6	49.2
7	24.6	26	26.6	41.2	25.6	34.1	34.8	35.1	9.5	15.1	15.9	64.9	64.8	50.8	49.3
8	25.1	26.8	26.9	40.8	26.3	34.8	35.8	34.2	8.7	15.2	15.56	65.8	65.0	50.0	48.63
											7				7
Mean value	24.8	26.6	26.6	41.1	25.7	34.6	34.8	34.8	9.2	15.3	16.1	65.2	65.1	50.1	49.0
Standard deviation	0.29	0.49	0.35	0.23	0.55	0.40	0.92	0.51	0.43	0.20	0.65	0.52	0.26	0.57	0.36
ALL SAMPLES															
Mean value	25.1	26.5	26.2	40.7	26.2	34.4	34.3	34.4	9.7	15.5	14.9	65.6	64.1	50.1	50.8
Standard deviation	0.32	0.41	0.51	0.42	0.53	0.67	0.89	0.53	0.64	0.75	1.41	0.53	0.92	1.12	2.06

Table 6: Fresh concrete analyses. Mixtures # 8-11.

The unshaded rows give the results of the concrete used for the CEMAGREF-IMG rheometer, while the shaded areas are for the other rheometers.

Nominal values	% of paste by mass fraction				% of 0.08/2 fraction				% of 2/10 fraction				% of 10/D fraction			
	29.3	28.8	40.8	26.9												
Mixtures	# 8	# 9	# 10	#11	# 8	# 9	# 10	#11	# 8	# 9	# 10	#11	# 8	# 9	# 10	#11
1	29.1	26.5	36.8	26.0	34.8	33.8	21.0	36.1	27.8	30.8	28.3	27.5	37.4	35.4	50.7	36.4
2	28.7	26.5	37.6	26.1	34.1	32.9	21.6	36.3	26.1	29.2	28.9	27.0	39.8	38.0	49.5	36.8
3	28.5	27.6	37.6	26.3	33.3	35.3	21.9	37.8	25.9	34.8	25.2	26.6	40.7	29.9	52.9	35.7
4	28.6	26.2	38.9	26.8	33.6	32.1	23.2	35.2	25.6	30.2	26.8	27.0	40.8	37.7	50.1	37.8
5	28.6	26.7	39.6	26.1	33.7	33.9	21.4	36.5	27.7	32.2	23.6	26.7	38.6	33.9	55.0	36.8
Mean value	28.7	26.7	38.1	26.3	33.9	33.6	21.8	36.4	26.6	31.5	26.5	27.0	39.5	35.0	51.6	36.7
Standard deviation	0.23	0.53	1.13	0.32	0.60	1.20	0.83	0.94	1.04	2.17	2.17	0.35	1.45	3.28	2.27	0.77
6	28.6	26.5	37.4	26.6	33.7	32.8	23.9	36.1	28.6	29.6	30.8	25.7	37.7	37.6	45.4	38.2
7	29.8	26.6	38.6	25.6	35.9	33.6	22.9	35.5	29.3	28.8	28.9	27.3	34.8	37.6	48.2	37.2
8	29.7	28.4		26.5	35.6	35.8		36.3	27.5	33.3		27.1	36.9	30.9		36.6
Mean value	29.4	27.2	38.0	26.2	35.1	34.1	23.4	36.0	28.5	30.6	29.8	26.7	36.5	35.3	46.8	37.3
Standard deviation	0.67	1.07	0.85	0.55	1.19	1.57	0.68	0.43	0.91	2.40	1.31	0.84	1.53	3.87	1.98	0.81
ALL SAMPLES																
Mean value	29.0	26.9	38.1	26.3	34.3	33.8	22.3	36.2	27.3	31.1	27.5	26.9	38.3	35.1	50.2	36.9
Standard deviation	0.53	0.74	0.98	0.38	0.99	1.27	1.06	0.77	1.33	2.13	2.46	0.54	2.08	3.24	3.12	0.79

3. Concrete Rheometers

3.1. The BML Rheometer

3.1.1. Description of apparatus

The ConTec BML viscometer 3, used in this test, is a coaxial cylinder rheometer for coarse particle suspensions such as cement paste, grout, mortars, cement-based repair materials, and concrete. It is based on the Couette rheometer [16] principle where the inner cylinder measures torque as the outer cylinder rotates at variable angular velocity. It was developed in Norway in 1987 [8, 9] after six years intensive work with the Tattersall Two-Point test instrument. Since then, about 30 ConTec instruments have been made (as of Feb. 2001). Several versions have been designed from the basic instrument. Figure 2 shows viscometer 3, which is the best known, and viscometer 4, which is a smaller model, designed mainly for mortar and very fluid concrete.

To perform the tests described in this report the ConTec BML viscometer 3 was used. To simplify the wording, this instrument will be referred as BML or BML rheometer in the rest of this report.



Figure 2: The ConTec viscometers: a) Version 3; b) Version 4.

The instrument is user-friendly, fully-automated, and is controlled by computer software called FreshWin. Each test takes about 3 min to 5 min, from filling the bowl/material container to emptying it. During testing, the material is exposed to shear for about one minute (depending on the set-up used). A trolley is used for transporting the container (the outer cylinder) full of concrete to ease the transport operation.

Several measuring systems can be used depending on the maximum aggregate size in the suspension to be tested. Details are given in Table 7. Each measuring system is related to the diameter of the inner cylinder. As an example, the most commonly used is the C-200, where the C stands for Concrete and 200 represents the diameter of the inner cylinder in millimeters. The C-200 measuring system was used for the tests reported here.

Table 7: Dimensions of the inner and outer cylinders of the five standard measuring systems. The configuration used in the tests presented here is highlighted in gray

Measuring system	Inner radius (mm)	Outer radius (mm)	Effective height (mm)	Volume of testing
				Material
M-130	65	78	100	~1 liter
M-170	85	100	120	~3 liters
C-200	100	145	150	~17 liters
C-200/1.3	100	131	150	~15 liters
C-240	120	Xx	150	~25 liters

The parameters for each measuring system are incorporated as a standard set-up in the FreshWin software. As shown in Figure 3 (to the left), a simple click and point allows changes to the relevant parameters. The figure to the right shows the basic output of a test result, namely a plot of torque vs. rotational frequency (velocity), displayed in real time during testing. Figure 4 shows the inner and outer cylinder. Both cylinders contain ribs parallel to their axis. Therefore, it is the material tested that will form the actual inner and outer cylinder. This leads to a larger cohesion (or stickiness) between the cylinders and the test material, hence reducing the danger of slippage.

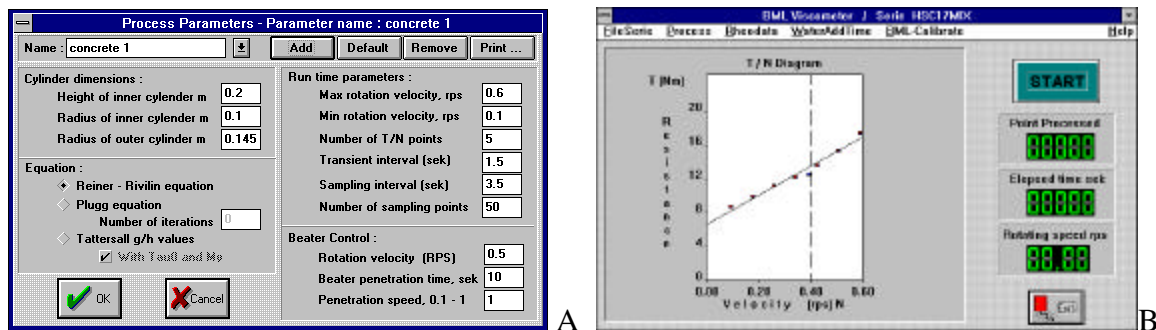


Figure 3: Output from the FreshWin software: A) The menu-driven window used to change relevant parameters; B) The basic output of a test result.

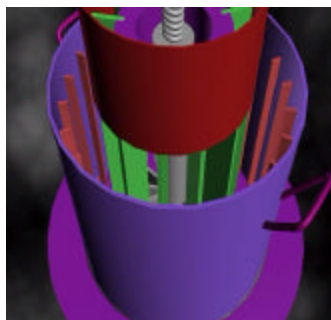


Figure 4: The inner and outer cylinder of the BML Viscometer 3 (or BML rheometer hereafter).

The inner cylinder consists of three parts; the upper measuring unit, the lower unit and the top ring (Figure 4 and Figure 5). It is only the upper unit that measures torque. The lower unit is present to eliminate, or at least minimize, the so-called bottom effects. This insures that only two-dimensional shearing of the testing material generates the torque, which the instrument records.

At the bottom of any coaxial cylinder viscometer there is a complex three-dimensional shearing in the material. In this bottom zone, the shear rate is not uniform for any given angular velocity. Also, in some locations of this zone, the material may not have reached equilibrium shear stress for the given angular velocity, even though it has reached equilibrium in the upper zone where two-dimensional shearing exists. The functionality of the pre-mentioned lower unit is to reduce this bottom effect.

The functionality of the top ring is somewhat less important, since its main objective is to keep a constant height h where torque is measured. This is done to simplify the calculations of the plastic viscosity and the yield value. If omitted, then the height has to be measured for each test and put manually in the FreshWin software.

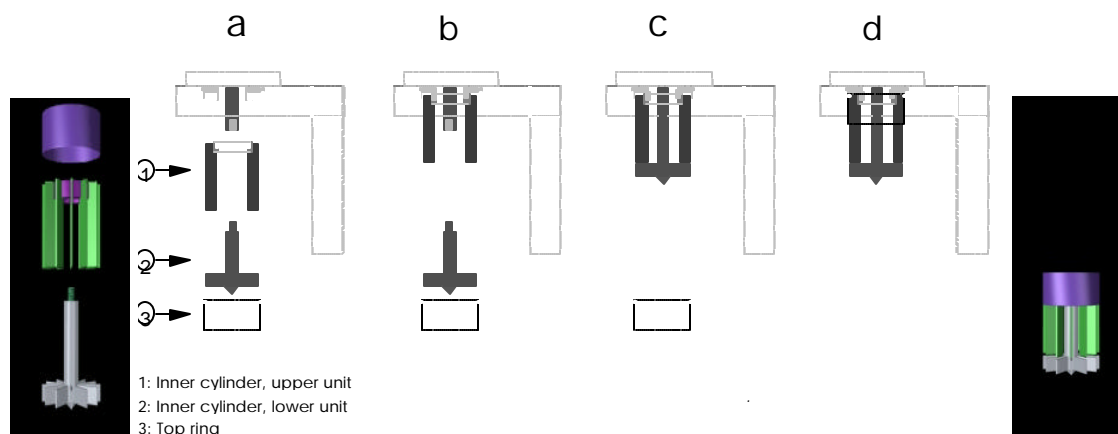


Figure 5: The assembly of inner cylinder of the BML viscometer 3. This figure shows the sequence for installing the inner cylinder.

Depending on mixture design, during initial shearing, a permanent volume increase in the material can be observed. This positive dilatancy occurs between the inner and outer cylinder (i.e. in the shearing zone). Generally, some amount of liquid, i.e., cement paste, fine aggregate, etc., would be extracted from the test material near the outer cylinder and move in the area of highest dilatancy, namely near the inner cylinder. As a consequence, a higher aggregate content would appear near the outer cylinder, which will result in a plug flow. This overall process is minimized in the BML, because the material within the inner cylinder can provide the liquid. The same mechanism applies to the material between the ribs of the outer cylinder.

3.1.2. Test procedures

Concrete and other cement-based materials, such as cement paste or mortar, are usually considered to be a Bingham fluid, at least as a first approximation. In this case the viscosity is given by:

$$\mathbf{h} = \mathbf{m} + \frac{\mathbf{t}_0}{\dot{\mathbf{g}}} \quad (1)$$

where

\mathbf{h}	Viscosity of the Bingham fluid [Pa·s]
\mathbf{m}	Plastic Viscosity [Pa·s]
τ_0	Yield value [Pa]
$\dot{\mathbf{g}}$	Rate of shear [1/s]

The equation for the shear stress is given by $\mathbf{t} = \mathbf{h}\dot{\mathbf{g}}$, where \mathbf{t} is the applied shear stress. With the above viscosity equation, then the well-known shear stress equation for the Bingham fluid is created:

$$\mathbf{t} = \mathbf{h}\dot{\mathbf{g}} = (\mathbf{m} + \mathbf{t}_0/\dot{\mathbf{g}})\dot{\mathbf{g}} = \mathbf{m}\dot{\mathbf{g}} + \mathbf{t}_0 \quad (2)$$

Since the fluid material in a coaxial cylinder rheometer is dominated by shear flow, the following constitutive equation or rheological equation of state is used [17]:

$$\mathbf{s} = -p\mathbf{I} + 2\mathbf{h}\dot{\mathbf{e}} \quad (3)$$

$\dot{\mathbf{e}}$	The strain rate tensor [1/s]
$\bar{\mathbf{v}}$	Velocity [m/s]
$\boldsymbol{\sigma}$	Stress tensor [Pa]
p	Pressure [Pa]
\mathbf{I}	The unit dyadic (or the unit matrix)

In rheology, an equation of this type is the most fundamental tool for describing the mechanical behavior of a fluid material. Its divergence describes the net force acting on a continuum particle from its surroundings.

A top view of coaxial cylinder rheometer is shown in Figure 6. The outer cylinder (radius r_o) rotates at angular velocity Ω (\mathbf{w}_o in the figure), while the inner cylinder (radius r_i) is stationary and registers the applied torque T from the rheological continuum (i.e. from the cement-based material).

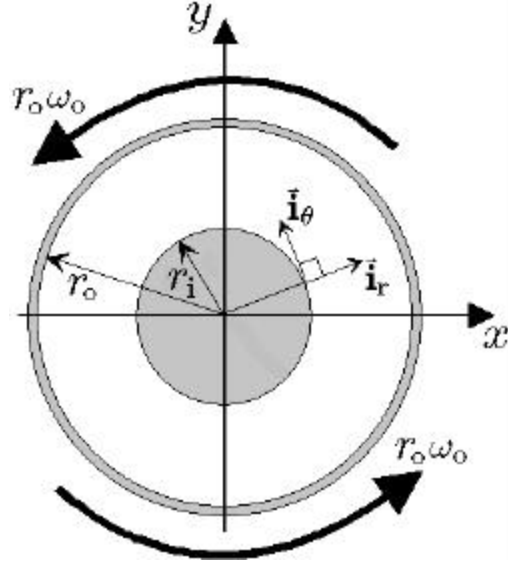


Figure 6: A top view of a coaxial cylinder rheometer. The outer cylinder (radius r_o) rotates at angular velocity ω_o , while the inner cylinder (radius r_i) is stationary and registers the torque transferred through the fluid material.

As can be seen from Figure 6, it is very convenient to work in cylindrical coordinates, as is done here. Using the general velocity field in Equation 3, it is only possible to achieve a solution by numerical means:

$$\vec{v} = v_r(r, \mathbf{q}, z, t) \vec{i}_r + v_q(r, \mathbf{q}, z, t) \vec{i}_q + v_z(r, \mathbf{q}, z, t) \vec{i}_z \quad (4)$$

But fortunately some reasonable assumptions about the flow can be made, which makes an analytical approach possible:

1. At a low Reynolds number (i.e. with low speed and high viscosity η) the flow is stable and it is possible to assume flow symmetry around the z -axis:

$$\vec{v} = v_r(r, \mathbf{q}, z, t) \vec{i}_r + v_q(r, \mathbf{q}, z, t) \vec{i}_q \quad (5)$$

2. If the bottom effect¹ in the rheometer is eliminated by some geometrical means, height independence can be assumed in the velocity function:

$$\vec{v} = v_r(r, \mathbf{q}, t) \vec{i}_r + v_q(r, \mathbf{q}, t) \vec{i}_q \quad (6)$$

¹ The “bottom effect” means the effect from the shear stress generated at the bottom plate of the container. This stress generates height dependence (i.e. z -dependence) in the velocity function.

3. Due to the circular geometry of the coaxial cylinder rheometer (see Figure 6), it is reasonable to assume pure circular flow with \mathbf{q} -independence:

$$\bar{\mathbf{v}} = v_q(r, t) \bar{\mathbf{i}}_q \quad (7)$$

Since the rheological continuum a coaxial cylinder rheometer is driven by shear stress from its outer cylinder and not by pressure distribution in the \mathbf{q} -direction, it is also reasonable to assume \mathbf{q} -independence in the pressure function:

$$p = p(r, z, t) \quad (8)$$

The governing equation comes from Newton's Second Law, more accurately called Cauchy's equation of motion [18]:

$$\mathbf{r} \frac{d\bar{\mathbf{v}}}{dt} = \bar{\nabla} \cdot \mathbf{s} + \mathbf{r} \bar{\mathbf{b}} \quad (9)$$

Solving the above equation with the given assumptions and with the boundary conditions of $v_\theta(r_i)=0$ and $v_\theta(r_o)=r_o \cdot \Omega$, produces:

$$v_q(r) = \frac{T r}{4 \mathbf{p} \mathbf{m} h} \left(\frac{1}{r_i^2} - \frac{1}{r^2} \right) - \frac{\mathbf{t}_o r}{\mathbf{m}} \ln \left(\frac{r}{r_i} \right) \quad (10)$$

$$T = \frac{4 \pi \mu h}{\left(\frac{1}{r_i^2} - \frac{1}{r_o^2} \right)} \Omega + \frac{4 \pi \tau_o h}{\left(\frac{1}{r_i^2} - \frac{1}{r_o^2} \right)} \ln \left(\frac{r_o}{r_i} \right) = H \Omega + G \quad (11)$$

In the above derivations, no assumption is made regarding the ratio of the cylinders, r_o/r_i . Therefore, any ratio can be used in the above two equations.

Solving Equation 11 for Ω gives the well-known Reiner-Rivlin equation. The variable T is the torque applied to the inner cylinder by the testing material. The relation between the rotational frequency (N) and the angular velocity (Ω) of the outer cylinder is:

$$\Omega = 2 \mathbf{p} \cdot N \quad (12)$$

In the M-170 measuring system, the ratio between the inner and the outer radii, r_o/r_i , is 1.18, which ensures that only small variations [19] exist in shear rate across the gap between the cylinders. For the standard C-200 system, which was used in the current test program, the ratio of the radii of the outer and inner cylinders is 1.45. With this ratio, the rate of shear will not be fully constant in the shearing zone at a given angular velocity of the outer cylinder. This, however, does not prevent the calculation of the Bingham parameters of yield stress and plastic viscosity, when the Reiner-Rivlin equation is used.

The software that controls the rheometer also calculates the speed, N_p , below which plug flow will occur [16] using Equation 13. If a data point is below the plug speed, it is removed manually, by a simple click of the mouse. The underlying physics for a coaxial cylinder rheometer and the derivation of Equation 13 has also been discussed by Tattersall and Banfill [16]:

$$N_p = \frac{\tau_0}{\mu} \cdot \left[\frac{1}{2} \left(\frac{r_o^2}{r_i^2} - 1 \right) - \ln \left(\frac{r_o}{r_i} \right) \right] \cdot \frac{1}{2\pi} \quad (13)$$

The likelihood for plug flow occurring between the inner and outer cylinder during testing is proportional to the ratio of τ_0/μ . If a plug occurs, then the error can be higher if the ratio of the outer to the inner cylinder radii (r_o/r_i) is as big or bigger than the square root of the ratio of G and T_0 (see Figure 7) is:

$$\frac{G}{T_0} = \left(\frac{r_o}{r_i} \right)^2 \quad (14)$$

The term T_0 is the torque value measured at the lowest rotational frequency possible. Its deviation from the term G occurs because of a plug inside the test material.

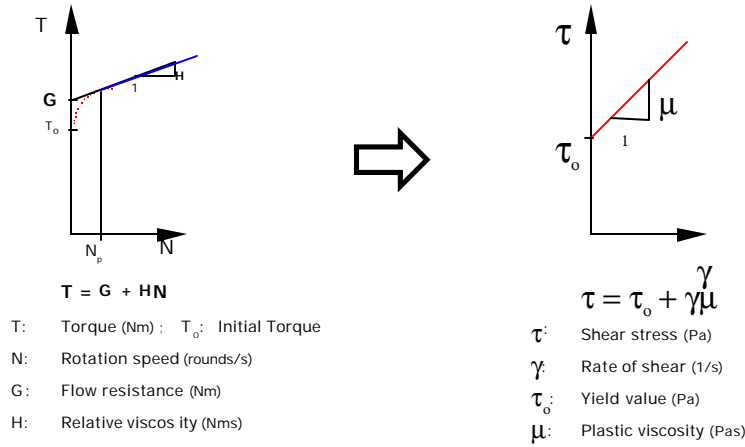


Figure 7: The relation between torque measured by the rheometer and shear stress

3.1.3. Calibration

The calibration of torque and angular velocity is performed by an external load cell and a stopwatch (or optical tachometer). The measured values are inserted into the FreshWin software, which calculates the calibration constants. To confirm that the calibration is correct, commercial products with known or stable rheological properties, like the oil, CylEso 1000, can be tested. Figure 8 shows the theoretical line and the kinematic viscosity measured with the ConTec BML viscometer 3. Also shown are values measured with a tube rheometer by the oil-testing laboratory Fjölver. Agreement is sufficiently accurate for

measurement of the viscosity of such a relatively low viscosity newtonian liquid such as the CylEso 1000 oil.

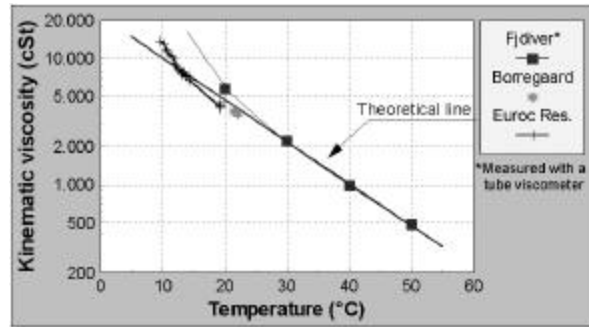


Figure 8: Output from the software during calibration of the BML rheometer

3.2. The BTRHEOM Rheometer

3.2.1. Description of the apparatus

The BTRHEOM is a parallel plate rheometer for soft-to-fluid concrete (slump higher than 100 mm, up to self-compacting concrete) with a maximum size of aggregate up to 25 mm. The rheometer is designed so that a 7 L specimen of concrete having the shape of a hollow cylinder is sheared between a fixed base and a top section that is rotated around the vertical axis (see Figure 9). A motor located under the container rotates the upper blade system (see Figure 10). The torque resulting from the resistance of the concrete to be sheared is measured through the upper blades.

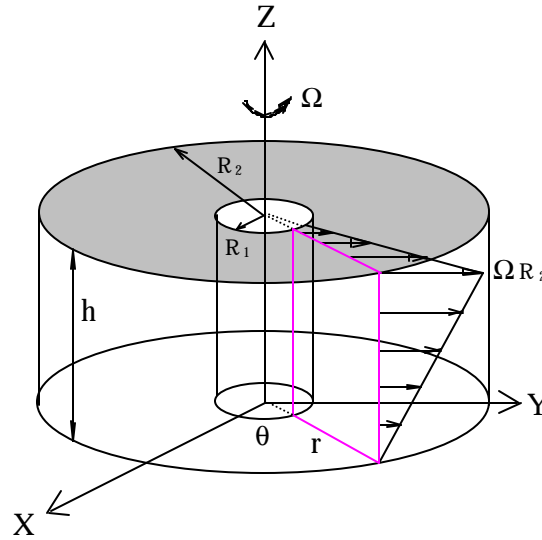


Figure 9: Principle of the BTRHEOM rheometer

The dimensions of the sample are: $R_1 = 20$ mm, $R_2 = 120$ mm, and $h = 100$ mm (Figure 9). The control of the rheometer (rotation speed, vibration), the measurements (torque and rotation speed) and the calculation of the rheological parameters from the raw data are all carried out by a special program (ADRHEO). The rotation speed can be varied between 0.63 rad/s (0.1 rev/s) and 6.3 rad/s (1 rev/s), though it is usually chosen between 0.63 rad/s (0.1 rev/s) and 5.02 rad/s (0.8 rev/s). The maximum torque that can be measured is about 14 N·m.

3.2.2. Test procedure

A seal is used to ensure that no concrete flows between the bucket and the rotating upper cylinder and blocks the apparatus. The mean friction due to the seal is first evaluated in the presence of water. From this value, the friction of the seal in the presence of concrete is calculated and subsequently subtracted from the torque measurements to obtain the part of the torque due to the concrete alone [11,1]. Once the bucket is filled, the concrete is vibrated for 15 s to ensure good compaction of the concrete in the bucket (except for self-compacting

concrete). This pre-vibration is optional. The frequency of pre-vibration can be selected in the range from 36 Hz to 55 Hz. After the pre-vibration, the measurement itself starts. The rheometer is controlled by the rotation speed.

The basic test consists of one or two consecutive series of five to ten measurement points, made at increasing or decreasing rotation speed. For example, if the test consists of two series, both may contain the same number of points, and have the same upper and lower limits, but each series can be made at either increasing or decreasing rotation speed, and with or without vibration. After completion of the test, the concrete can be vibrated again if required. For each data point, a torque measurement (Γ) is taken after a time interval of about 20 s during which the rotation speed N is constant. This delay allows for stabilization of the torque.

3.2.3. Analysis of the data

The recording of the various (Γ , N) data pairs is carried out by the computer. The relationship between torque and rotation speed is a function of the form:

$$\Gamma = \Gamma_0 + A N^b \quad (15)$$

From this relationship and the strain field shown in Figure 9, the rheological behavior of the concrete can be deduced. It is assumed that the concrete has a Herschel-Bulkley behavior that means that the shear stress τ is related to the shear velocity gradient by the following equation:

$$\mathbf{t} = \mathbf{t}_0 + a \dot{\mathbf{g}}^b \quad (16)$$

For practical purposes, b is fixed between 1 and 3 (see [33]). Finally, the flow behavior of the concrete is approximated by the Bingham law with only two rheological parameters:

$$\tau = \tau_0 + \mu \dot{\gamma} \quad (17)$$

where τ_0 is the shear yield stress calculated with Equation 17 and μ the plastic viscosity deduced from a and b in Equations 18 and 19 [20]. The details of the derivation of the equations relating τ_0 and μ to Γ_0 , A and b in Equation 15 are given in Reference [20]. These equations are:

$$\tau_0 = \frac{3}{2\pi(R_2^3 - R_1^3)} \Gamma_0 \quad (18)$$

$$a = 0.9 \frac{(b+3)}{(2\pi)^{b+1}} \frac{h^b}{(R_2^{b+3} - R_1^{b+3})} A \quad (19)$$

$$\mu = \frac{3a}{b+2} \dot{\gamma}_{\max}^{b-1} \quad (20)$$

where $\dot{\gamma}_{\max} = \frac{\Omega_{\max} R_2}{h}$ is the maximum strain rate used in the measurement.

Alternatively, the Bingham parameters may be directly calculated from Equation 15 assuming $b = 1$. However, the result (in terms of τ_0 and μ values) is different from the value calculated using Equations 17 to 19 [20].

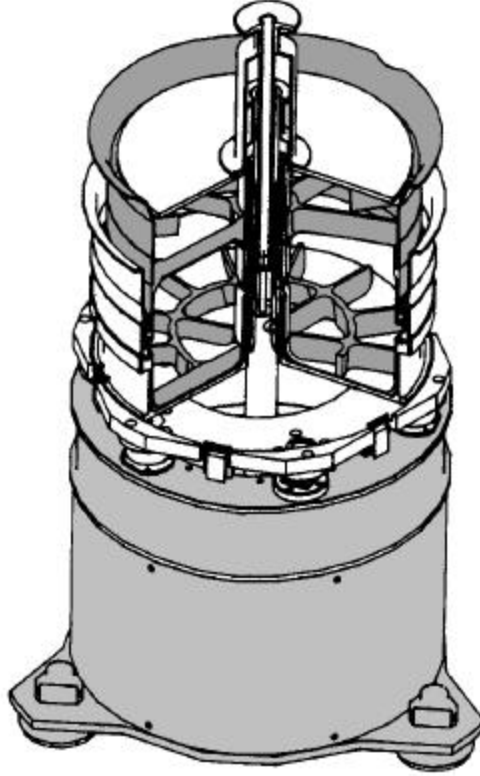


Figure 10: The BTRHEOM rheometer showing the blades at the top and bottom of the bucket containing the concrete.

3.3. The CEMAGREF-IMG Rheometer

3.3.1. Description of the apparatus

The CEMAGREF-IMG rheometer is a large coaxial-cylinder rheometer that contains approximately 500 L of concrete (see Figure 11 and Figure 12). The outer cylinder wall is equipped with vertical blades, and the inner one with a metallic grid in order to limit the slippage of concrete (see Figure 13). A rubber seal is fitted to the base of the inner cylinder to avoid any materials leakage between the cylinder and the container bottom.

This apparatus was originally developed to study mud flow rheology [21]. The primary advantage of this instrument is the large dimensions with respect to the maximum aggregate size. However, the geometry is not a pure Couette one, because the ratio of the inner radius to the outer radius is too large, 1.57. Therefore, some plug flow is to be expected when testing viscoplastic materials that have a yield stress. It means that for most tests, only the inner part of the concrete sample will be sheared, at least for the lower values of rotation speed (see Figure 13).

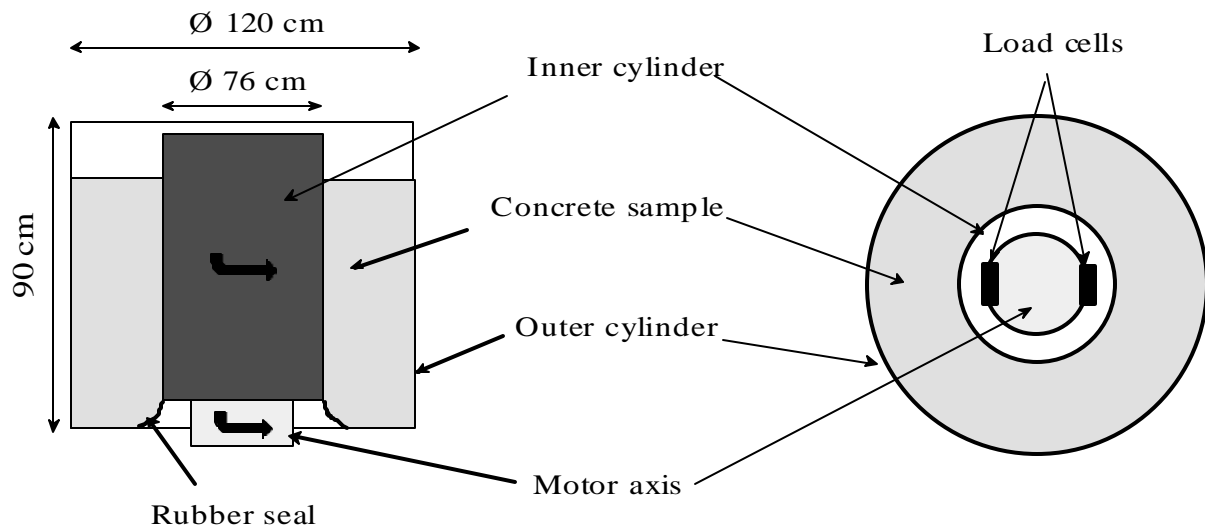


Figure 11: Schematic of the CEMAGREF-IMG rheometer



Figure 12: Picture of the CEMAGREF-IMG rheometer

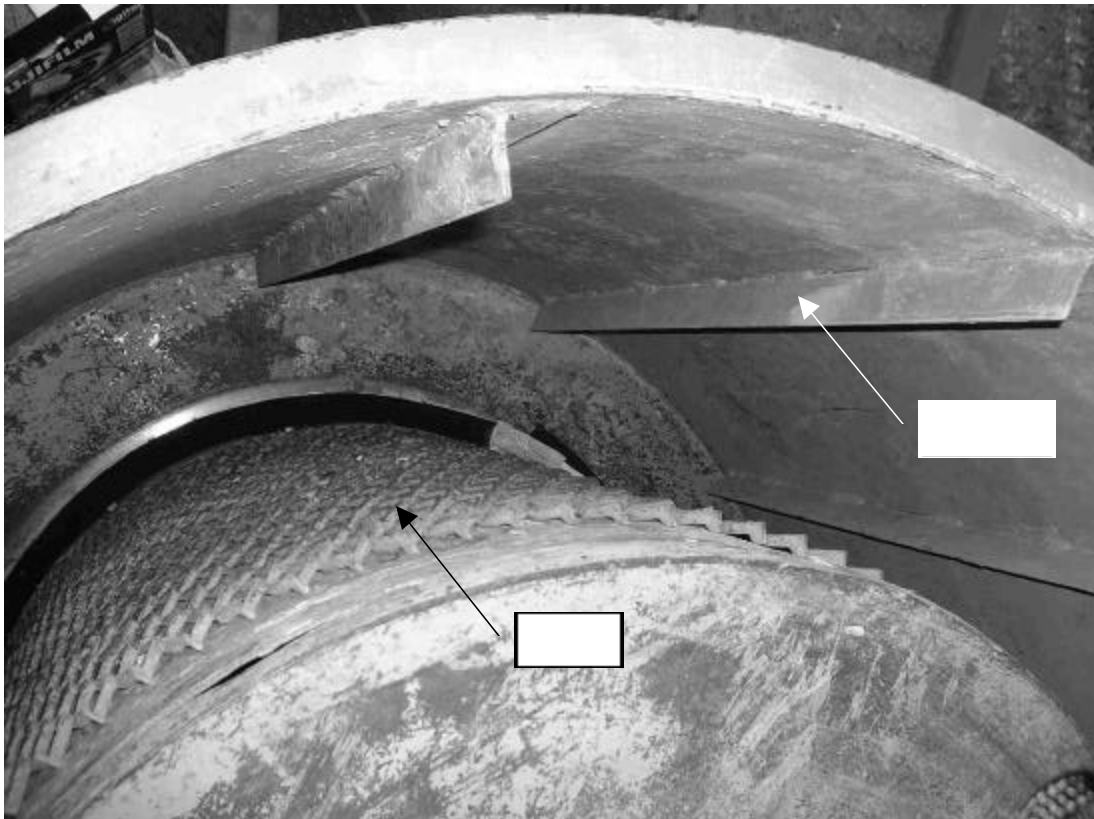


Figure 13: Top view of the CEMAGREF-IMG rheometer with grid on the inner cylinder and blades on the outer one.

The rotation movement is transmitted from the motor axis to the inner cylinder through two mechanical linkages, both of which include a load cell (see Figure 14). The load cells, which were calibrated by LCPC prior the tests reported here (see calibration report in Appendix D), measure the total torque transmitted to the concrete.

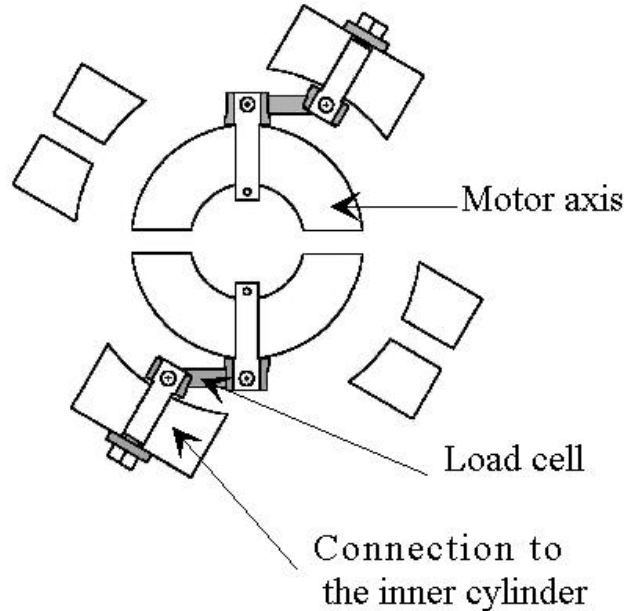


Figure 14: Sketch showing set-up of the calibrated load cells to measure the torque

The rotation velocity is measured by a dynamo, the axis of which is connected by a wheel to the cap of the rotating inner cylinder (see Figure 15). This speed-meter was also calibrated by LCPC prior to the tests reported here (see calibration report in Appendix D).

Thus, during a test, three voltages are recorded at a frequency of 5 Hz with a PCMCIA acquisition card IOTEK DAQCARD 112B (see verification report in Appendix D):

- two for the load cells;
- one for the speed-meter.

Data are saved in text files with the following format:

- first column (CH00): the torque value $C1$ (in N·m) given by the load cell n°1;
- second column (CH01): the torque value $C2$ (in N·m) given by the load cell n°2;
- third column (CH02): the rotation speed Ω (in rad/s) of the inner cylinder;

The total torque C is given by the equation $C=C1+C2$

The following relationships were used for conversion of the voltages measured ($V1, V2, V3$ in volts).

- for the load cell n°1: $C1 = 998.84 \cdot V1$
- for the load cell n°2: $C2 = 1000.2 \cdot V2$
- for the speed-meter: $\Omega = -0.6225 \cdot V3 + 0.0322$

The calibration curves are shown in Appendix D.

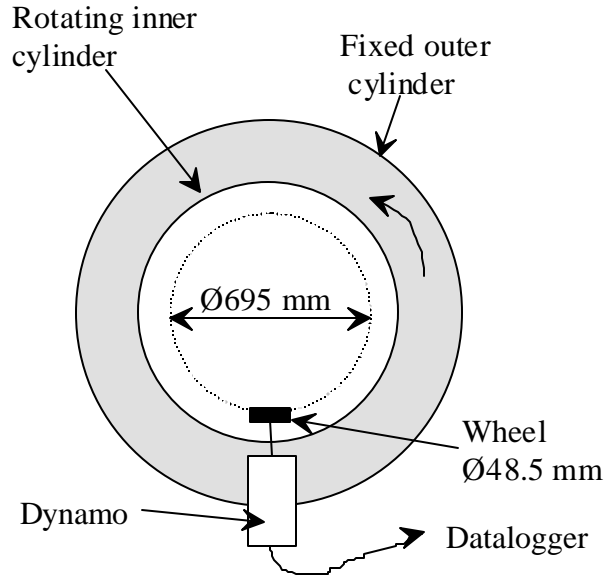


Figure 15: Description of the speed-meter

3.3.2. Test procedure

Tests are carried out by manual control of the engine power. The procedure is as follows:

- The torque needed to counteract the seal friction is measured in presence of a small amount of concrete in the rheometer (approximately 55 mm of concrete is needed to cover the seal) for different decreasing rotation speeds.
- The rheometer is then filled with concrete and the height of the concrete is measured.
- The rotation speed is rapidly increased up to a maximum and then decreased in 6 to 8 steps lasting around 10 s each, down to a minimum. Torque and rotation speed are recorded at a frequency of 5 Hz.
- During the test, the width of the sheared zone is manually evaluated with a ruler on the top surface of the concrete for different rotation speeds.

3.3.3. Analysis of the data

Notation

$R_{int} = 0.38$ m: inner cylinder radius

$R_{ext} = 0.60$ m: outer cylinder radius

h (in m): height of concrete test sample (total height of concrete minus 0.055 m, corresponding to the concrete used for the seal calibration)

C (in N·m): torque applied to the concrete sample

Ω (in rad/s): rotation speed of the inner cylinder

r (in m): radial coordinate of a unit concrete cylinder

ω (in rad/s): rotation speed of a unit concrete cylinder

$\dot{\gamma}$ (in s^{-1}): strain rate

τ (in Pa): shear stress

τ_0 (in Pa): shear yield stress in Bingham model
 μ (in Pa s): plastic viscosity in Bingham model
 R_c (in m): critical radius beyond which the concrete is not sheared (dead zone)
 E_c : width of the sheared zone ($E_c = R_c - R_{int}$)

Direct calculation of the shear yield stress

During a test, the width E_c of the sheared zone beyond which there is a “dead zone” (see Figure 16) was measured for different rotation speeds. For the sheared part of the concrete sample, the equilibrium equation gives a theoretical value of τ_0 which depends on E_c and C :

$$\tau_0 = \frac{C}{2\pi h(R_{int} + E_c)^2} \quad (21)$$

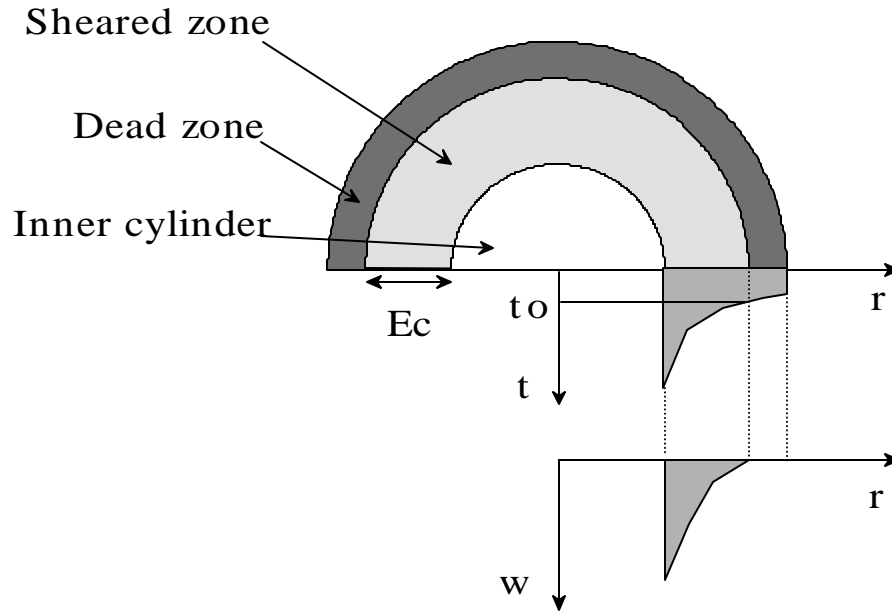


Figure 16: Diagram of plug flow phenomenon

For each rotation speed, the corresponding torque C was calculated according to the best fit curve (see Section 3.3.3). Then it was possible to calculate a set of theoretical values of the shear yield stress τ_0 for the given set of C values (i.e. the set of rotation speeds).

This analysis is particularly interesting because it does not need any assumption about the strain rate field between the concrete sample and the inner cylinder. On the contrary, to calculate both τ_0 and μ , it is necessary to assume that there is no slippage, which means that Ω is the rotation speed of the concrete near the surface of the inner cylinder. In this case, it is possible to analyze the best-fit torque-rotation speed curves according to Bingham models accounting for the plug flow phenomenon. This equation is known as the Reiner-Rivlin

equation. As the Bingham model gave a good fit to the experimental results, the Herschel-Bulkley model was not used in the analysis.

Analysis with Bingham model

Fresh concrete can be considered to be a Bingham fluid with the following equations:

$$\tau = \tau_0 + \mu \dot{\gamma} \quad (22)$$

$$\tau = \frac{C}{2\pi h r^2} \quad (23)$$

$$\dot{\gamma} = -r \frac{\partial \omega}{\partial r} \quad (24)$$

The critical radius R_c beyond which the concrete is not sheared (dead zone) is given by:

$$R_c = \max \left(R_{\text{int}} ; \min \left(R_{\text{ext}} ; \sqrt{\frac{C}{2\pi h \tau_0}} \right) \right) \quad (25)$$

If we make the assumption that there is no slippage between the inner cylinder and concrete, we have:

$$\Omega = - \int_{R_{\text{int}}}^{R_c} \frac{\partial \omega}{\partial r} dr \quad (26)$$

$$\Omega = \frac{1}{\mu} \int_{R_{\text{int}}}^{R_c} \left(\frac{C}{2\pi h r^2} - \tau_0 \right) \frac{1}{r} dr = \frac{C}{4\pi h \mu} \left(\frac{1}{R_{\text{int}}^2} - \frac{1}{R_c^2} \right) + \frac{\tau_0}{\mu} \ln \frac{R_{\text{int}}}{R_c} \quad (27)$$

Then for $C \geq 2\pi h R_{\text{int}}^2 \tau_0$:

$$\Omega = F(C) = \frac{\tau_0}{2\mu} \left[\ln(2\pi h \tau_0 R_{\text{int}}^2) - 1 \right] + \frac{C}{4\pi h \mu R_{\text{int}}^2} - \frac{\tau_0}{2\mu} \ln C \quad (28)$$

or else $\Omega=0$.

Fitting of the torque versus rotation speed curves

The curve of torque versus rotation speed data obtained for the seal is fitted with the following empirical function:

$$C_{\text{seal}}(\Omega) = C_{0,\text{seal}} + a \Omega \quad (29)$$

In the second step, the test performed with the rheometer full of concrete gives a set of points $(\Omega_i, C_{\text{all},i})$ where $C_{\text{all},i}$ is the total torque applied to the cylinder. The net torque C_i actually applied on the concrete sample is obtained with the following equation:

$$C_i = C_{\text{all},i} - (C_{0,\text{seal}} + a \Omega_i) \quad (30)$$

The set of experimental points (Ω_i, C_i) obtained is then fitted with the curve $\Omega = F(C)$ (see equation 25) as follows:

- for a given τ_0, μ and for each Ω_i , we calculate $C_{\text{th},i} = F^{-1}(\Omega_i)$. Unfortunately, the function F has the following form $F(x) = \Omega_0 + a x + b \ln x$, so F^{-1} can not be analytically written. A function was therefore created under MSExcel™ that calculates each $C_{\text{th},i}$ by solving $F(C_{\text{th},i}) - \Omega_i = 0$ with the Newton method.
- τ_0 and μ are adjusted with the MSExcel™ solver, in order to minimize the mean quadratic error:

$$\varepsilon = \sqrt{\frac{\sum_n (C - C_{\text{th},i})^2}{n}} \quad (31)$$

For the two curve-fittings, only the points from the decreasing part of the curve and for rotation speeds higher than 0.1 rad/s are used (see Figure 17 and Figure 18). The lower limit of 0.1 rad/s is chosen because the speed-meter was calibrated only for speeds higher than this value and because below this value, the inner cylinder rotates by jerks, which generates dynamic effects that disturb the torque measurements.

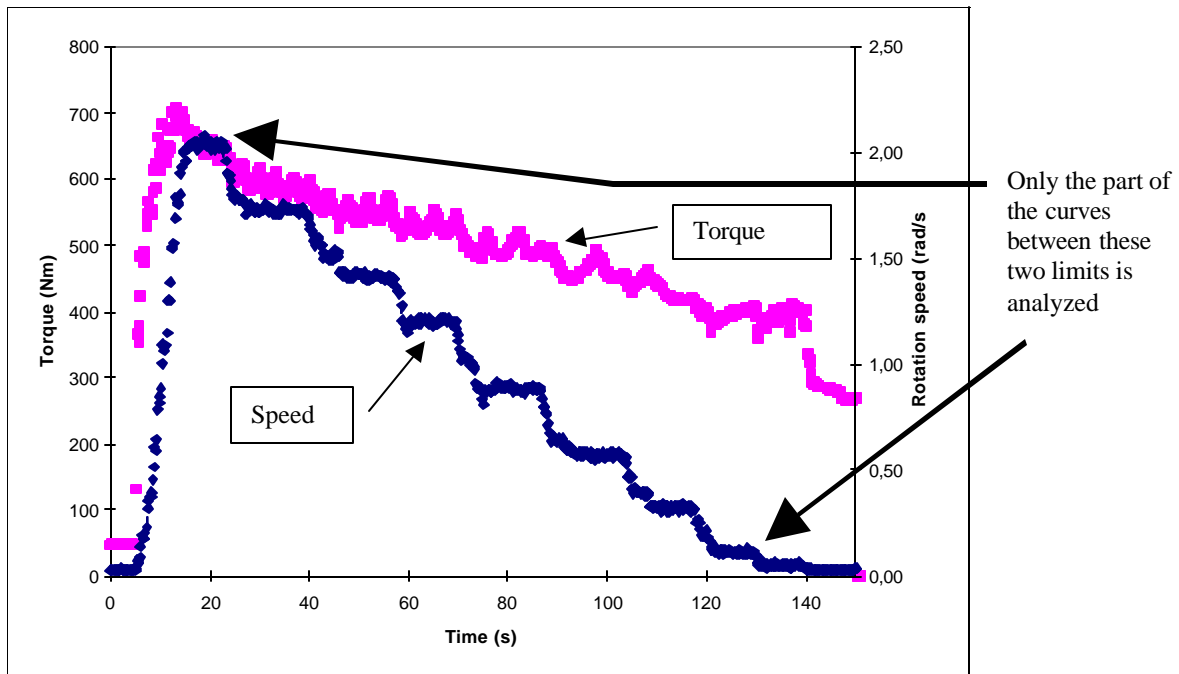


Figure 17: Typical curves versus time obtained during a test.

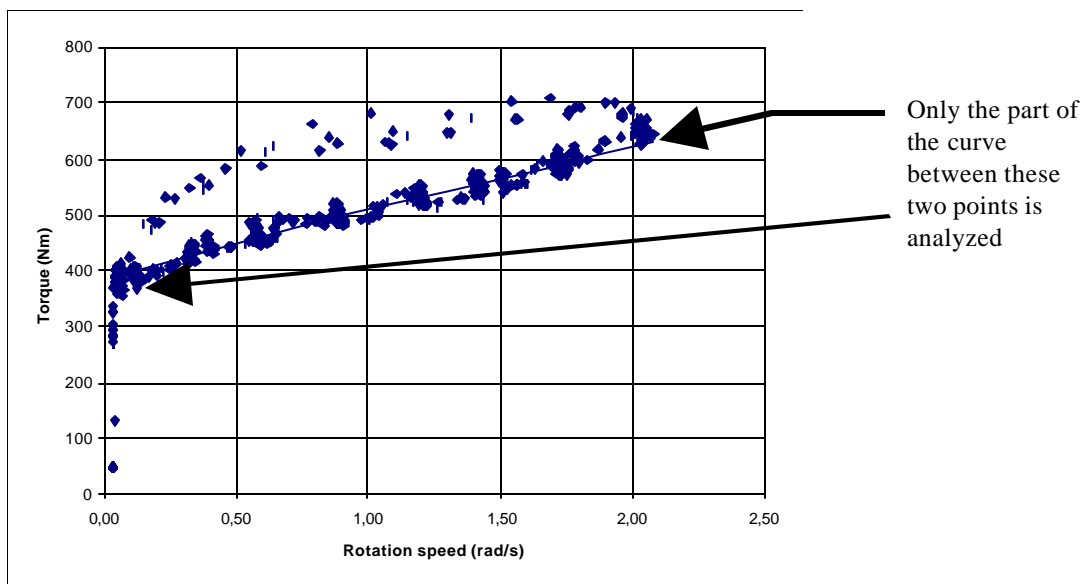


Figure 18: Torque-rotation speed curve for the same test as in Figure 17.

3.4. The IBB rheometer

3.4.1. Description of the apparatus

This apparatus is an instrumented and automated version of the existing apparatus (MKIII) developed by Tattersall [16]. It was modified in Canada by Beaupré [12] to study the behaviour of high-performance, wet-process shotcrete. The apparatus is fully automated and uses a data acquisition system to drive an impeller rotating in fresh concrete. The test parameters are easy to modify in order to produce any required test sequence. The analysis of the results is also automated and the rheological parameters, yield stress (in N·m) and plastic viscosity (in N·m·s), are displayed on the screen. The user may also retrieve an individual data set to plot the flow curves manually.

This apparatus can be used to test concrete with slumps ranging from 20 mm to 300 mm. It has been successfully used for self-compacting concrete, high-performance concrete, pumped concrete, dry and wet-process shotcrete, fiber reinforced concrete, and normal concrete. It has also been used on a few job sites as a means of quality control.

The general view of the apparatus is shown in Figure 19, while Figure 20 shows the detail of the bowl and impeller used for concrete and mortar respectively. The impeller shape and the planetary motion are as developed for the Tattersall MKIII (LM) apparatus. The concrete bowl leaves a 50 mm gap between the impeller and the bowl while the mortar bowl gives a 25 mm gap. The recommended maximum size aggregate is 25 mm for the concrete bowl and 12 mm for the mortar bowl. The sample size is 21 L for the concrete bowl and 7 L for the mortar bowl.



Figure 19: The IBB Rheometer

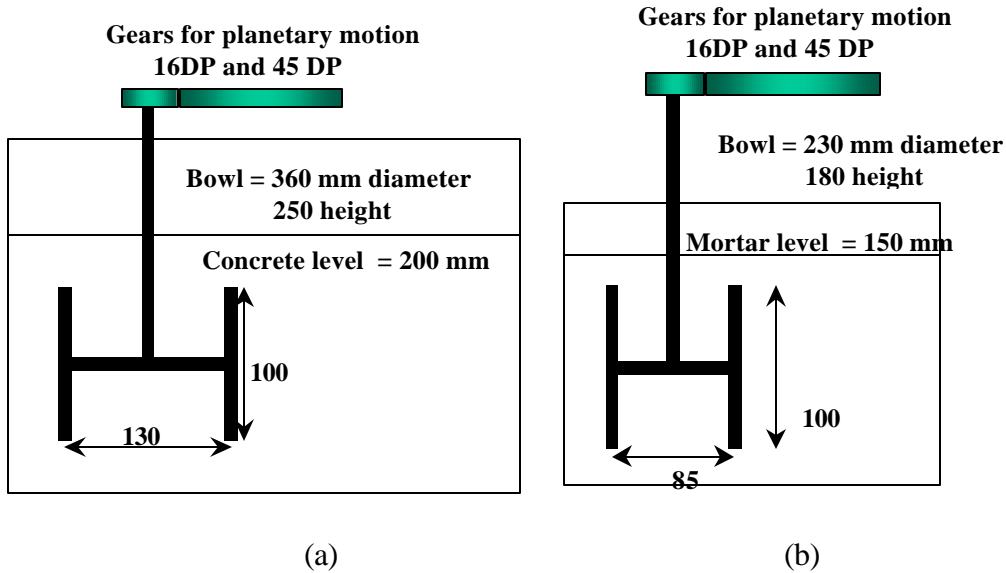


Figure 20: Details of the H-shaped impellers, bowls and planetary motion for IBB rheometer for concrete (a) and mortar (b) . Dimension in mm

3.4.2. Analysis of the data

The computer software, developed for use with the rheometer, calculates the following parameters from the torque/speed data: H , G , M , B and R^2 . Figure 21 indicates the meanings of these parameters. H and G could be related to plastic viscosity and yield stress respectively. R^2 is used to determine the significance of the calculations. A R^2 of 1 indicates that the data points lie on a straight line, while a value lower than 0.90 indicates that the data points are not on a straight line. The first point and the points for which the speed is 0 are not used in the calculations.

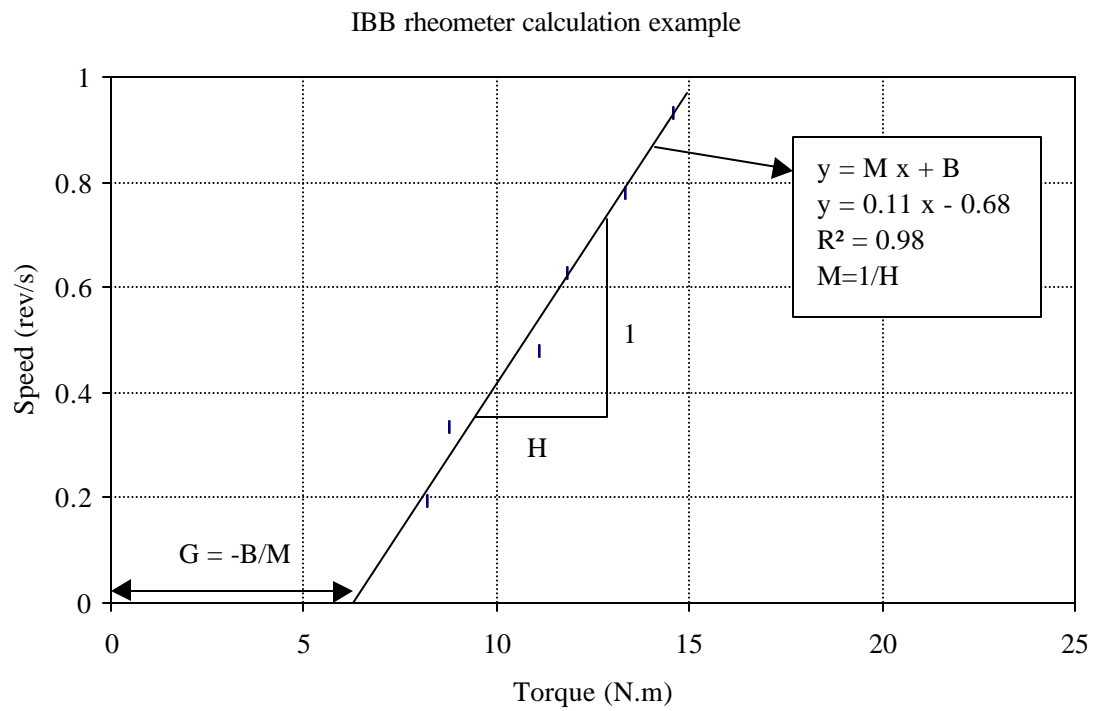


Figure 21: Example of calculation with indication of the meaning of the parameters. Y= speed; x = Torque

3.5. The Two-Point Rheometer

3.5.1. Description of the apparatus

The Two-Point workability test used in the program is an updated version of the apparatus first described by Tattersall and Bloomer [22]. The principles remain the same, with the option of two impeller systems - an axial impeller with four angled blades set in a helical pattern around a central shaft which imparts a stirring and mixing action to the concrete (the MH system), and an offset H-impeller with a planetary motion through the concrete (the LM system). The former, which is suitable for slumps in excess of about 100 mm, was used in the current program. Dimensions of the impeller and bowl are given in Figure 22.

The impeller is driven by a variable speed hydraulic drive unit motor through a gearbox; the overall arrangement is shown in Figure 23. Torque is measured indirectly through the oil pressure in the drive unit. The linear relationship between the oil pressure and torque was obtained by prior calibration with a plunger block, radius arm and spring balance system fully described elsewhere [16]. During testing, the oil pressure can be observed on a pressure gauge, or captured digitally on a computer via a pressure transducer fitted to a tapping in the drive unit casing. The impeller speed is similarly captured from a tachometer fitted to the drive shaft. The speed is controlled manually.

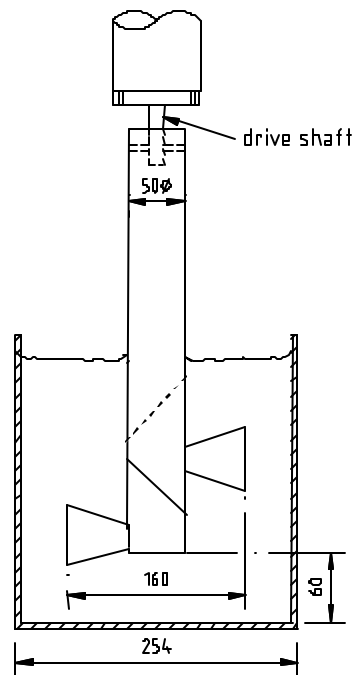


Figure 22: Impeller and bowl dimensions (in mm)

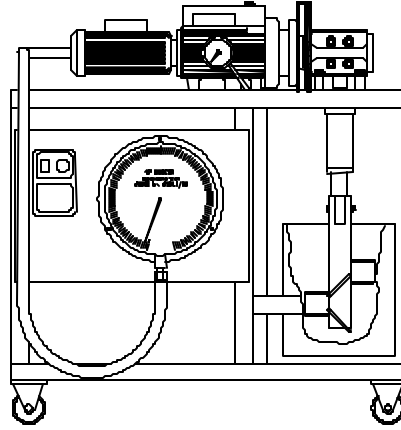


Figure 23: The overall arrangement of the Two-Point test apparatus

3.5.2. Test procedure

Previous studies [23] had shown that a suitable testing procedure was to obtain the torque/impeller speed relationship in a single downward sweep of the speed from 6.2 rad/s to 0.62 rad/s (1 rev/s to 0.1 rev/s) in about 30 s. A guide trace on the computer screen was used to ensure consistency between tests. The voltages corresponding to speed and pressure were recorded four times per second, giving approximately 120 data points per test. As well as testing with the impeller rotating in the concrete, it is necessary to record the oil pressure with the impeller rotating in air (called the idling test) over a similar speed range. The net pressure between the idling and concrete test then gives the torque needed to rotate the impeller in the concrete.

This relationship between torque and speed is of the familiar Bingham form:

$$T = g + hN \quad (32)$$

where g is the yield value term and h the plastic viscosity term.

Prior calibration was also carried out to determine the relationship between these two terms and the Bingham parameters of yield stress (τ_0) and plastic viscosity (μ) in fundamental units. The calibration theory is described in full in Chapter 7 of Tattersall and Banfill [16]. The principles can be summarized as follows.

It is assumed that in the apparatus there is an average effective shear rate given by

$$\dot{\gamma} = KN \quad (33)$$

where N is the impeller speed about its own axis and K is a constant. Knowing the value of K and another constant G permits g and h to be expressed in terms of τ_0 and μ using

$$\mathbf{t}_0 = K / Gg \quad (34)$$

$$\mathbf{m} = 1 / Gh \quad (35)$$

The value of G is determined by observing the linear relationship between T and N in the apparatus for a Newtonian liquid of known viscosity η . G is the constant of proportionality in:

$$T / N = Gh \quad (36)$$

The value of K is determined by comparing the power law relationship between T and N of the form

$$T = pN^q \quad (37)$$

obtained in the two point apparatus for a power law fluid with the flow curve determined separately in a rheometer as

$$\mathbf{t} = rg^a \quad (38)$$

(p , q , r and s are constants)

Provided that the range of shear rates are similar in the Two-Point apparatus and in the rheometer then

$$K = (p / rG)^{1/(s-1)} \quad (39)$$

The indices for the power law fluid, q and s , should be equal and Equation 33 assumes this. If they are not equal, it should be written as [23]

$$\dot{\mathbf{g}} = KN^{(q-1)/(s-1)} \quad (40)$$

The Newtonian fluid used was a silicone with a viscosity of about 28 Pa·s at 22 °C. The value of G was determined at three temperatures, 22 °C, 27 °C and 32 °C, with the average value being 0.0587 m³.

The power law fluid was an aqueous solution of carboxymethyl cellulose, at two concentrations, 2.5 % and 3 % by mass fraction. The average value of K was 7.1.

The test procedure was as follows:

- The machine was run with the impeller rotating for at least 0.5 h before testing to allow the oil in the drive unit to reach equilibrium temperature.
- An idling test was carried out

- The concrete was loaded into the bowl with the impeller rotating at about 1.2 rad/s (0.2 rps) until the impeller blades were completely immersed in concrete
- The speed was increased to 6.2 rad/s (1 rev/s), and the data recording was then started and continued whilst reducing the speed to zero over about 30 s.
- The impeller was disconnected and the idling test repeated.

3.5.3. Analysis of the data

The data in the form of voltages proportional to speed and torque was recorded directly into an Excel spreadsheet. After discarding the tail of data at either end of the test, the following procedure was used for the concrete test data to eliminate the falsely high pressure kicks that can arise from aggregate particles trapping and interlocking:

- A best fit relationship between pressure and speed was obtained by linear regression
- The standard deviation of the residuals between the measured and predicted values was calculated
- Data points more than twice this standard deviation from the predicted value are substituted by the predicted value and a second 'corrected' regression line obtained.

In practice, this increases the correlation coefficient of the regression line, but does not significantly alter the slope and intercept.

The slope and intercept were also obtained for each of the two idling tests and averaged. The two regression equations were then converted from voltages to oil pressure and impeller speed and the net pressure/speed relationship (Equation 32) obtained by subtraction.

This gave the yield value and plastic viscosity terms g and h , which were converted into yield stress and plastic viscosity in fundamental units using the values of G and K determined by calibration and Equations 34 and 35 above.

4. Results

4.1. Quality control measurements: Slump, modified slump, density

The concrete quality was checked immediately after mixing with the measurement of the slump according to the ASTM C143 standard. These results are reported in Table 8 as “slump at mixer”. If the slump was not on target, water or HRWRA were added to the mixer and the concrete remixed as described in Section 2.3. In some but not all cases, the concrete slump was re-measured at the mixer. At the same time the tests were conducted, using the various rheometers, a slump was measured using the standard method (ASTM C143) and a modified method [24]. This latter method also gives the rate of slumping by measuring the time for the concrete to slump by 100 mm. These times are reported along with the slump measured in Table 8. The final slump is also recorded. The relationship between the slumps measured by the two methods is shown in Figure 24. The correlation coefficient, R^2 , of 0.95 is considered satisfactory (see also the critical review of R^2 in Section 5.1.2).

The density of the fresh concrete was also measured using a volumetric method. The results are reported in Table 8. These results were used to calculate the exact concrete composition as reported in Section 2.2.

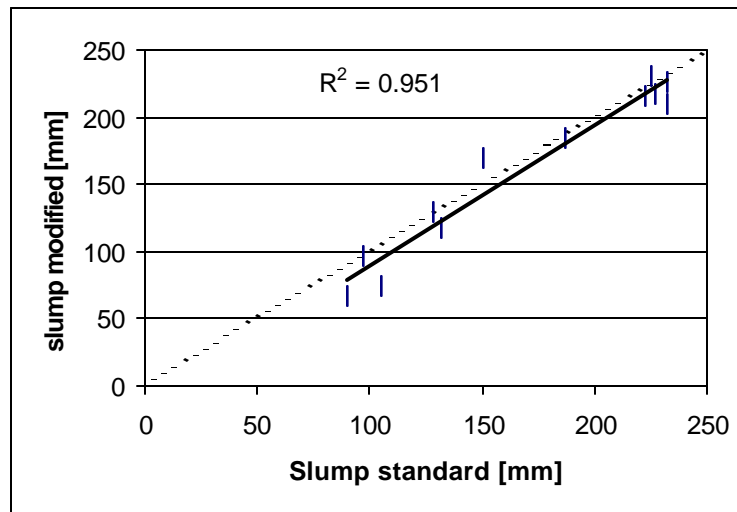


Figure 24: Comparison of the slumps measured by the standard method and the modified method. The dotted line represents the 45 ° line.

Table 8: Slump Measurements

Mixture #	Date/time ^g MM/DD/YY	Slump		Spread		Modified Slump		Density [kg/m ³]	Comments
		at mixer [mm]	in hall [mm]	Std. [mm]	Mod. [mm]	Slump [mm]	Time [s]		
1	10/24/00 10:19	110	97			97	NA	2407	
2	10/24/00 12:05	240	225	475	420	230	1.9	2361	
3	10/24/00 14:53	160 ^a	187			184	2.22	2372	
4	10/24/00 16:57	110	90			67	NA	2373	
5	10/25/00 9:56	120 ^b	105			74	NA	2409	
6	10/25/00 12:11		227	338 ^e	351	217	2	2427	
7 7 repeat	10/25/00 15:14		232	467 ^f	391 398	210 237	NA 1.26	2399	Spread at 15:26 was 479 mm
8	10/25/00 18:03 ^d	160	128			130	1.6	2356	
9	10/26/00 9:54 ^d	220 ^c	232	400	360	226	2.76	2318	
10 10 repeat	10/26/00 11:40	225	222			216 225	NA 1.45	2344	
11	10/26/00 15:10 ^d	185	132			117	2.17	2275	
12	10/27/00 10:17	150 ^c	150			169	1.57	2349	

Notes:

- a) Water was added after this slump was measured
- b) 2nd measurement at 10:10 was 11.2 cm; 3rd measurement at 10:26 was 10.8 cm
- c) HRWRA added after this measurement
- d) Time estimated from recorded pictures
- e) Flow spread at mixer was 440 mm
- f) Flow spread at mixer was 610 mm
- g) all times use 24 h clock

NA = Non Available

4.2. Comparison between rheometers

For each rheometer, the yield stress and the plastic viscosity were calculated as described in Section 3. Detailed data and graphs can be found for each rheometer in Appendix C. Table 9 shows the data obtained. It should be noted that one of the rheometers, IBB, does not provide the results in fundamental units. Therefore, most graphs have double axes to ensure that the IBB data are correctly represented.

Table 9: Yield stress and viscosities calculated from the measurements

Mix- ture #	BML		BTRHEOM		CEMAGREF- IMG*		IBB		Two-Point	
	Yield stress	Plastic Viscosity	Yield stress	Plastic Viscosity	Yield stress	Plastic Viscosity	Yield stress	Plastic Viscosity	Yield stress	Plastic Viscosity
	Pa	Pa·s	Pa	Pa·s	Pa	Pa·s	N·m	N·m·s	Pa	Pa·s
1	738	114	1619	181	1832		10.84	14.72	919	61
2	76	17.4	406	18	437	3	0.34	5.34	80	13
3	408	82.4	771	136			3.67	13.20	314	83
4	840	72	2139	51	2138		7.44	11.65	1059	
5	910	108	1753	94			3.91	14.61	698	19
6	139	45	505	78	487	63	1.80	10.31	145	41
7	90	32.7	549	54	410	43	0.86	9.31	98	38
8	717	29	1662	67	1417		5.71	8.84	689	22
9	125	15	624	25	504	3	0.95	6.06	159	19
10	248	35.9	740	50	535	43	1.98	8.88	253	19
11	442	29	1189	27	1034	21	3.97	6.57	516	16
12	584	39	1503	38	929	47	6.23	9.07	525	22

Note: * See Appendix C, Section 5.3.3 for the explanation for the empty cells

In this chapter we will present some comparisons between the data. A more detailed discussion of the data is found in Section 5. The data will be shown in various ways to:

- Determine the relationship between the rheometer measurements and the slump or modified slump measurements
- Examine the relative responses of the rheometers for each mixture.
- Establish the correlation functions and coefficients between any pair of rheometers

Figures and tables will be presented with comments to illustrate each of these points.

4.2.1. Comparison with the slump and modified slump test

As the use of these rheometers is not wide spread at this time, it was interesting to determine the correlations between values obtained with the rheometers and the more commonly used slump test. In this series of tests, two versions of the slump test were performed: the standard slump test as described in ASTM C143 and the modified slump test developed by Ferraris and de Larrard [24]. The slump is expected to be correlated with the yield stress, [24, 25] while the modified slump test time and final slump value should be used to compare to the plastic viscosity.

Figure 25 and Figure 26 show the results obtained. It seems that the yield stress (Figure 25) is correlated with the slump for each rheometer, as expected. This point is further developed in Section 5.3. On the other hand, the plastic viscosity measured by the rheometers (Figure 26) is not correlated with the plastic viscosity calculated from the modified slump tests results. This is probably due to the fact that the coefficients used to calculate the plastic viscosity from the slumping time were fitted from a set of data points using only round aggregates. Also, the coefficients were calculated from a set of data [26] with a range of plastic viscosities from 20 Pa·s to 1000 Pa·s while here the range is from 20 Pa·s to 140 Pa·s. Therefore, the modified slump test was not able to distinguish between concretes within this narrower range of plastic viscosities. Other type of models could perhaps be applied to more successfully correlate the plastic viscosity measured with the rheometers and the results from the modified slump tests [27].

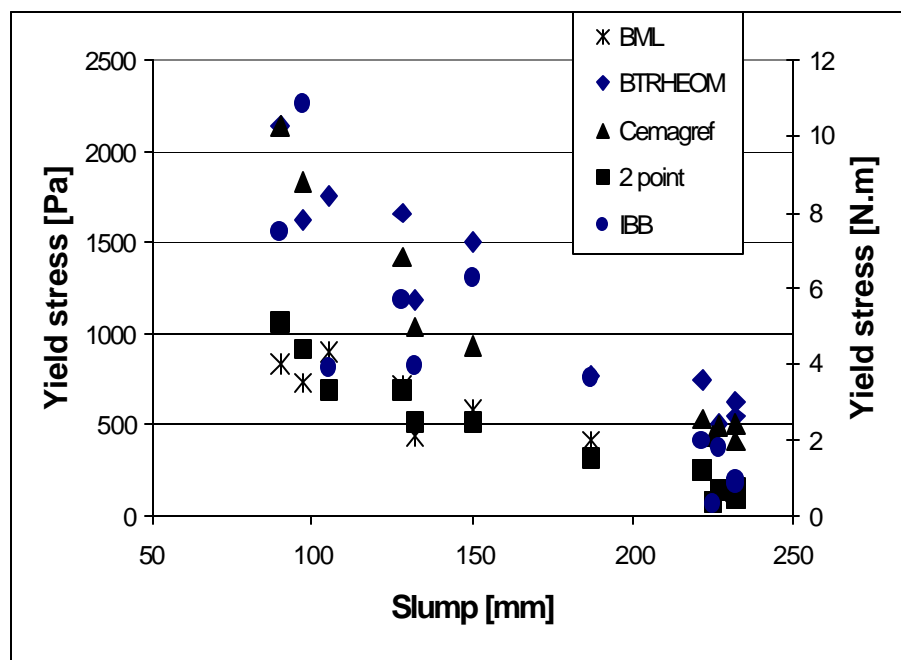


Figure 25: Comparison of standard slump and yield stress as measured with the five rheometers. The second axis in N·m gives the results obtained with the IBB.

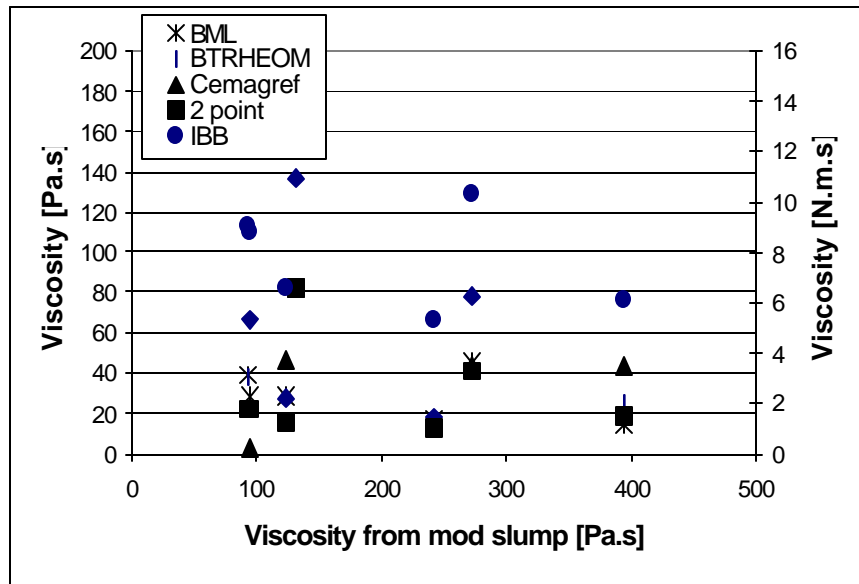


Figure 26: Comparison of plastic viscosity calculated from the modified slump test and plastic viscosity as measured with the five rheometers. The second axis in N.m.s gives the results obtained with the IBB.

4.2.2. Variation of the values by concrete composition

The concrete mixtures used were designed to cover a wide range of rheological performance as stated in Section 2.2. It might be expected that all the rheometers would rank the yield stresses in the same order, and similarly for the plastic viscosities. In other words, the values should be high or low for the same mixtures. There are two ways to represent the rankings:

- Plot the measured value versus the mixture number.
- Rank all the concretes according to each rheometer and see if the rankings are the same, using the Kendall's coefficient of concordance W [see Appendix E]

4.2.2.1. Analysis of variation of the yield stress and plastic viscosity by mixture

At first glance, Figure 27 and Figure 28 seem to show that the yield stress values are synchronized better between rheometers than are the plastic viscosity values. In Sections 4.2.3 to 4.2.5, it will be shown that a certain correlation between plastic viscosities measured with the various rheometers does, however, exist.

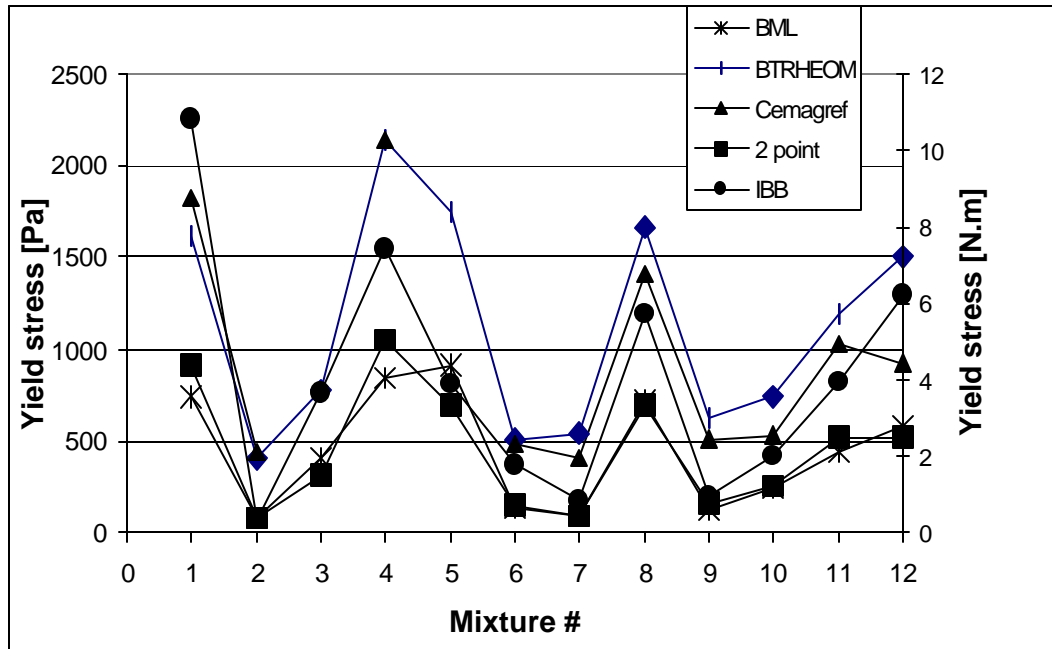


Figure 27: Comparison of the yield stresses as measured with the rheometers

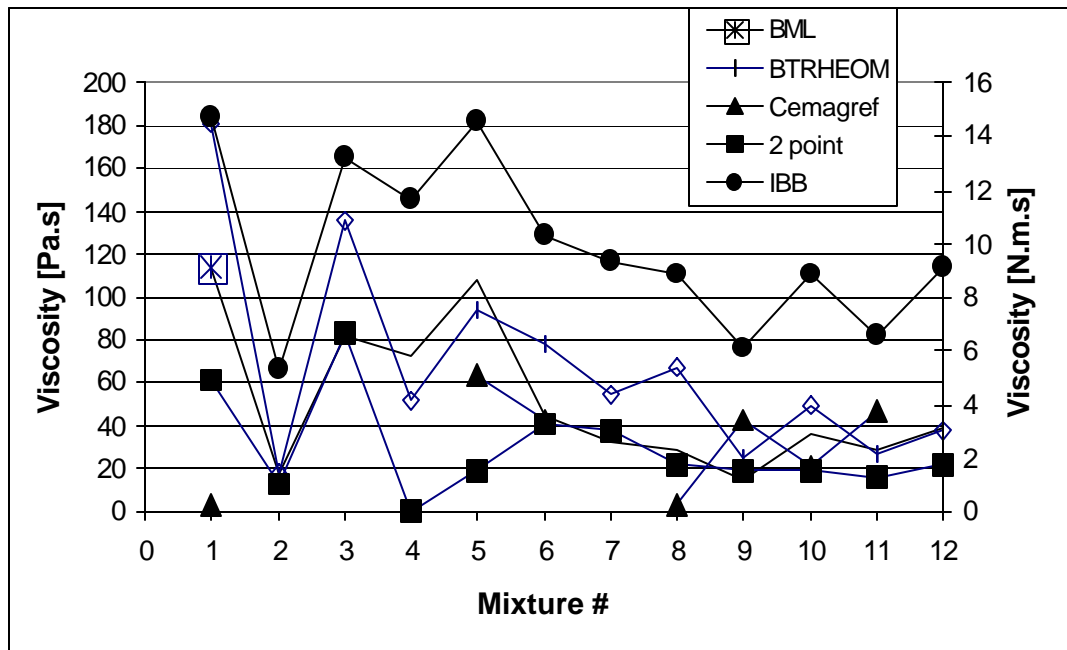


Figure 28: Comparison of the plastic viscosities as measured with the rheometers

4.2.3. Relative rank of the data by each rheometer

The graphs of yield stress and plastic viscosity versus mixture number (Figure 27 and Figure 28) show there is some similarity between the results of the different rheometers (especially for yield stress). The next step is to compare the classification of the concretes by apparatus: will the mixtures be ranked in the same order by yield stress and plastic viscosity?

This type of comparison can be quantified by Kendall's coefficient of concordance, W , [28] (see Appendix E). First, the ranking needs to be established for each concrete by each rheometer, both for yield stress (Table 10) and plastic viscosity (Table 11). This comparison is made only on the rank given by each apparatus, which enables one to include also the slump test (with yield stress) and the IBB (for both "equivalent" yield stress and plastic viscosity). Nevertheless, the same number of data points should be available for each rheometer. This precludes the CEMAGREF-IMG from the comparison². When the measurements obtained with two different mixtures are identical, the rank assigned to both of them is the average between the two ranks. For instance, with the BML, mixtures #8 and #11, both give a plastic viscosity value of 29 Pa·s. The rank would be 8 and 9 for these mixtures for the plastic viscosity. The rank assigned will be 8.5 for both mixtures. The same procedure is applied for the Two-Point tests for mixtures #8 and #12, and mixtures #5, #9 and #10.

From the tables, it is clear that there is some correlation between the various devices for both yield stress and plastic viscosity. We have already seen (Figure 27) a strong correlation between the yield stress ranking, but Table 11 shows a correlation also on the plastic viscosity measurements. For instance, Mixtures #2, #3, #8 and #10 show similar rankings for yield stress (Table 10). Mixtures #1, #10 and #11 show similar ranking for the plastic viscosity (Table 11).

Calculations of the Kendall's coefficient of concordance, W (Appendix E), show it to be equal to 0.941 for the results in Table 10 and 0.910 for the results in Table 11. These values of W need to be compared with a reference value taking into account the number of samples (12 in this case) and the number of devices (5 for yield stress and 4 for plastic viscosity). The reference values obtained from Ref. [28] are 0.336 for the yield stress and 0.415 for the plastic viscosity. This is a test of the independence of the classifications, i.e., the classifications are **not** independent (at the 95% confidence level) if the value of the W parameter is greater than the reference value. The test shows that the classifications by the various devices are not independent, and this implies that concretes would be classified in the same order by whatever instrument was used.

² To also compare the results of Cemagref, another comparison should be made on the mixes for which it has given a reliable result.

Table 10: Ranking of the yield stresses of the mixtures as determined by the rheometers and the slump. The mixtures are ranked in decreasing order of yield stress from 1 to 12. The higher the slump, the lower the yield stress.

Ranking according to	Mixture #	1	2	3	4	5	6	7	8	9	10	11	12
BML		3	12	7	2	1	9	11	4	10	8	6	5
BTRHEOM		4	12	7	1	2	11	10	3	9	8	6	5
IBB		1	12	7	2	6	9	11	4	10	8	5	3
Two-Point		2	12	7	1	3	10	11	4	9	8	6	5
slump		2	9	7	1	3	10	12	4	11	8	5	6

Table 11: Ranking of the plastic viscosity of the mixtures as determined by the rheometers. The mixtures are ranked in decreasing order of plastic viscosities from 1 to 12.

Ranking according to	Mixture #	1	2	3	4	5	6	7	8	9	10	11	12
BML		1	11	3	4	2	5	8	8.5	12	7	8.5	6
BTRHEOM		1	12	2	7	3	4	6	5	11	8	10	9
IBB		1	12	3	4	2	5	6	9	11	8	10	7
Two-Point		2	11	1	12	8	3	4	5.5	8	8	10	5.5

4.2.4. Graphical comparison of pairs of rheometer results

A graphical comparison of the Bingham parameters, yield stress and plastic viscosity, for each pair of rheometers should give a qualitative estimate of the correlation between the results obtained by the various rheometers. If any pair of rheometers gave identical values, the data points, plotted on a scatter graph with identical scales for both axes, should be on a 45 degree straight line, or a line of equality, passing through the origin. For each pair of rheometers, plots were made for yield stress and for plastic viscosity. In each plot, the equality line is shown together with linear regression (Section 4.2.5) and the 95% confidence range. Due to the fact that no mixture was repeated, the 95% confidence range is calculated based on a single value and a linear regression. Note that the line of equality was not plotted for the IBB rheometer because the units are not the same as for the other rheometers. Figure 29 to Figure 38 at the end of this section show all these plots. The regression line parameters are given in Section 4.2.5. As shown in Table 15 and Table 16, the correlation functions coefficients are not the same on both sides of the symmetry, therefore, we show two graphs for each pair of rheometers.

As discussed below, one of the plastic viscosities measured with the Two-Point test was probably an outlier. This is discussed in Section 3.5.3 and in Appendix C. Therefore, a

second set of pair graphs in Figure 39 and Figure 40, omit the value for plastic viscosity from Mixture #4 as measured by the Two-Point test.

These figures show, at a glance, how the results from different rheometers correlate with each other.

4.2.5. Correlation functions and coefficients between pairs of rheometers

One objective of this project was to determine the degree of correlation between the rheometers. Correlation relationships allow the user of any one rheometer to compare results with those obtained with any of the other rheometers. Two methods were selected to show the correlation between any two rheometers:

- Calculation of the correlation coefficient
- Fitting of a linear function to data from pair of rheometers.

These functions and correlation coefficients were calculated for yield stress and plastic viscosity separately.

The correlation coefficient R measures the degree of association between two variables. For two variables, x and y , R is calculated from [29]:

$$R = \frac{\sum (x_i - \bar{x})(y_i - \bar{y})}{\sqrt{\sum (x_i - \bar{x})^2 \sum (y_i - \bar{y})^2}} \quad (41)$$

The correlation coefficient R measures the degree of linear association between variables. It is possible for two variables to have a high degree of non-linear association and still have a low correlation coefficient. The value of R range between -1 and 1 . For negative values of R , y decreases as x increases. For yield stress and plastic viscosity the correlation coefficients R were calculated for each pair of rheometers. The calculated R values for each pair of results are shown in Table 12 and Table 13. Discussion of the significance of these results is given in Section 5.1.2.

During the testing and subsequent analysis, it was apparent that the properties of some of the mixtures approached the limits of suitability for some rheometers. A case in point is mixture # 4 when tested in the Two-Point test. This mixture had the lowest slump, and may not therefore have been efficiently mixed by the impeller. A plastic viscosity of near-zero was obtained, which should be treated with suspicion. There are, however, no rigorous reasons for excluding it from the statistical analysis, even though this has added to the degree of scatter. If this point is not considered in the calculation of the correlation coefficients for the plastic viscosity, the results in Table 14 are obtained. In this case, the correlation coefficients between the results from Two-Point tests and the other rheometers are higher.

Table 12: Correlation coefficients for yield stress

	BML	BTRHEOM	CEMAGREF-IMG	IBB	Two-Point	Slump
BML		0.97	0.95	0.81	0.94	-0.96
BTRHEOM			0.94	0.82	0.97	-0.95
CEMAGREF-IMG				0.90	0.99	-0.95
IBB					0.90	-0.86
Two-Point						-0.96
Slump						

Table 13: Correlation coefficients for plastic viscosity

	BML	BTRHEOM	CEMAGREF-IMG	IBB	Two-Point	Mod Slump
BML		0.84	0.98	0.96	0.45	-0.41
BTRHEOM			0.91	0.86	0.79	-0.29
CEMAGREF-IMG				0.98	0.75	-0.41
IBB					0.52	-0.40
Two-Point						-0.15
Mod Slump						

Table 14: Correlation coefficients for plastic viscosity if Mixture #4 for Two-Point test is not considered (see text for rationale).

	BML	BTRHEOM	CEMAGREF-IMG	IBB	Two-Point	Mod Slump*
BML		0.84	0.98	0.96	0.58	-0.41
BTRHEOM			0.91	0.86	0.82	-0.29
CEMAGREF-IMG				0.98	0.75	-0.41
IBB					0.65	-0.40
Two-Point						-0.15
Slump						

Note: * no changes from

Table 13 because no data is available for Mixture # 4 in the modified slump

A second objective was to determine the relationships between the Bingham constants measured by pairs of rheometers and results of the slump and modified slump test. Only 12 data points were available in each case (fewer from the CEMAGREF-IMG), and no mixture was repeated. Therefore, there was an insufficient number of results for fitting any other than a linear relationship. The computed regression coefficients are shown in Table 15 and Table 16. For example, in Table 15, the yield stress equation relating BML and BTRHEOM rheometers is:

$$\text{BML Yield stress} = 0.50 * (\text{BTRHEOM Yield stress}) - 122.0 \quad (42)$$

For those rheometers that determine the Bingham constants in fundamental units, the ideal case would be for the slope coefficient to be 1 or close to it, and the intercept coefficient to be zero or near zero, i.e., the different tests would give similar results. Clearly, this is not the situation in most cases. The significance of the results, the confidence with which they can be used, and the possible reasons for the differences, are discussed in the next section.

Table 15: Between-rheometer linear correlation functions for the yield stress. The rheometers in the column head are Y and those in the row head are X. In each cell the coefficients of the equation $Y=AX +B$ are shown. The rheometers are listed in alphabetical order.

A;B	BML [Pa]	BTRHEOM [Pa]	CEMAGREF -IMG [Pa]	IBB [N/m]	Two-Point [Pa]	Slump [mm]
BML [Pa]		1.85; 300.9	1.98; 179.89	0.008;0.334	1.010; 7.007	-0.18; 248.2
BTRHEOM [Pa]	0.50; -122.0		0.974; -93.6	0.004; -0.91	0.54; -153.9	-0.09; 273.0
CEMAGREF- IMG [Pa]	0.45; -40.7	0.91; 204.7		0.0049;-0.824	0.56; -99.79	-0.09; 261.1
IBB [N/m]	79.7; 126.2	155.3; 504.3	163.4; 316.9		95.4; 75.4	-15.8; 231.6
Two-Point [Pa]	0.87; 46.3	1.72; 338.3	1.75; 194.6	0.008;0.114		-0.17; 244.9
Slump [mm]	-5.59; 1387.3	-10.77; 2942.2	-11.1; 2898.1	-0.063; 14.7	-5.99; 1466.8	

Table 16: Between-rheometer linear correlation functions for the plastic viscosity (all data available are used). The rheometers in the column head are Y and those in the row head are X. In each cell the coefficients of the equation $Y=AX +B$ are shown. The rheometers are listed in alphabetical order.

A;B	BML [Pa·s]	BTRHEOM [Pa·s]	CEMAGREF -IMG [Pa·s]	IBB [N/m·s]	Two-Point [Pa·s]	Mod Slump [Pa·s]
BML [Pa·s]		1.202; 6.20	2.06; -31.19	0.089; 5.3	0.37; 13.84	-0.08; 51.6
BTRHEOM [Pa·s]	0.59; 11.16		1.01; -9.91	0.056; 6.07	0.36; 7.20	-0.11; 75.24
CEMAGREF- IMG [Pa·s]	0.47; 15.7	0.81; 15.50		0.081; 5.36	0.35; 12.68	-0.039; 51.7
IBB [N/m·s]	10.37; -50.9	13.2; -62.60	11.9; -62.9		4.43; -10.97	-0.009; 10.5
Two-Point [Pa·s]	0.926; 20.06	1.87; 9.88	1.59; -6.19	0.0961; 6.64		-0.034; 36.8
Mod Slump [Pa·s]	-2.03; 263.1	-0.79; 233.3	-1.79; 269.9	-16.4; 331.1	-0.69; 210.9	

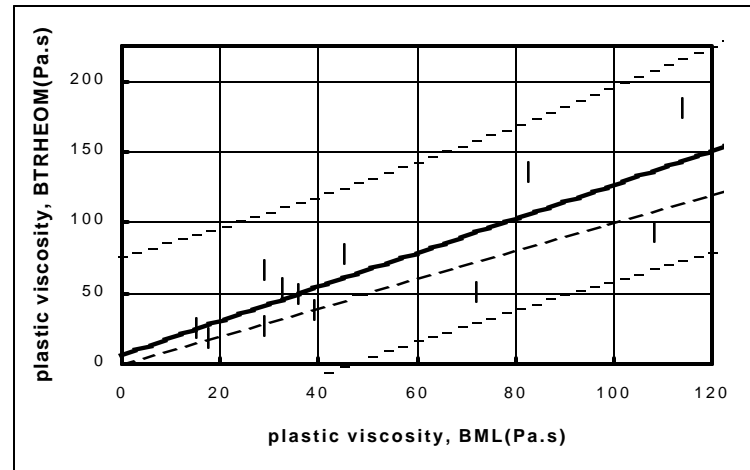
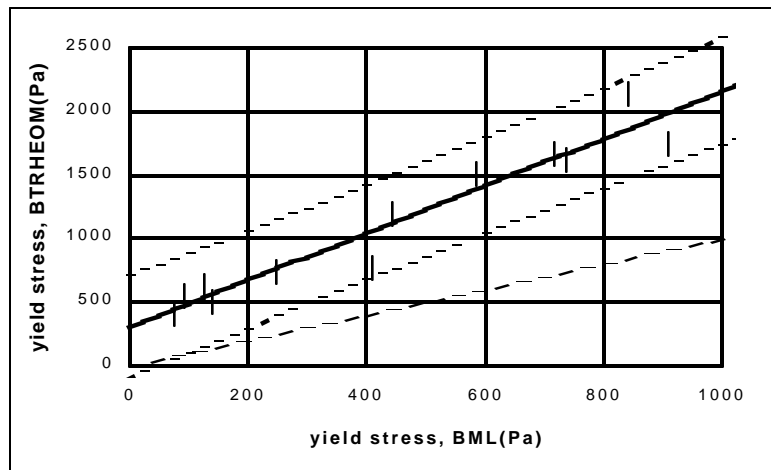
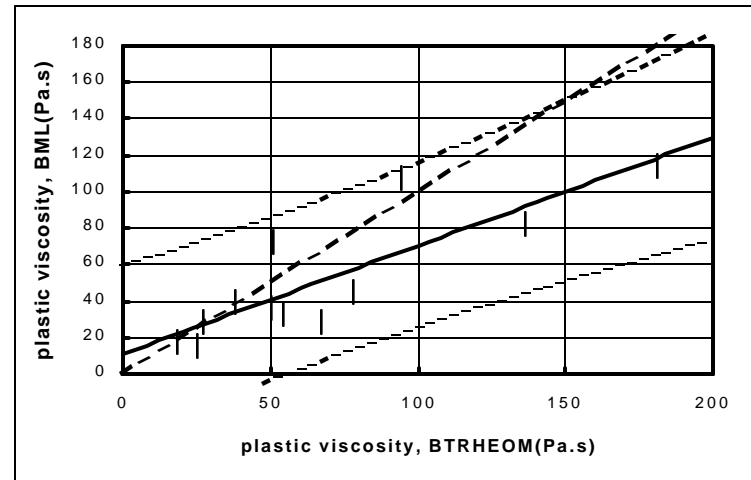
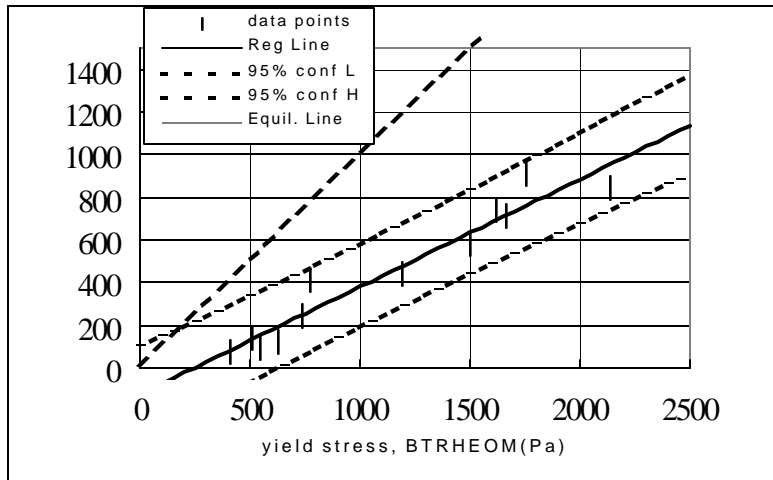


Figure 29: Comparison between BML and BTRHEOM

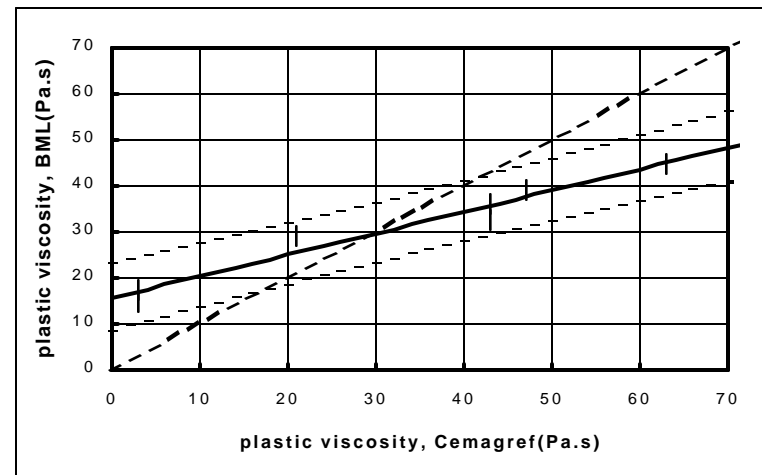
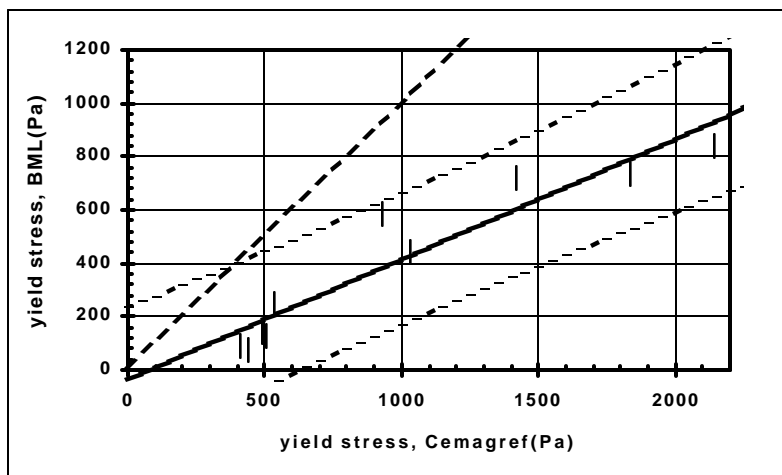
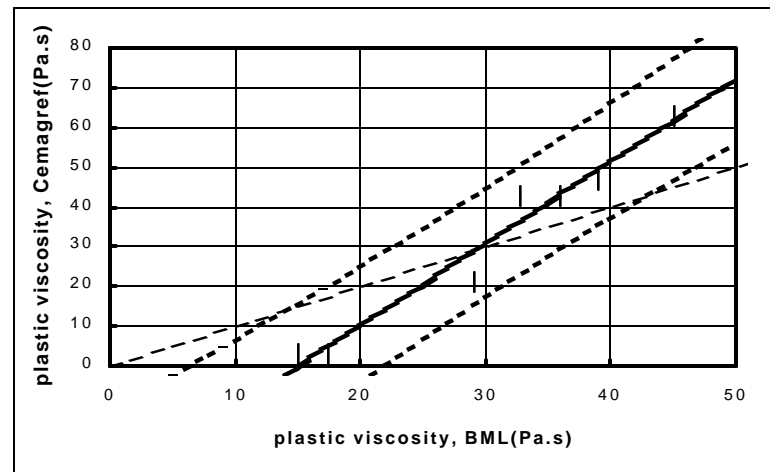
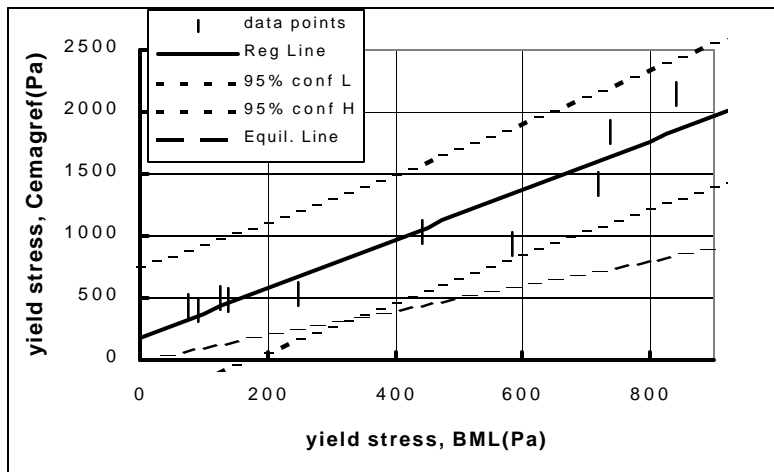


Figure 30: Comparison between BML and CEMAGREF-IMG

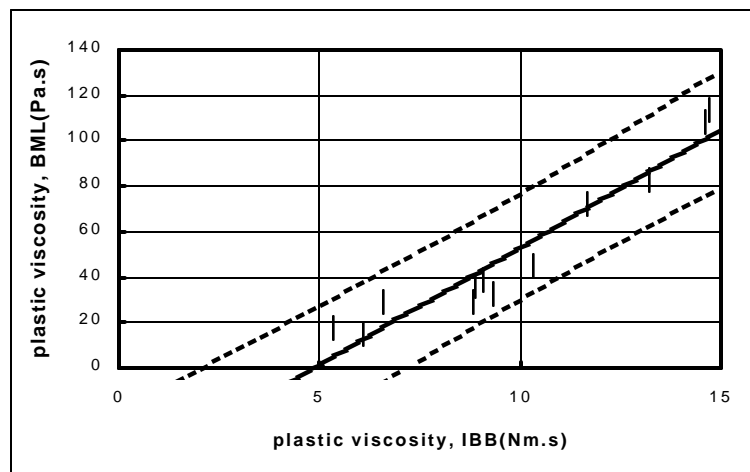
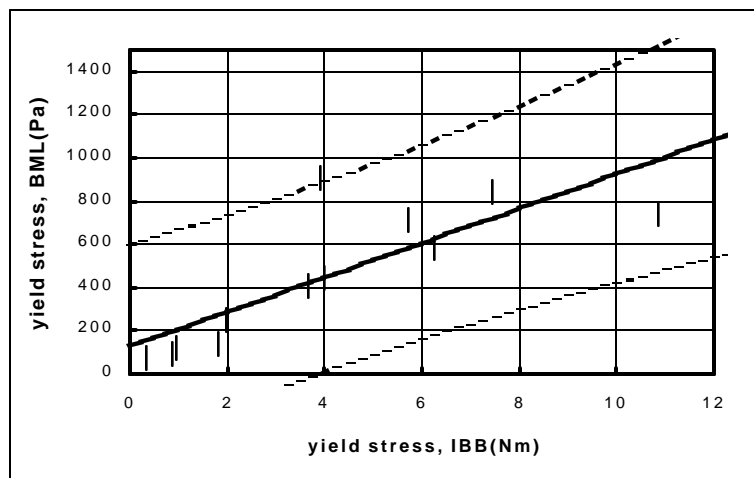
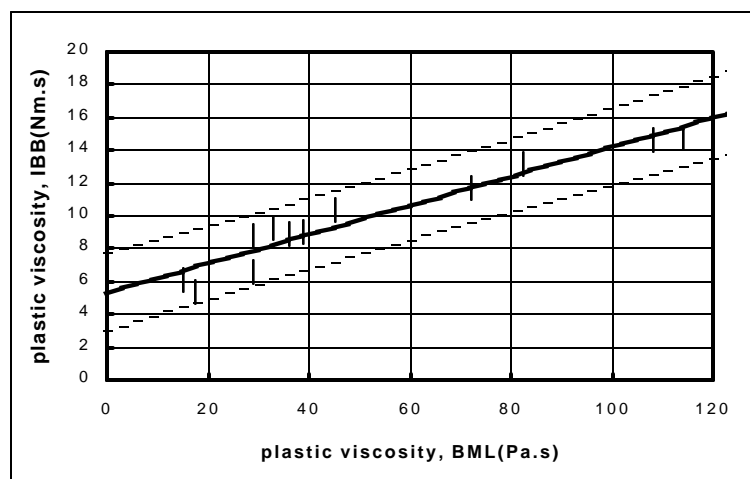
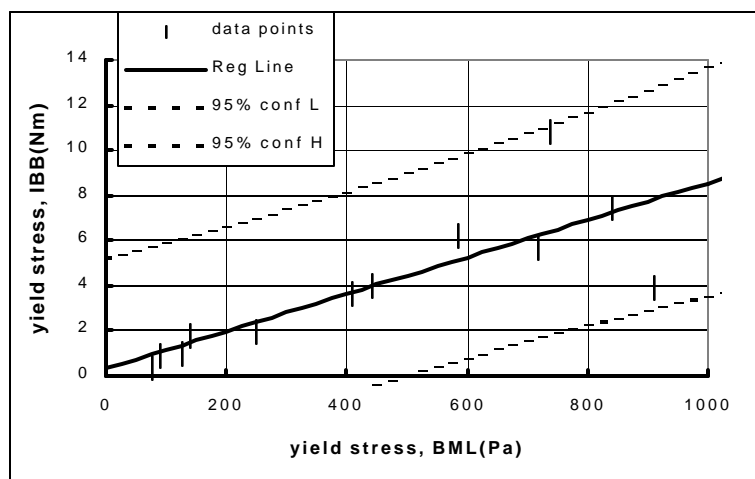


Figure 31: Comparison between BML and IBB

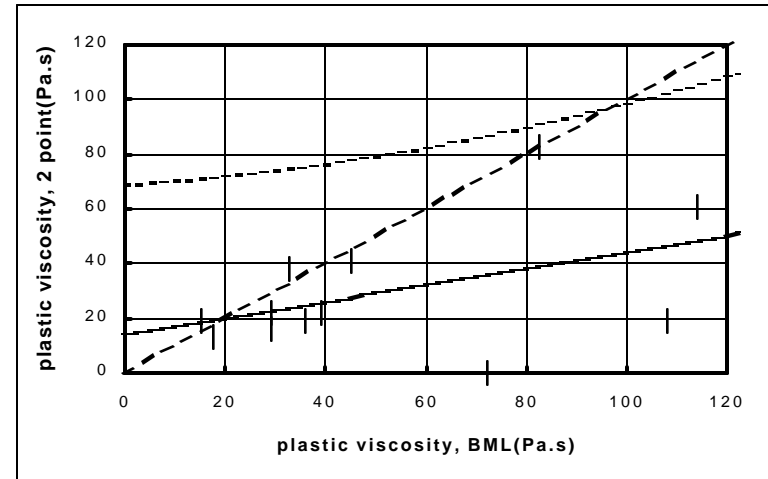
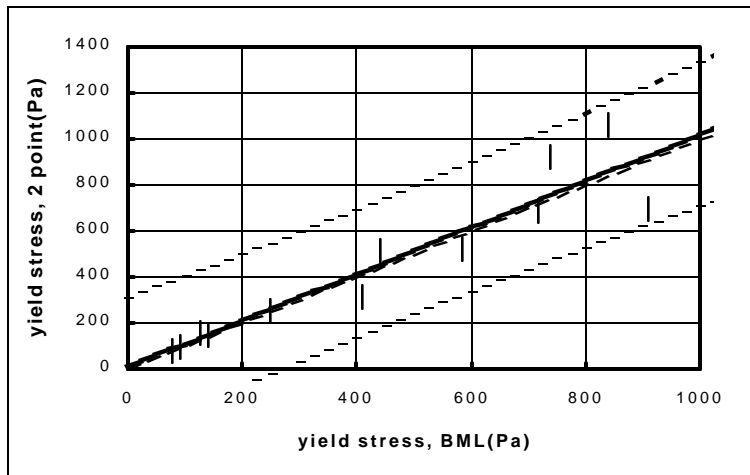
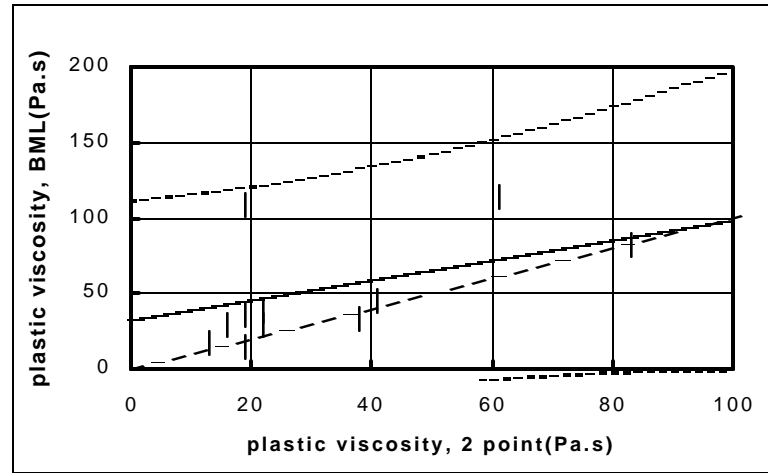
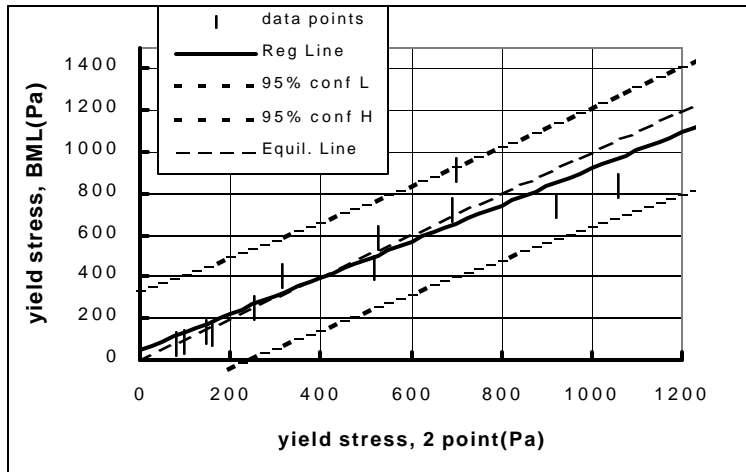


Figure 32: Comparison between BML and Two-Point test

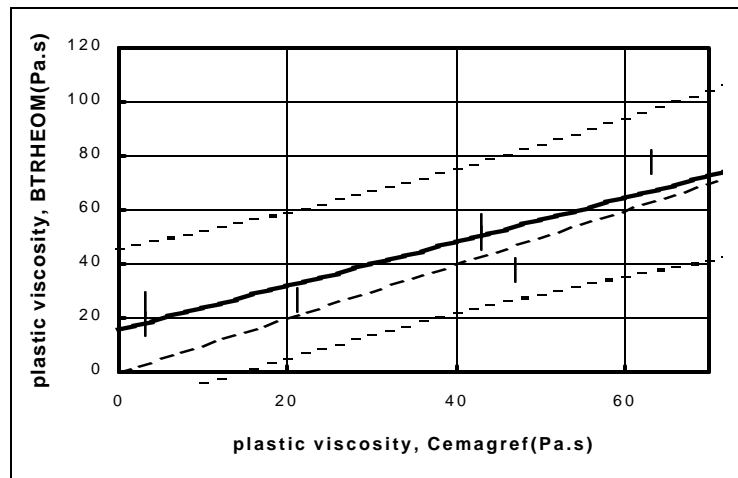
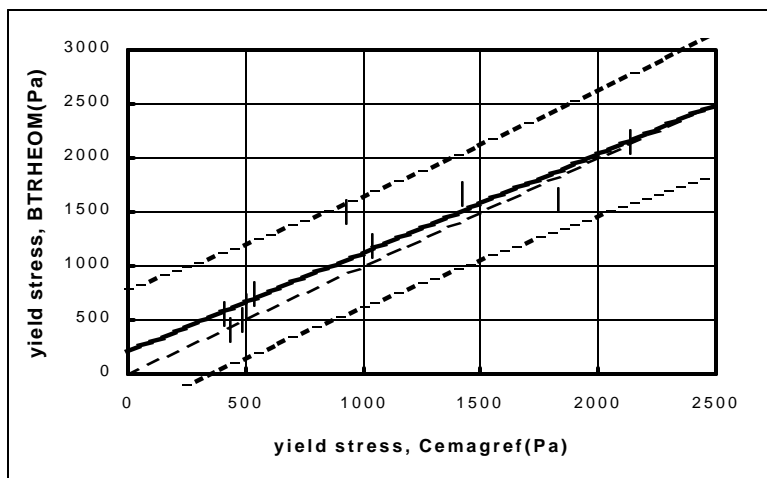
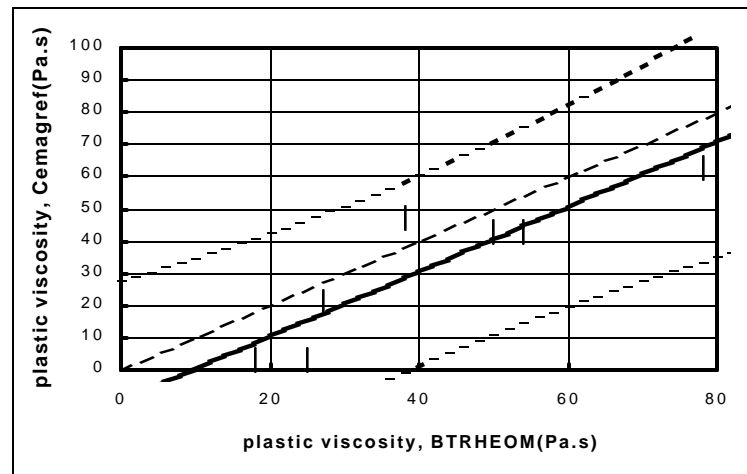
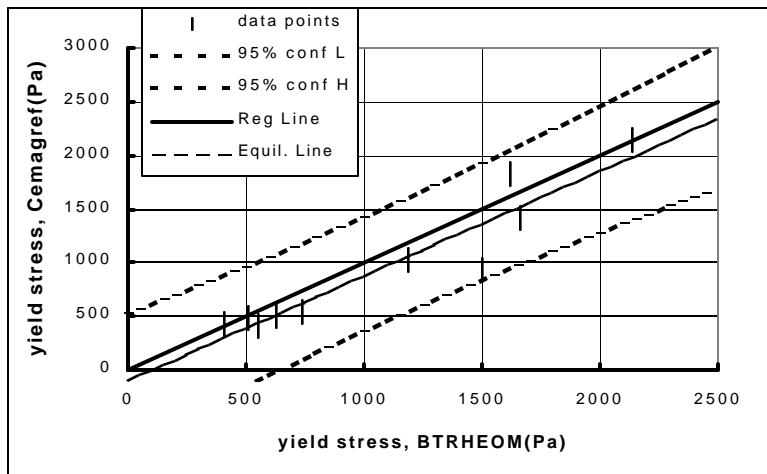


Figure 33: Comparison between BTRHEOM and CEMAGREF-IMG

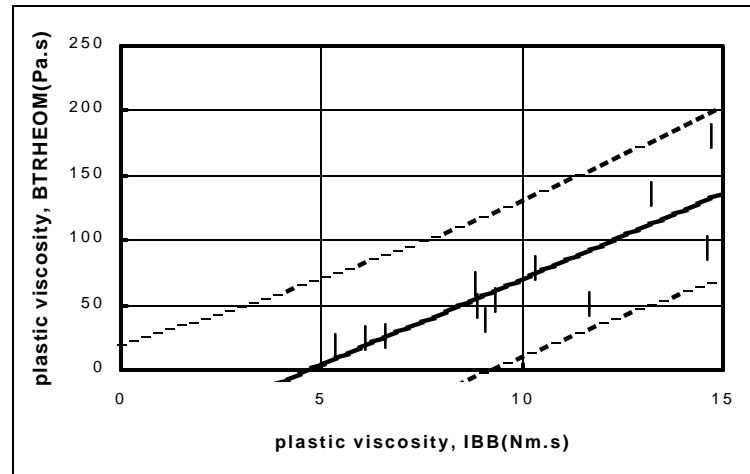
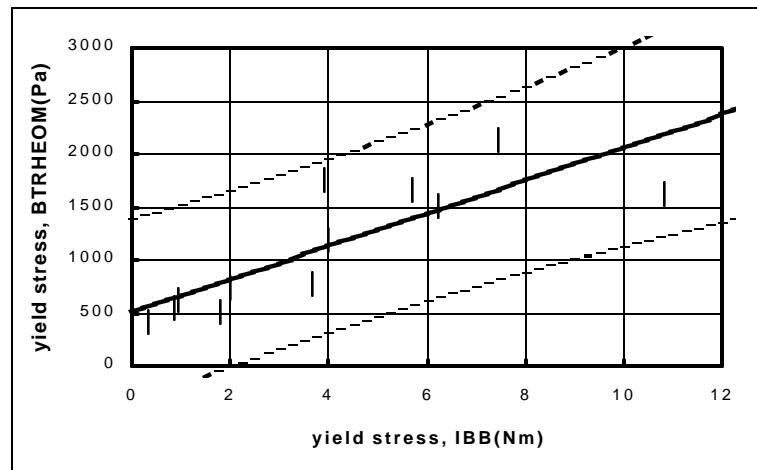
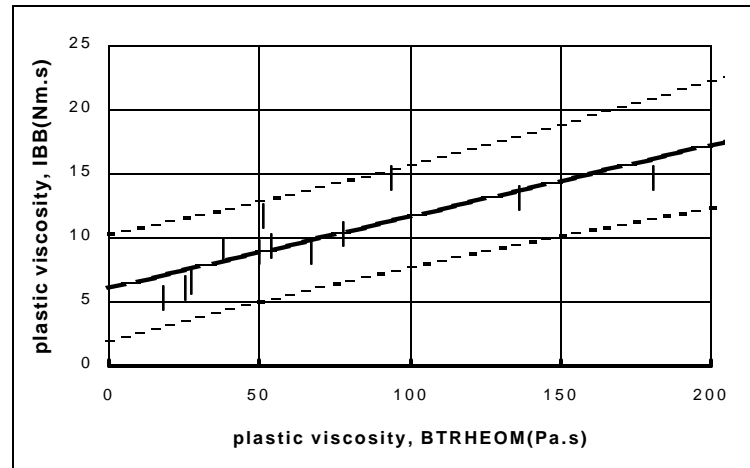
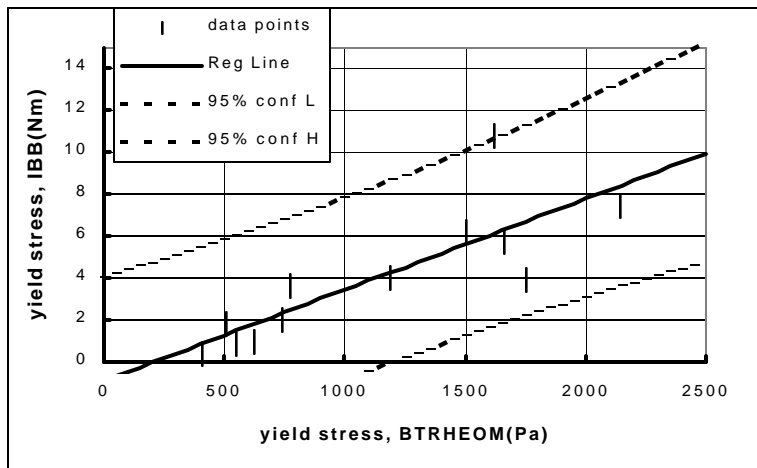


Figure 34: Comparison between BTHEOM and IBB

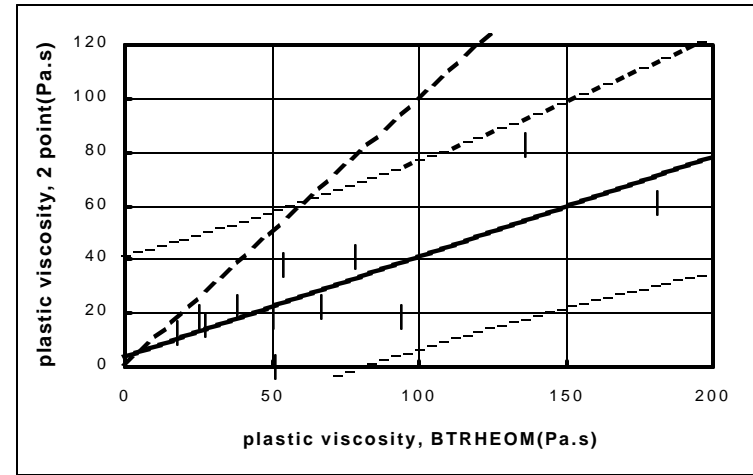
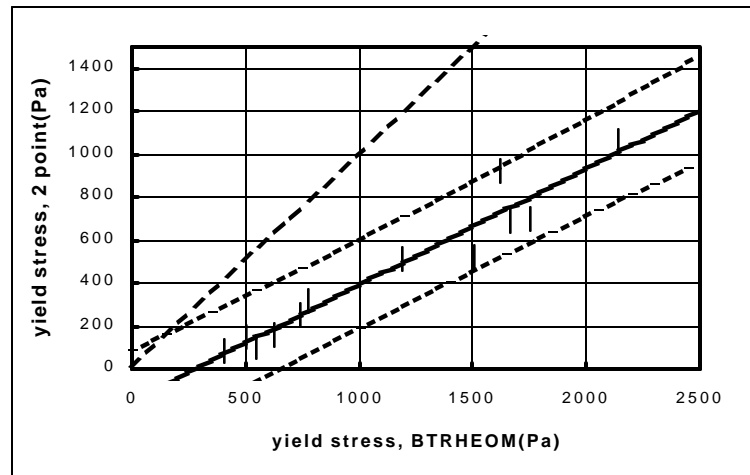
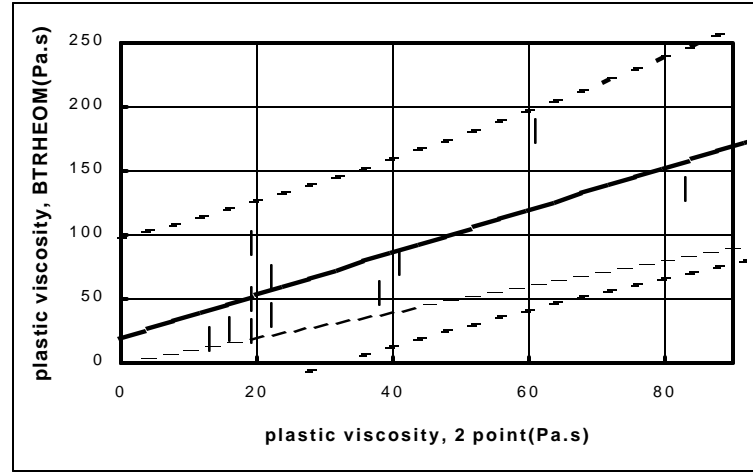
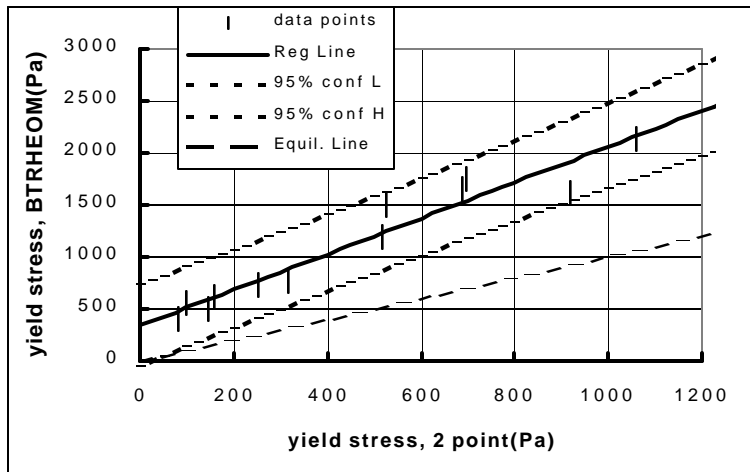


Figure 35: Comparison between BTRHEOM and Two-Point test

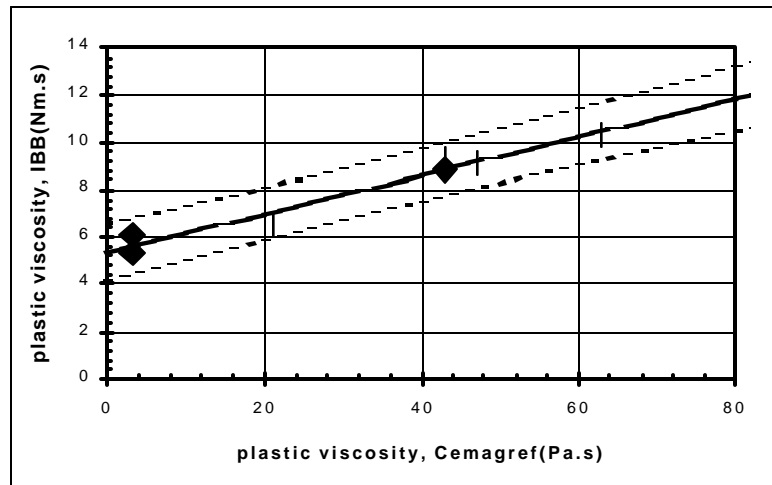
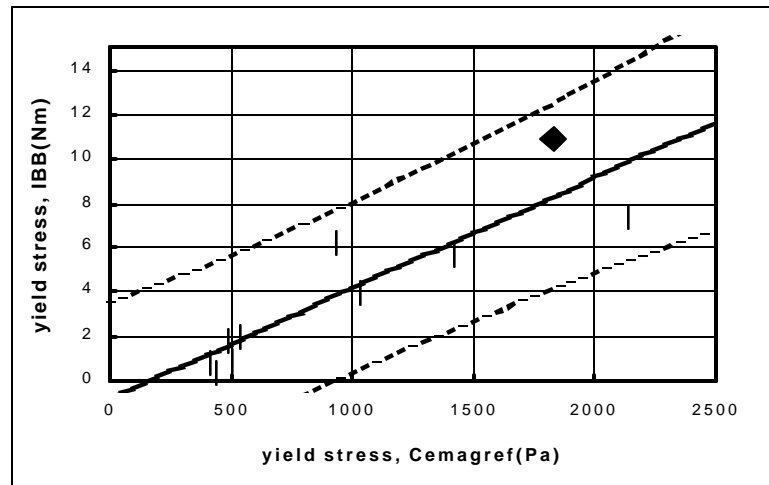
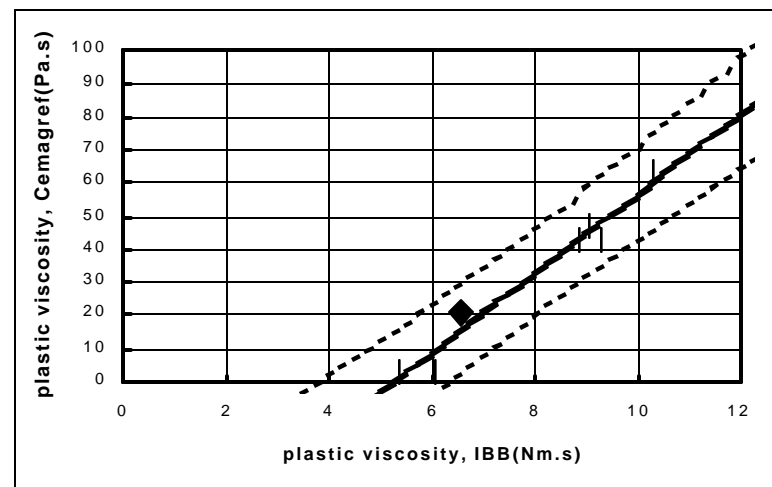
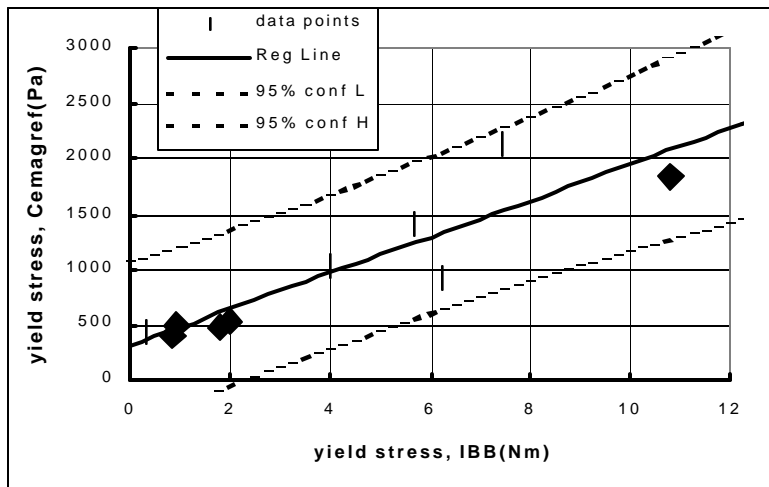


Figure 36: Comparison between IBB and CEMAGREF-IMG

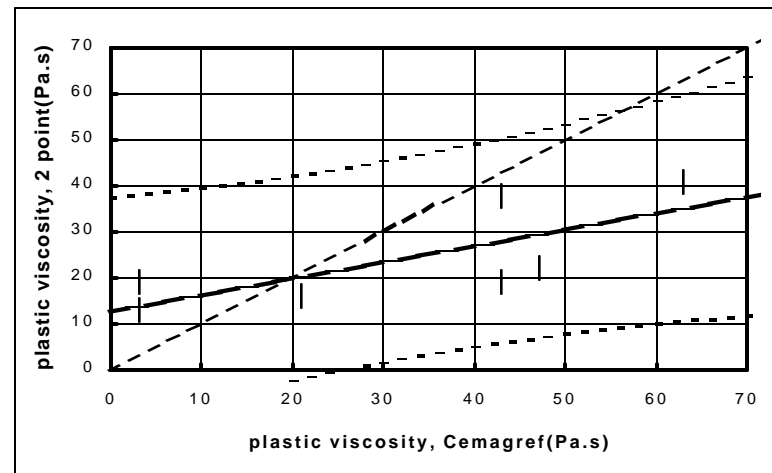
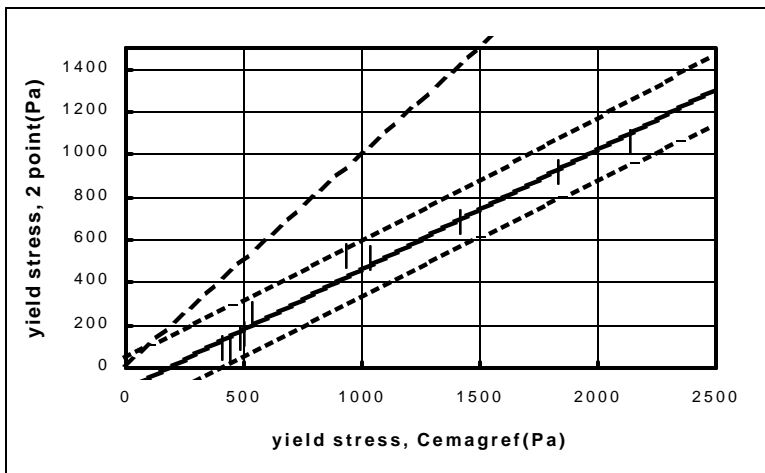
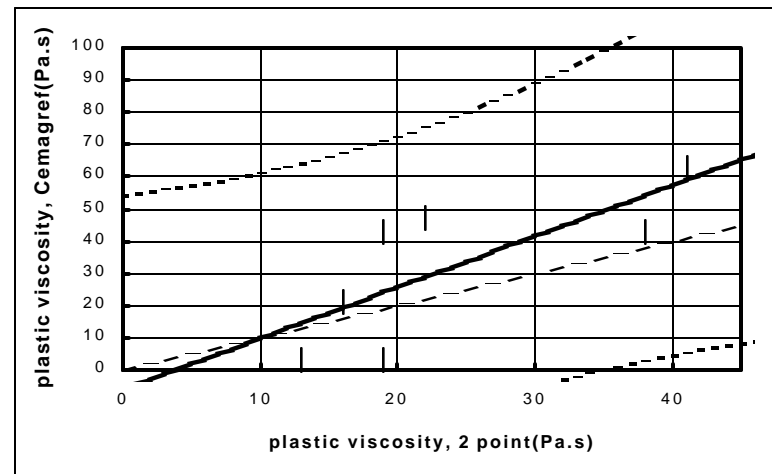
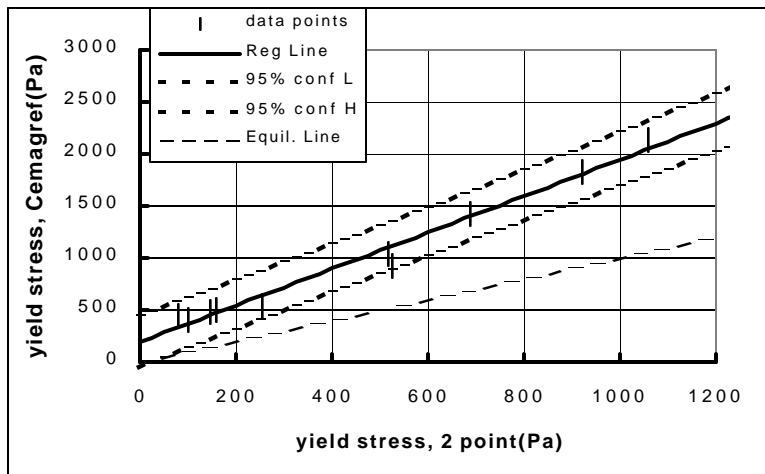


Figure 37: Comparison between CEMAGREF-IMG and Two-Point test

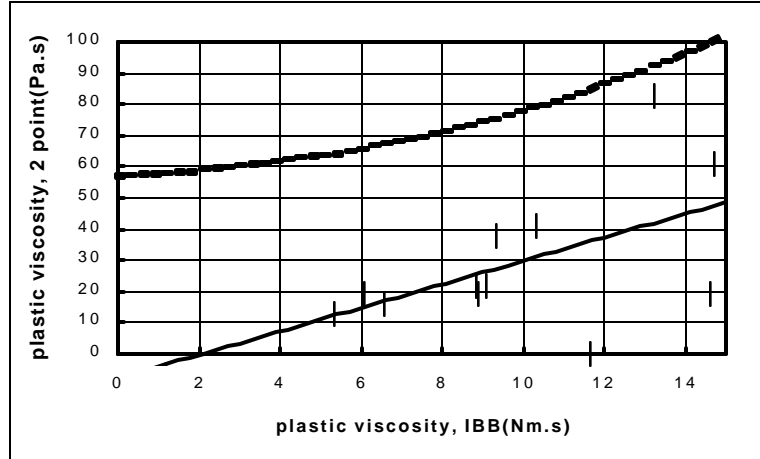
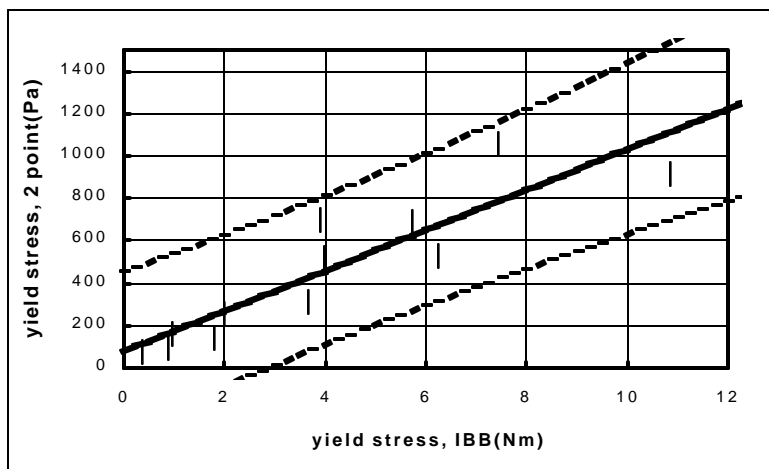
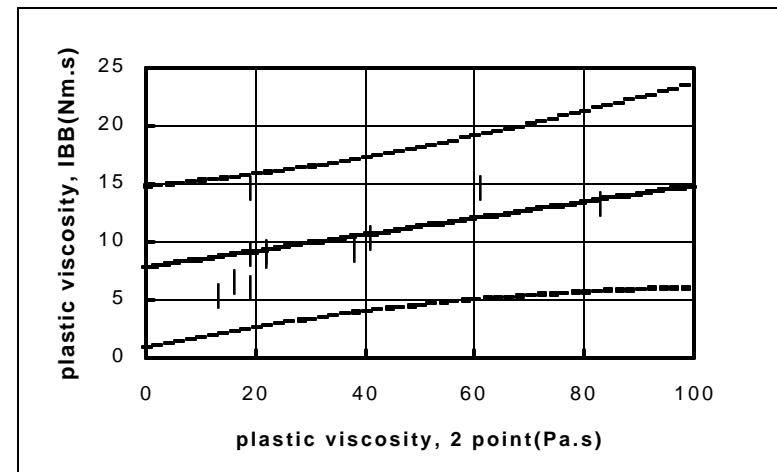
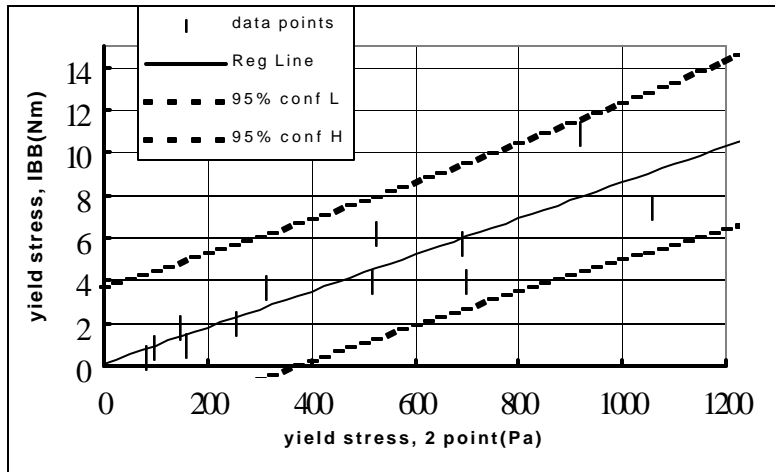


Figure 38: Comparison between IBB and Two-Point test

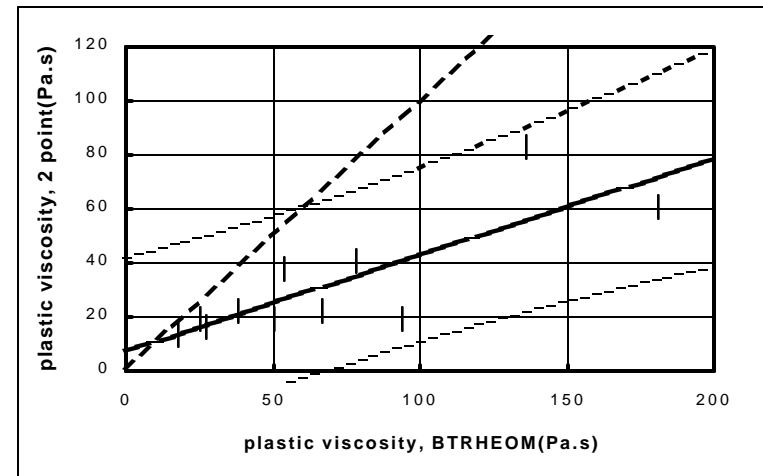
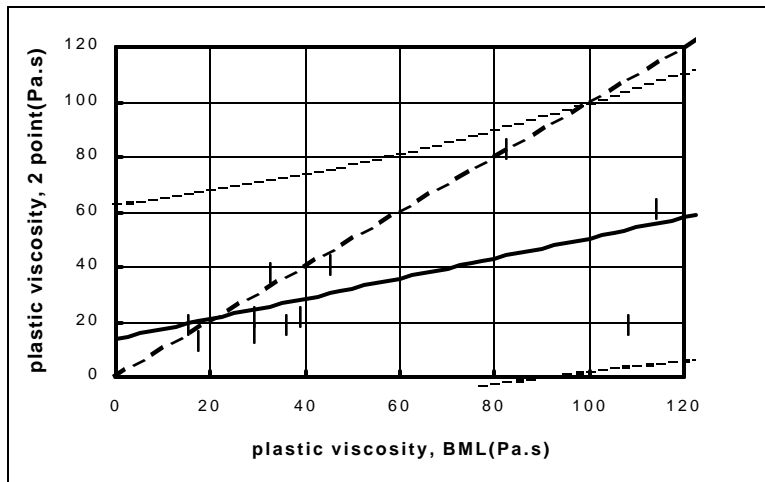
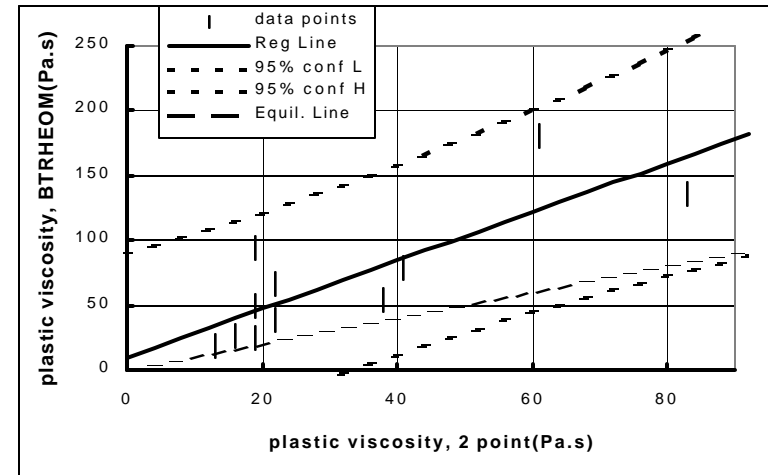
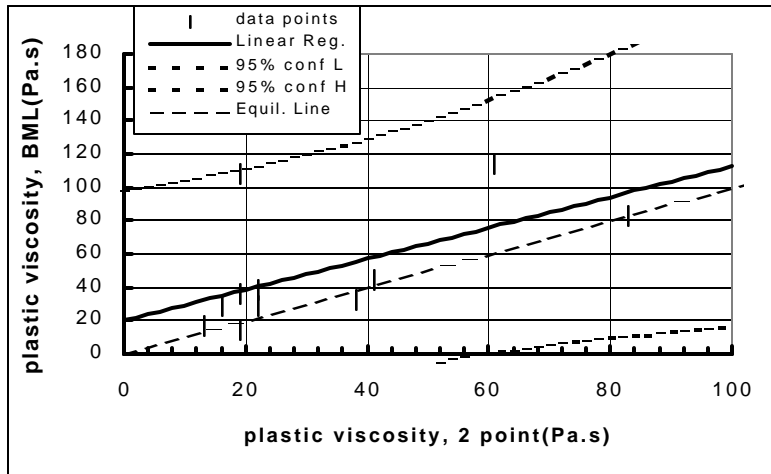


Figure 39: Comparison of plastic viscosities between BML, BTRHEOM and Two-Point test when the data points from Mixture #4 were omitted.

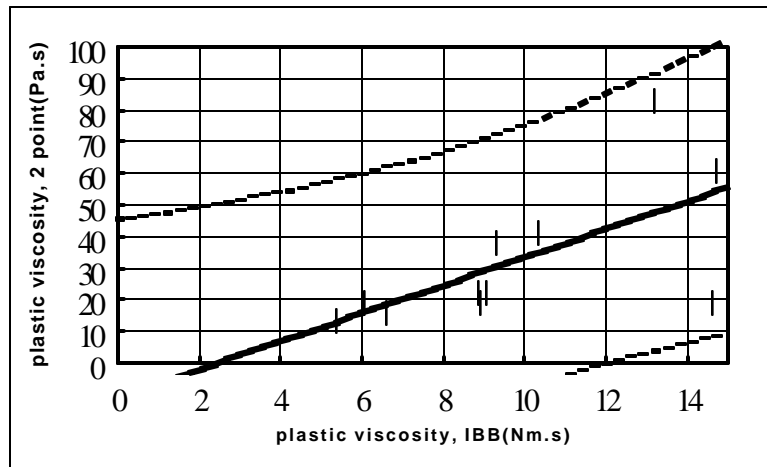
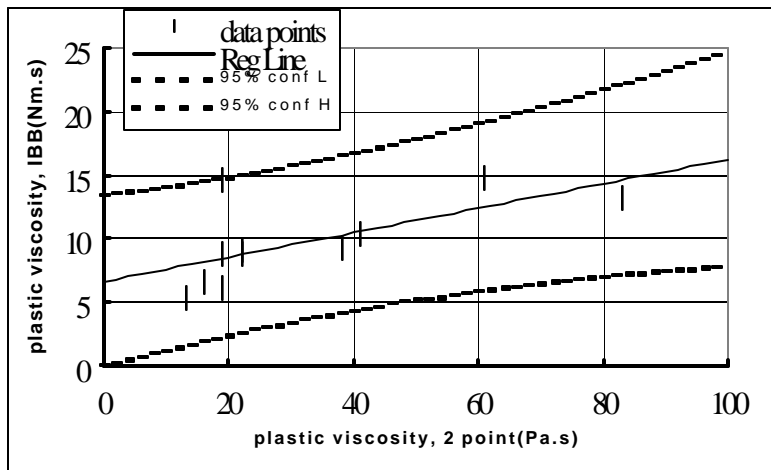


Figure 40: Comparison of plastic viscosities between IBB and Two-Point test. The data from Mixture #4 were omitted.

5. Discussion

5.1. Comments on correlations between pairs of rheometers

5.1.1. Linear regression or not?

It is clear from the results that there is some correlation between the values given by the different rheometers for both yield stress and plastic viscosity. The correct correlation function between any two instruments should be of the type $Y = X$ (yield stress according to one rheometer Y = yield stress according to another rheometer X ; similarly for plastic viscosity). The slope should be 1 and the line should go through the origin. This is obviously not the case for most pairs of rheometers (Table 15 and Table 16 or Figure 29 to Figure 40). Therefore, some effects are not fully taken into account in the calculation of the yield stress and plastic viscosity from the raw data from the rheometers. This leads to erroneous values for yield stress and plastic viscosity. Without knowledge of the source of the errors or the availability of a standard material or rheometer, it is impossible to determine the correct correlation between the rheometers.

As the results presented are not related by a function $Y=X$, the question is raised, could we approximate the relationship between rheometers to allow users to compare their results? For this, a linear relationship was selected, but the coefficients should be used with caution. The reason is that the small number of points available does not allow a clear selection of the correct function. Most of all, the R coefficient should be used with caution. It implies several hypotheses that were not tested during the tests, mainly that the distribution of the results follows a normal distribution for each apparatus. Moreover, the value against which R must be compared depends on the number of points considered, and this number is not the same for all the apparatus (between 7 and 12 data points).

5.1.2. Critical review of R

In Table 12 to Table 14, the value of R for the correlations are listed for each pair of rheometers. To be correctly interpreted, the value of R (or R^2) must be compared to a reference value that depends on the number of points used for the correlation. In our case, depending on the rheometers compared, this number ranges from 7 to 12.

For 12 points, at the 1 % level ($\alpha=0.01$, $\nu=10$), the reference value of R is 0.7079, i.e. $R^2=0.5011$ (see Table 17).

Table 17 Critical values for the correlation coefficient R of a sample extracted from a normal distributed population. α is the probability, and $n = n-2$, n being the number of points. If the calculated value of R is higher than the reference value shown in the table, there is a probability α that X and Y are dependent.

α	0.1	0.05	0.01
n			
5	0.6694	0.7545	0.8745
6	0.6215	0.7067	0.8343
7	0.5822	0.6664	0.7977
8	0.5494	0.6319	0.7646
9	0.5214	0.6021	0.7348
10	0.4973	0.5760	0.7079

Table 12 to Table 14 show that these levels are exceeded by all correlations except those involving the modified slump. There is no correlation between modified slump and plastic viscosity and this test will not be considered further. However, slump correlates well with yield stress, confirming the observation originally made by Tattersall and Banfill [16].

5.2. Discussion on discrepancies on absolute values

When attempting to compare the absolute values measured with the various rheometers, an immediate conclusion is that the instruments fall into two groups consisting of (a) the BTRHEOM and CEMAGREF-IMG, and (b) the Two-Point and BML. The agreement is excellent within group (a), acceptable within group (b), but less satisfactory between the two groups. In one sense this is encouraging because of the level of agreement between instruments whose principles of operation differ. The BTRHEOM is essentially a parallel plate rheometer, whereas the CEMAGREF-IMG is a coaxial cylinder rheometer. The Two-Point consists of a blade rotating in a concrete container whereas the BML has a coaxial cylinder rheometer. However, better agreement between the BML and the CEMAGREF-IMG, both coaxial cylinder instruments, would have been expected. Plastic viscosity agrees adequately but the difference in yield stress is large.

In a perfect world, all rheometers would give the same values for yield stress and for plastic viscosity for a given concrete. Although there is a high correlation between the rheometers, the absolute values are not identical. Discussions were conducted on this topic and some hypotheses were put forward, which need to be tested through further research. The hypotheses are:

- Each rheometer was calibrated using a different method. Some were calibrated using oil as a reference material, while others were calibrated through the load cell used to

measure the torque. Calculations to convert torque and rotational speed to plastic viscosity and yield stress in fundamental units rely on known equations for specific geometries. Most equations assume that the flow between the moving parts is linear. This assumption was not always verified in practice.

- The shearing surfaces are usually designed to avoid slippage. Nevertheless, it was not always possible to avoid slippage in the tests reported here. Slippage might explain some lower values as compared to a rheometer with no slippage. It is relevant that Mannheimer has pointed out that for cement pastes [30], slippage can have a significant effect on the measured yield stress. Further, the gap between parts of a rheometer must be high as compared to the maximum size of particles. If this condition is not fulfilled, *confinement* effects may occur. These issues are discussed in Appendix F.
- The CEMAGREF-IMG has a seal at the bottom to avoid concrete seeping under the moving cylinder. The seal friction is calibrated using an empty rheometer. A question that could be raised is whether the pressure on the seal exerted by the concrete might alter the seal friction. Calculations presented in Appendix G show that a very pessimistic assumption on the nature of the friction at the seal level only leads to an overestimation of the yield stress by 40 Pa to 50 Pa. This is far from the difference shown between the CEMAGREF-IMG and the other instruments.
- The other instrument that has a seal is the BTRHEOM. This instrument is calibrated using water before loading the instrument with concrete. Extensive investigations [11] were conducted to evaluate the difference between the seal friction in the presence of concrete (where cement grout fills the gap between seal and container) from that in the presence of water. Further, owing to the dimensions of this apparatus, concrete pressure is not likely to have significant influence on seal friction. So the discrepancy could not be attributed to an incorrect estimate of seal friction in the BTRHEOM.

5.3. Correlation between the slump and the yield stress

It was stated earlier and it can be seen from Figure 25 that slump is correlated with yield stress. Several attempts to determine an equation to relate the two entities can be found in the literature [26, 31, 32, 33]. Some of the equations are based on finite element simulations of slump cone tests [31, 32] while others are based on the fitting of sets of data [26, 33]. They all have the common form:

$$\tau_0 = \frac{\rho(A - S)}{B} + C \quad (43)$$

where

S is the slump in mm

τ_0 is the shear yield stress in Pa

ρ is density in kg/m³

A, B, C are constants to be determined either by fitting data or by simulation

The two cases we will compare with our data were developed by Hu et al. [31] and Kurokawa [32]. In these cases the constants are:

Hu's constants: $A = 300$; $B = 270$ and $C = 0$

Kurakawa's constants: $A = 300$; $B = 303$ and $C = 0$.

These constants were deduced from finite-element calculations based on the equilibrium of the concrete sample at the end of the slump test, and not on fit of experimental data.

Figure 41 shows the data obtained in this study compared with the Hu and Kurokawa equations. It seems that these equations are on the high end of the data obtained in this study.

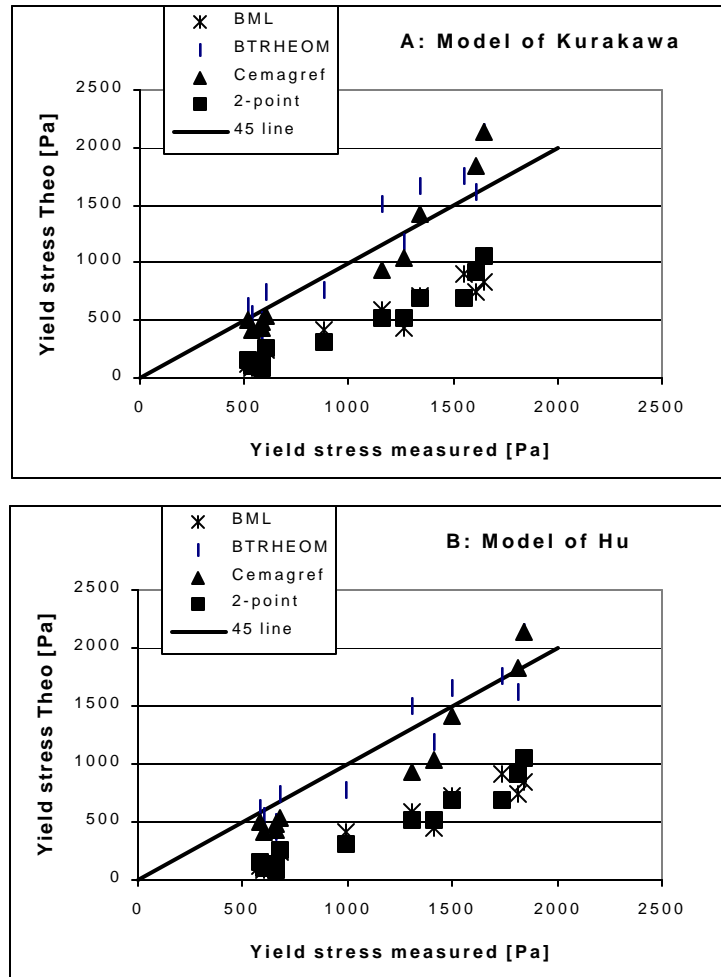


Figure 41: Comparison of measured and predicted yield stress according to equations developed by Hu and Kurakawa

6. Summary of findings

This report relates the results obtained from the first ever systematic comparison of concrete rheometers. It was carried out in France in October 2000.

A series of twelve concrete mixtures was tested in five rheometers. The mixtures had slumps ranging from 90 mm to 235 mm, but more importantly, they had a wide range of combinations of yield stress and plastic viscosity. The rheometers were all rotational, but were based on different principles and could be grouped as follows:

- Coaxial: BML and CEMAGREF-IMG
- Parallel plate: BTRHEOM
- Mixing action with an impeller: IBB and Two-Point apparatus

There were widely different geometries both within and between groups.

It was found that the rheometers gave different values of the Bingham constants of yield stress and plastic viscosity, even for those instruments that give these directly in fundamental units. However, it was found that:

- All the mixtures were ranked statistically in the same order by all the rheometers for both yield stress and for plastic viscosity.
- The degree of correlation of both yield stress and plastic viscosity measurements between any pair of rheometers was reasonably high. Relationships with 95 % confidence levels have been proposed to relate measurements with one rheometer to those with another.
- Differences in absolute values given by the various rheometers may be attributed to several causes, like slip at the concrete/wall interface, or confinement of concrete between moving parts of the rheometers (Appendix F). Further research is needed to quantify and, if necessary, to correct these effects.
- The slump test correlates well with the yield stress as measured with any of the rheometers
- The slumping time measured with the modified slump test does not correlate with the plastic viscosity. Therefore, it was concluded that this test is not useful for concretes having a relatively narrow range of plastic viscosities such as those investigated in this project.
- One future utilization of concrete rheology is to predict the flow kinematics of concrete operations. For this purpose, it is necessary to have sound basic rheological parameters. This report has shown that rheometers could be used to provide this information.

The fact that findings (1) and (2) above apply to instruments operating on different principles and with a range of geometries is encouraging and an important step forward for the subject as a whole. All the rheometers are therefore able to describe the rheology or flow of fresh

concrete, and the correlations obtained will assist in the analysis and comparison of results from different rheometers in different laboratories on different concretes. There are, however, some consistent differences that cannot be unambiguously explained at this point. Some hypotheses were discussed but further research is needed.

There is a great need for standardization of rheological measurements on concrete. This study is the first step in attempting to compare methodologies.

7. Future work

This report answered some questions but raised many more. Further research is needed to address the issues raised.

The authors suggest that the following points be considered in a new series of tests:

- A wider range of mixtures, to include self-compacting concretes.
- A wider range of plastic viscosities.
- Concretes with similar rheological properties designed with a wide range of aggregate sizes and shapes (crushed and round).
- A set with repetition of mixtures, to give greater confidence in the correlations between results from the various test systems, and perhaps identifying non-linear relationships if these exist.
- Tests and analysis to explain the consistent difference between the results of those instruments that give values of the Bingham constants in fundamental units. This would include consideration of calibration, wall slippage and volumetric confinement. It would be beneficial if some progress could be made with this before further comparative tests are made.
- Apply numerical simulations to exhibit the various artifacts that can occur in different rheometers.
- Investigate the possibility of developing a standard material for calibration of rheometers.

8. References

- 1 Hu, C., “Rhéologie des bétons fluides,” Etudes et Recherches des Laboratoires des Ponts et Chaussées, OA 16, 203 p., Paris, France, 1995
- 2 Ferraris C., Brower L., Ozyildirim C., Daczko J., “Workability of Self-compacting Concrete,” Symp. Proc. of PCI/FHWA/FIB Int. Symposium on ‘High Performance Concrete: The Economical Solution for Durable Bridges and Transportation Structures’ ,Orlando (FL) Sept 25-27, pp. 398-407, 2000
- 3 de Larrard F., “ Why rheology matters,” Concrete International, vol. 21 #8, pp. 79-81, 1999
- 4 Tattersall, G.H., *The workability of concrete*, A Viewpoint Publication, Cement and Concrete Association, 1976
- 5 Urano S., Hashimoto C., Tsuji Y., “Evaluation of flow of self-compacting concrete by visualization technique,” Proc. 1st Inter. RILEM Symp. On ‘Self-compacting Concrete’, Sweden, PROC 7 pp. 25-34, 1999
- 6 Ferraris, C.F., “Measurement of the Rheological Properties of High Performance Concrete: State of the Art Report,” Journal of Research of NIST, vol. 104 #5, pp. 461-478, 1999
- 7 Hackley V. A., Ferraris C. F., “Guide to Rheological Nomenclature: Measurements in Ceramic Particulate Systems,” NIST Special Publication 946, February 2001
- 8 Wallevik O.H., “The Rheology of Fresh Concrete and its Application on Concrete with and without Silica Fume.” Dr.ing. thesis 1990:45, NTH Trondheim. p. 185 (in Norwegian), 1990
- 9 Wallevik O.H., Gjorv, O.E., “Development of a Coaxial Cylinder Viscometer for Fresh Concrete,” Properties of Fresh Concrete, proceedings of the Rilem Colloquium, Chapman & Hall, Hanover, October, 1990, pp. 213-224
- 10 de Larrard, F., Szitkar J.-C., Hu, C., Joly M., “Design of a Rheometer for Fluid Concretes,” RILEM Workshop Special Concretes – Workability and Mixing, 201-208, 1993
- 11 de Larrard, F., Sedran, T., Hu, C., Szitkar, J.C., Joly, M., Derkx, F., “Evolution of the Workability of Superplasticized Concretes: assessment with BTRHEOM Rheometer,” RILEM International Conference on Production Methods and Workability of Concrete, RILEM Proceedings 32, , Glasgow, Scotland, June 3-5, pp. 377-388, 1996.
- 12 Beaupré, D., “Rheology of High Performance Shotcrete,” Ph. D. Thesis Uni. Of British Columbia (Canada), 1994

- 13 Domone P.L.J., Xu Yongmo, Banfill P.F.G., "Developments of the Two-Point workability test for high-performance concrete," Magazine of Concrete Research, vol. 51, pp. 181-190, 1999
- 14 Sedran T., de Larrard F., "BétonlabPro 2 - Logiciel de formulation de bétons - Version exécutable sous Windows" (BétonlabPro 2 – Software for computer-aided concrete mixture-proportioning – Ms. Windows version), Presses de l'Ecole Nationale des Ponts et Chaussées, Paris, June, 2000
- 15 Vandanjon P.O., "Evaluation et utilisation du banc d'analyse granulométrique, un appareil de mesure de l'homogénéité des mélanges (Evaluation and use of the Automatic Fresh Mix Analyser, an apparatus for mix homogeneity assessment)," Bulletin des Laboratoires des Ponts et Chaussées, No. 222, pp. 3-12, July-August, 1999.
- 16 Tattersall, G.H., Banfill, P.F.G., *The rheology of fresh concrete*, Pitman, London, 356, 1983
- 17 Barnes H.A., Hutton, J.F., Walters, K., "An introduction to Rheology," Elsevier, p. 10, p. 128, p. 141, pp. 148-149 and p.156, 1989
- 18 Malvern L.E., *Introduction to the Mechanics of a Continuous Medium*, Prentice Hall Inc, , p. 214 and p. 357, 1969
- 19 Banfill, P.F.G., "A Coaxial Cylinders Viscometer for Mortar: Design and Experimental Validation," *Rheology of fresh cement and concrete*, E. & F.N. Spon, Liverpool, pp. 217-227, 1990
- 20 De Larrard F., Ferraris C. F. and Sedran T., "Fresh Concrete: a Herschel-Bulkley Material," Technical note, Materials and Structures, Vol. 31, pp. 494-498, August-September, 1998.
- 21 Coussot, P., "Rheologie des boues et laves torrentielles - Etudes de dispersions et suspensions concentrées," Thèse de doctorat de l'institut National Polytechnique de Grenoble, et Etudes du Cemagref, série Montagne n°5, 418 p, 1993
- 22 Tattersall, G.H., Bloomer, S.J., "Further development of the Two-Point test for workability and extension of its range," Magazine of Concrete Research 31: pp. 202-210, 1979
- 23 Domone, P.L.J., Xu, Y., Banfill, P.F.G. , "Developments of the Two-Point workability test for high-performance concrete," Magazine of Concrete Research vol. 51, pp. 171-179, 1999
- 24 Ferraris, C.F., de Larrard, F. "Modified Slump Test to Measure Rheological Parameters of Fresh Concrete," Cement, Concrete and Aggregates, Vol. 20 #2, pp. 241-247, 1998

- 25 De Larrard, F., Hu, C., Sedran, T., Sitzkar, J.C., Joly, M., Claux, F., Derkx F., "A New Rheometer for Soft-to-Fluid Fresh Concrete," ACI Materials Journal, Vol. 94, No. 3, pp. 234-243, 1997
- 26 Ferraris, C.F., F. de Larrard, F., "Testing and Modelling of Fresh Concrete Rheology," NISTIR 6094, 1998
- 27 Chidiac, S.E., Maadani, O., Razaqpur, A.G., and Mailvaganam, N.P., "Controlling the quality of fresh concrete A new approach," Magazine of Concrete Research, vol. 52 (5) pp.353-364, 2000
- 28 Saporta, G., *Probabilités, analyse des données et statistiques*, Editions TECHNIP, 1990 (in French)
- 29 Meyer, S.L., *Data Analysis for Scientists and Engineers*, John Wiley & Sons, p. 143, 1975
- 30 Mannheimer, R.J., "Effect of slip on flow properties of oilwell cement slurries," Oil and Gas Journal, Dec 5, pp. 144-147, 1983
- 31 Hu, C., de Larrard, F., Sedran, T., Boulay, C., Bosc, F., Deflorenne, F., "Validation of BTRHEOM, the new rheometer for soft-to-fluid concrete," Materials and Structures, Vol. 29, No. 194, pp. 620-631, 1996
- 32 Kurokawa, Y., Tanigawa, Y., Mori, H., Komura, R., "A Study on the Slump Test and Slump-Flow Test of Fresh Concrete," Transactions of the Japan Concrete Institute, vol. 16, pp. 25-32, 1994
- 33 Sedran R., "Rheologie et rhéométrie des bétons. Application aux bétons autonivelants," Thèse de l'ENPC ("Rheometry and rheology of concrete. An application to Self Compacting Concrete," PhD Thesis), 220 p, Mars, 1999

APPENDIXES

TABLE OF CONTENTS

APPENDIX A: PICTURES OF RHEOMETERS AND THE LCPC FACILITY.....	73
APPENDIX B: PICTURES FROM THE SLUMP TESTS.....	79
APPENDIX C: DATA FROM THE RHEOMETERS	85
DATA AND GRAPHS FROM THE BML.....	85
DATA AND GRAPHS OBTAINED USING THE BTRHEOM	89
DATA AND GRAPHS OBTAINED USING THE CEMAGREF-IMG.....	94
DATA AND GRAPHS OBTAINED USING THE IBB	117
DATA AND GRAPHS OBTAINED USING THE TWO-POINT TEST	122
APPENDIX D: CALIBRATION REPORT FOR THE CEMAGREF-IMG.....	125
APPENDIX E: CALCULATION OF THE KENDALL COEFFICIENT OF CONCORDANCE.....	131
APPENDIX F: ARTIFACTS IN RHEOLOGICAL MEASUREMENTS	133
SIZE OF TESTED SPECIMEN.....	133
SLIP AT THE BOUNDARIES OF THE SPECIMEN	133
WALL EFFECT	136
ARTIFACTS AND RHEOMETERS – A CRITICAL REVIEW	140
APPENDIX G: SEAL FRICTION IN CEMAGREF-IMG TEST: EFFECT OF CONCRETE HEIGHT.....	143
INTRODUCTION	143
QUANTITATIVE ANALYSIS.....	143
CONCLUSION	145
REFERENCES FOR THE APPENDIXES	147

Appendix A: Pictures of Rheometers and the LCPC Facility

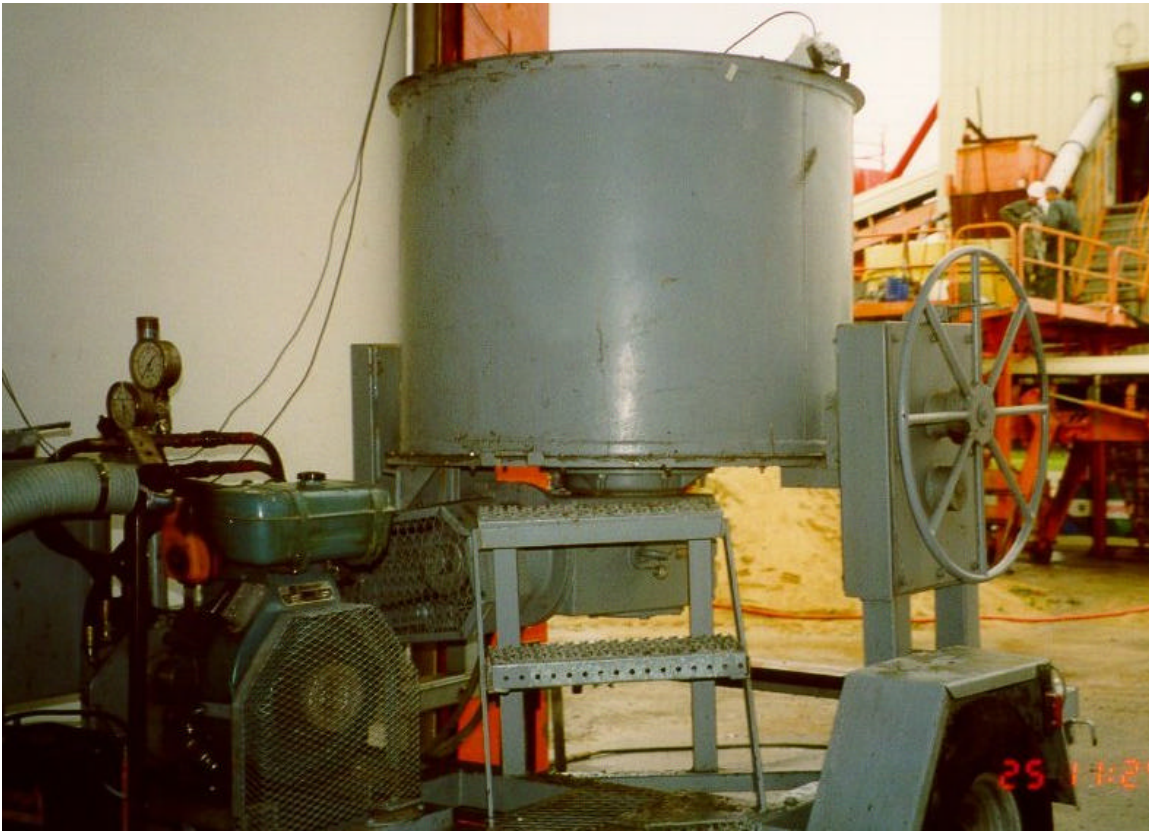
BML



BTRHEOM



CEMAGREF-IMG



IBB



Two-point test



Batch plant



Transportation of concrete to the rheometers



Appendix B: Pictures from the slump tests

The slump tests, depicted here, were carried out at the same time as the concrete was being tested in the rheometers.

Mixture #1



Mixture #2



Mixture #3



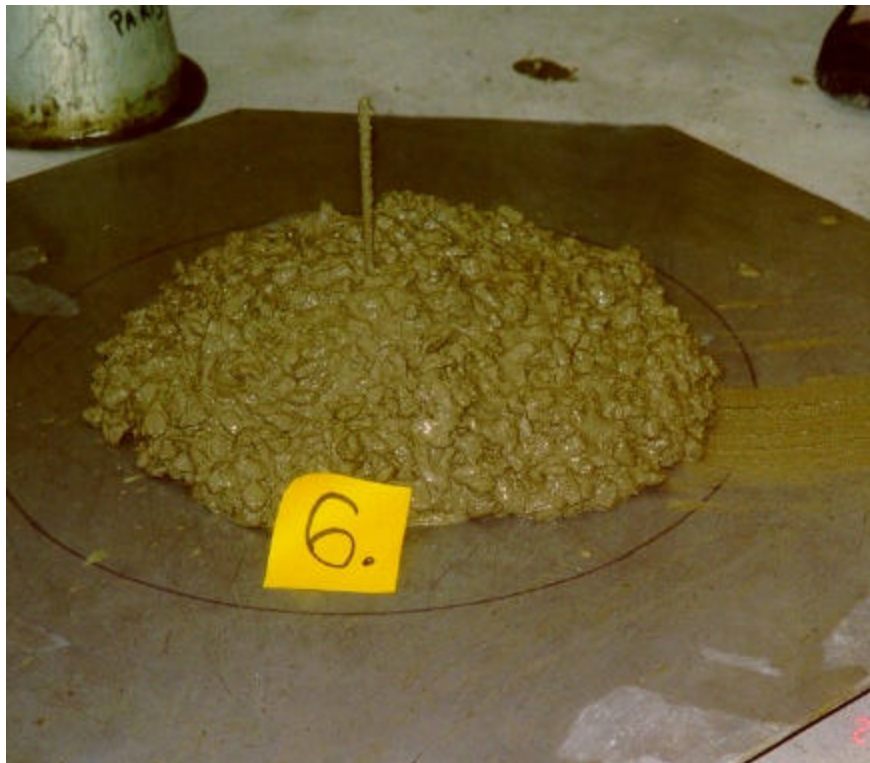
Mixture #4



Mixture #5



Mixture #6



Mixture #7



Mixture #8



Mixture #9



Mixture #10



Mixture #11



Mixture #12

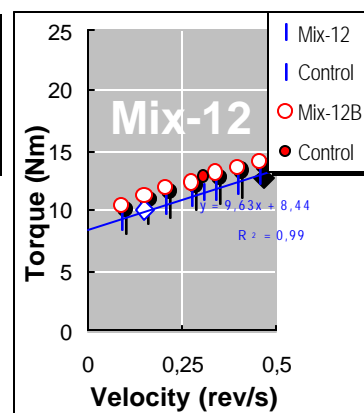
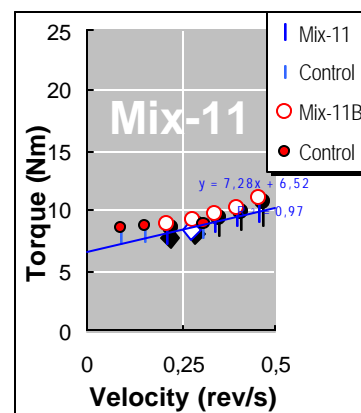
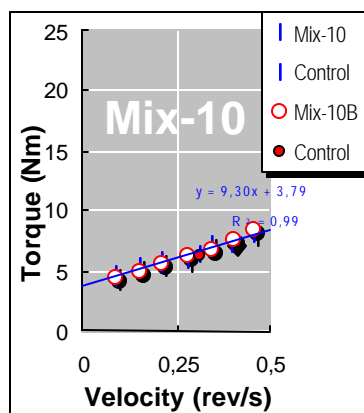
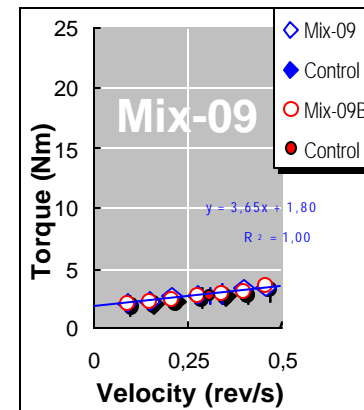
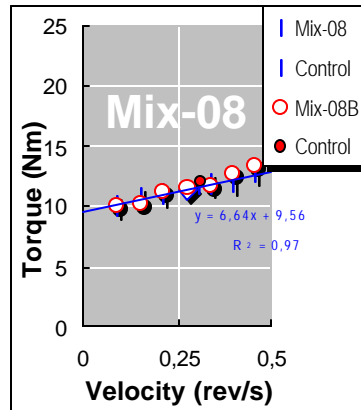
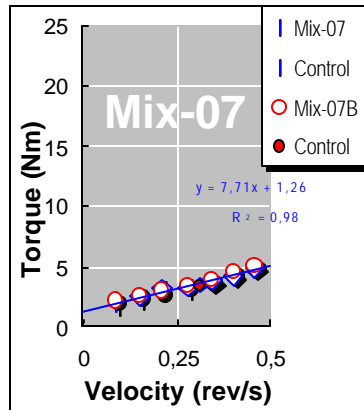
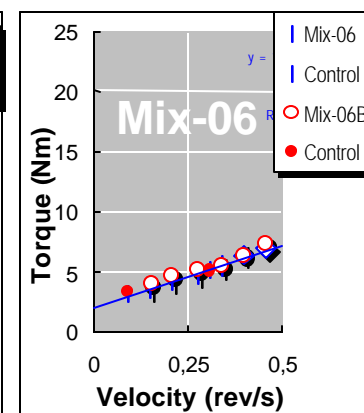
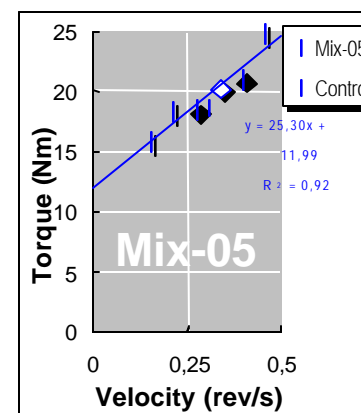
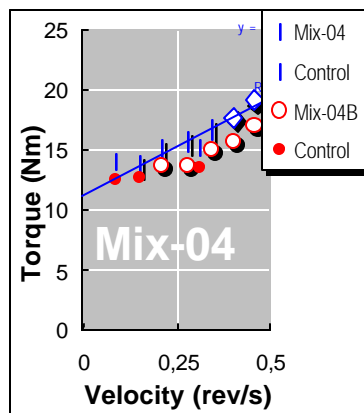
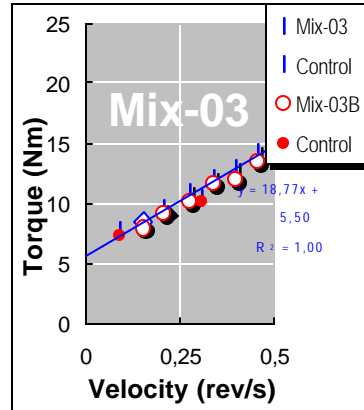
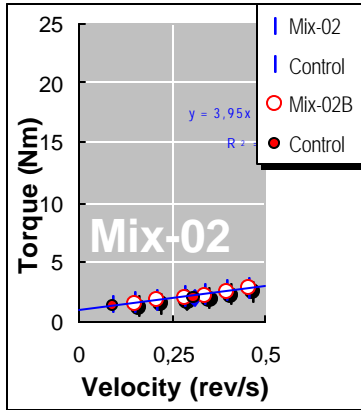
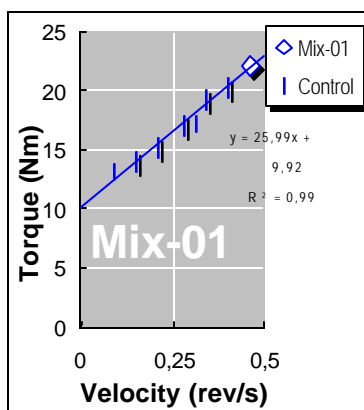


Appendix C: Data from the rheometers

Data and graphs from the BML

All the mixes were run twice and are shown here and in the graphs, but only the first run was used in the report to compare with the other rheometers.

Velocity	Mix-01	Mix-02	Mix-03	Mix-04	Mix-05	Mix-06	Mix-07	Mix-08	Mix-09	Mix-10	Mix-11	Mix-12
(rev/s)	(Nm)	(Nm)	(Nm)	(Nm)	(Nm)	(Nm)	(Nm)	(Nm)	(Nm)	(Nm)	(Nm)	(Nm)
0,46	21,92 No	2,84 No	14,18 No	19,01 No	24,83 No	6,85 No	5,00 No	12,82 No	3,51 No	8,19 No	9,80 No	12,93 No
0,4	20,17 No	2,64 No	12,87 No	17,66 No	21,02 No	6,35 No	4,25 No	11,98 No	3,23 No	7,43 No	9,59 No	12,22 No
0,34	19,11 No	2,34 No	11,98 No	16,66 No	20,23 No	5,42 No	3,73 No	11,80 No	3,01 No	7,01 No	8,98 No	11,64 No
0,28	16,92 No	2,09 No	10,78 No	15,64 No	18,45 No	4,84 No	3,32 No	11,32 No	2,83 No	6,16 No	8,41 No	11,14 No
0,21	15,23 No	1,86 No	9,38 No	14,92 No	18,19 No	4,25 No	3,05 No	11,07 No	2,60 No	5,75 No	8,13 No	10,55 No
0,15	13,99 No	1,63 No	8,34 No	13,71 No	15,80 No	3,59 No	2,44 No	10,62 No	2,34 No	5,26 No	7,87 Yes	10,01 No
0,09	13,13 Yes	1,43 Yes	7,69 Yes	14,03 Yes	14,64 No	3,07 Yes	1,95 No	10,11 No	2,12 No	4,66 No	7,69 Yes	9,18 No
0,3	17,1	2,0	10,6	15,1	18,6	5,0	3,4	11,6	2,7	6,4	8,2	11,6
Velocity	Mix-01B	Mix-02B	Mix-03B	Mix-04B	Mix-05B	Mix-06B	Mix-07B	Mix-08B	Mix-09B	Mix-10B	Mix-11B	Mix-12B
(rev/s)	(Nm)	(Nm)	(Nm)	(Nm)	(Nm)	(Nm)	(Nm)	(Nm)	(Nm)	(Nm)	(Nm)	(Nm)
0,46		2,79 No	13,46 No	16,97 No	No	7,33 No	5,13 No	13,28 No	3,54 No	8,38 No	11,08 No	14,20 No
0,4		2,45 No	12,01 No	15,69 No	No	6,45 No	4,54 No	12,74 No	3,17 No	7,49 No	10,26 No	13,63 No
0,34		2,19 No	11,63 No	15,02 No	No	5,47 No	3,96 No	11,68 No	2,94 No	6,76 No	9,62 No	13,13 No
0,28		1,97 No	10,12 No	13,66 No	No	5,09 No	3,42 No	11,52 No	2,76 No	6,21 No	9,22 No	12,39 No
0,21		1,81 No	9,14 No	13,69 No	No	4,54 No	2,90 No	11,17 No	2,47 No	5,67 No	8,83 No	11,89 No
0,15		1,51 No	7,96 No	12,74 Yes	No	3,88 No	2,63 No	10,20 No	2,34 No	4,99 No	8,77 Yes	11,14 No
0,09		1,40 Yes	7,25 Yes	12,51 Yes	No	3,29 Yes	2,13 No	10,03 No	2,12 No	4,37 No	8,60 Yes	10,30 No
0,3		2,0	10,2	13,5		5,2	3,5	12,0	2,7	6,2	8,9	12,9

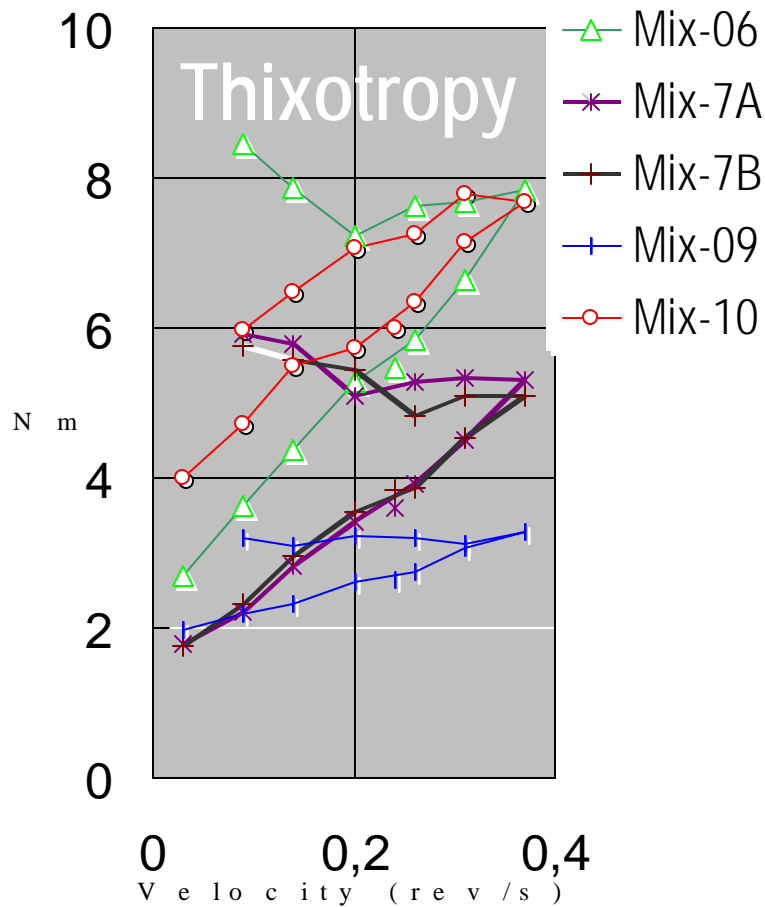


The following table gives the summary of the calculated results.

Mix no.	Test no.	G-value (Nm)	H-value (Nm s)	r	dG (Nm)	dH (Nm s)	Seg.	Yield (Pa)	Pl. Visc (Pa s)	Time (min)	Date (dd/mm/yy)	Time (hh/mm/ss)
1	1	9,81	25,93	0,997	0,28	0,29	4	738	114,1	1 32	24/10/2000	10:17:26
	2	10,13	21,21	0,991	0,37	0,39	6	761	93,3	1 45	24/10/2000	10:30:32
2	1	1,01	3,95	0,999	0,06	0,07	11	76	17,4	1	24/10/2000	12:04:21
	2	0,90	3,91	0,995	0,14	0,15	6	68	17,2	1	24/10/2000	12:13:45
3	1	5,42	18,72	0,999	0,16	0,17	6	408	82,4	1	24/10/2000	14:51:54
	2	5,36	17,22	0,994	0,33	0,34	5	403	75,8	1	24/10/2000	14:59:40
4	1	11,17	16,36	0,997	0,22	0,24	7	840	72,0	1	24/10/2000	16:55:39
	2	10,30	13,74	0,968	0,81	0,85	7	774	60,5	1	24/10/2000	17:03:33
5	1	12,11	24,64	0,974	0,70	0,73	6	911	108,4	1	25/10/2000	09:56:18
	2 Error	45,11	33,13	0,956	1,07	1,13	10	3391	145,8	1	25/10/2000	10:03:11
6-SCC	1	1,91	10,61	0,997	0,16	0,17	3	139	45,0	1	25/10/2000	12:10:45
	2	2,13	10,69	0,990	0,33	0,35	6	155	45,4	1	25/10/2000	12:18:30
3 Thixotro		2,19	14,58	0,997	0,19	0,20	6	159	61,4	4	25/10/2000	12:21:58
7	1	1,24	7,69	0,994	0,19	0,20	6	90	32,7	1	25/10/2000	15:13:22
	2	1,31	7,93	0,996	0,16	0,17	7	98	34,9	1	25/10/2000	15:18:43
	3 Thixo	1,30	10,34	0,998	0,13	0,14	7	98	45,2	4	25/10/2000	15:26:02
4 Thixo		1,43	9,77	0,998	0,11	0,12	1	108	42,7	4	25/10/2000	15:29:45
8	1	9,53	6,62	0,989	0,23	0,24	0	717	29,1	1	25/10/2000	18:02:19
	2	9,05	8,79	0,983	0,33	0,35	-2	680	38,7	1	25/10/2000	18:09:28
9	1	1,79	3,64	0,999	0,05	0,06	6	125	15,0	1 36 min	26/10/2000	09:53:42
	2	1,74	3,65	0,993	0,13	0,14	6	122	15,0	1 min	26/10/2000	09:59:48
	3 Thixotro	1,81	3,83	0,995	0,11	0,12	5	128	15,6	4 min	26/10/2000	10:06:21
10	1	3,75	9,27	0,997	0,15	0,16	4	248	35,9	1	26/10/2000	11:40:45
	2	3,36	10,38	0,997	0,15	0,15	6	232	41,9	1	26/10/2000	11:47:38
	3 Thixo	3,69	10,62	0,996	0,18	0,19	5	253	42,0	4	26/10/2000	11:51:56
11	1	6,50	7,24	0,989	0,34	0,36	6	443	28,9	1	26/10/2000	15:11:20
	2	6,77	8,86	0,986	0,42	0,45	7	509	39,0	1	26/10/2000	15:17:08
12	1	8,41	9,59	0,998	0,12	0,13	-2	584	39,0	1	27/10/2000	10:14:02
	2	9,51	10,24	0,997	0,16	0,16	-2	669	42,1	1	27/10/2000	10:22:22
	3	11,84	13,28	0,996	0,19	0,20	2	890	58,4	1	27/10/2000	10:49:33
Oil error 1 plug		7,74	10,74	0,995	0,20	0,21	-1	528	42,9	1	27/10/2000	11:31:05

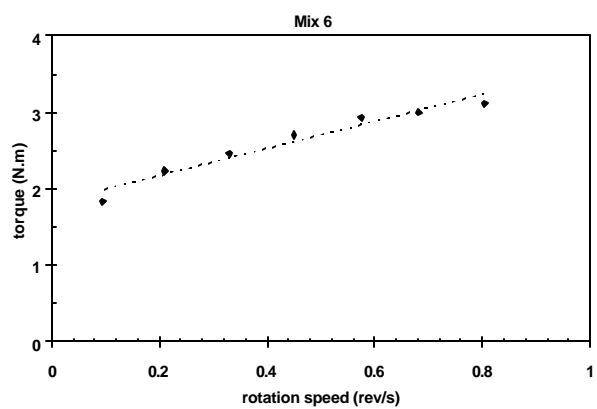
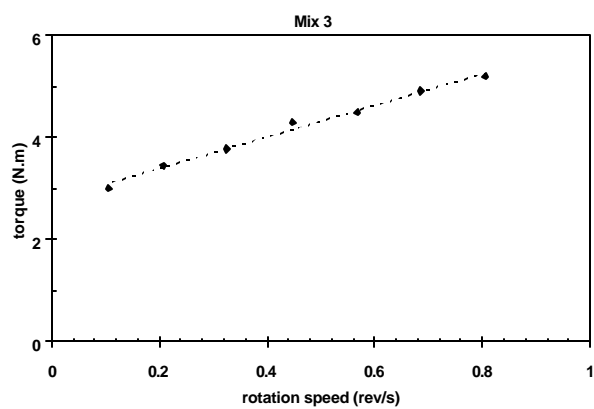
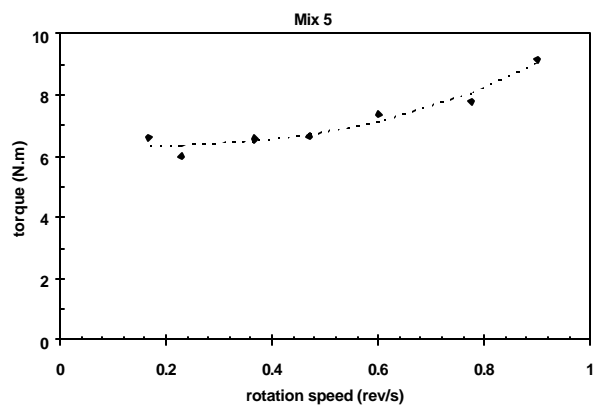
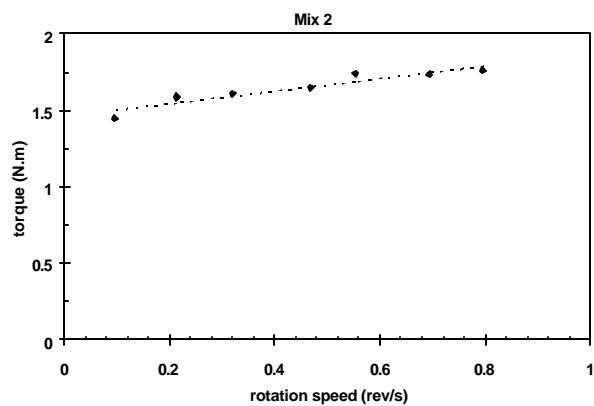
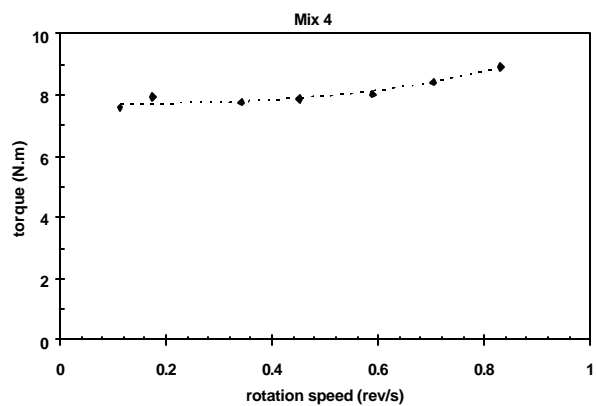
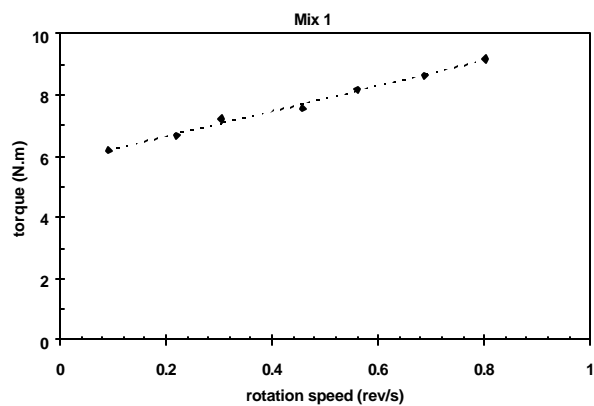
The thixotropy was evaluated for four mixtures; Mixture #6, Mixture #7, Mixture #9 and Mixture #10. Mixture #7 was tested twice (Na-7A and Na-7B) with almost identical results. The thixotropic properties were evaluated by determining up and down curves (up and down refer to the increase or decrease of the velocity). The area between the up and down curves is “the rate of work per unit volume”; it cannot be directly characterized as a material parameter as it depends heavily on the shear history of the material tested. The size of the “thixotropy area” should also be related to the yield value of the material.

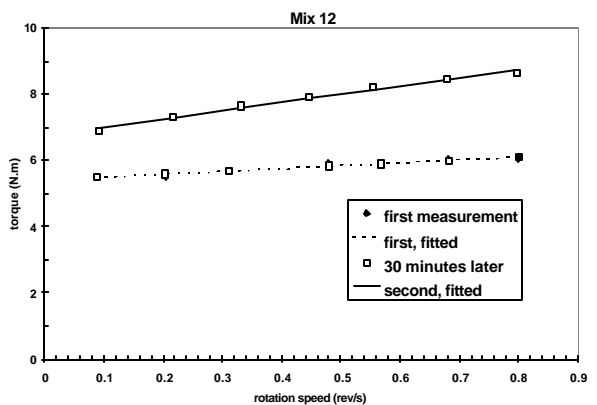
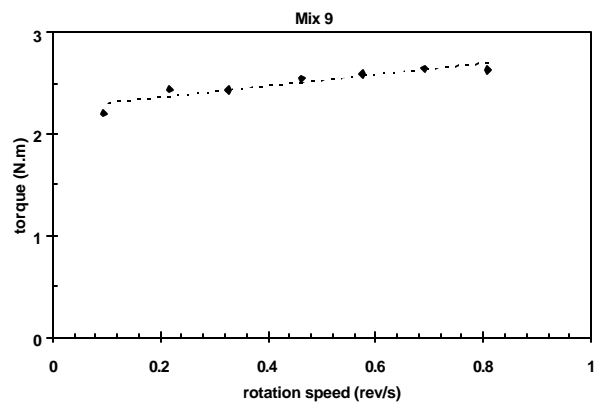
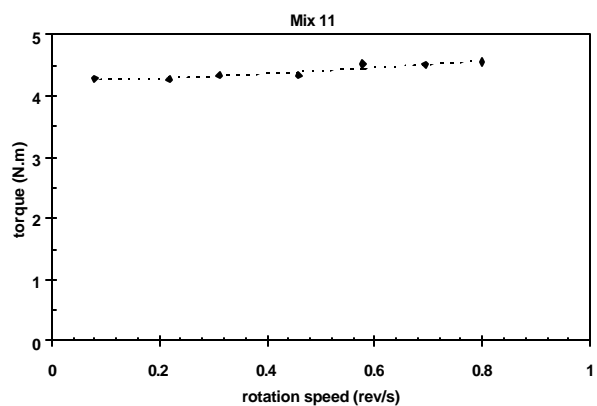
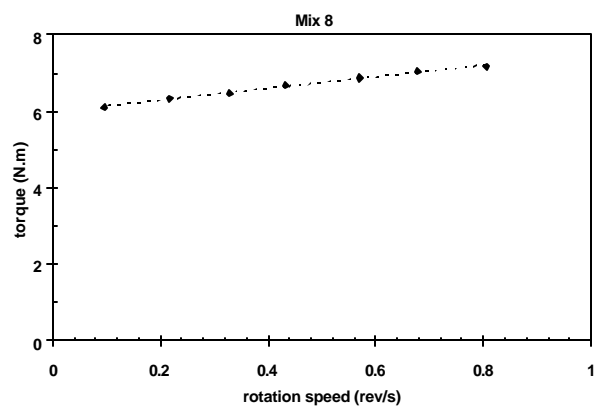
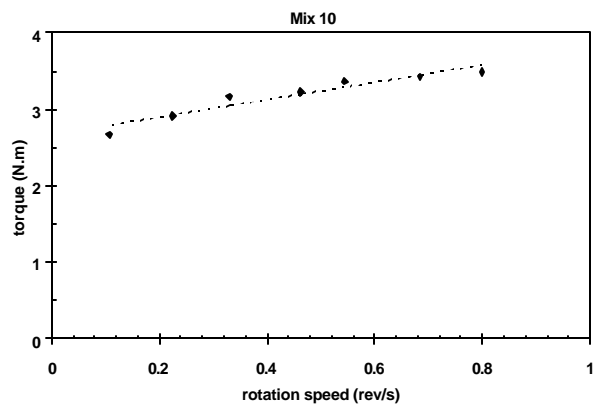
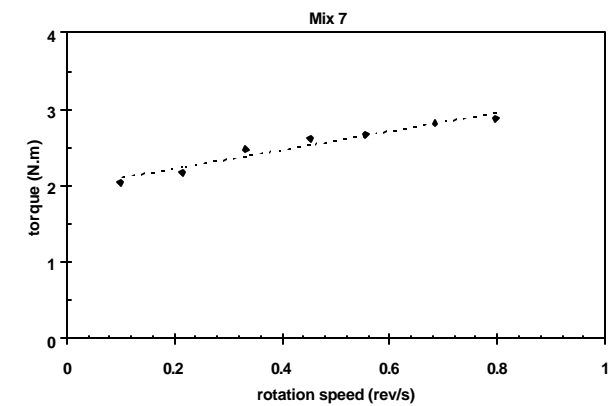
The “thixotropy” is lower for mixture #9 though relative to the yield value for mixture #10 is the lowest. The “thixotropy” is significantly higher for mixture #7.



Data and graphs obtained using the BTRHEOM

The dotted line represents the modified Bingham model fitted to the points.





The following tables show the data points used for the graph above. The readings were recorded by decreasing rotation speed. The concrete was vibrated prior to start of the measurements to ensure good filling of the bucket, unless stated otherwise.

Mixture #1

Point	Speed	Torque
n°	(rev/s)	(N·m)
1	0.803	9.173
2	0.687	8.623
3	0.56	8.173
4	0.457	7.57
5	0.305	7.219
6	0.219	6.676
7	0.091	6.181

Mixture #4

Point	Speed	Torque
n°	(rev/s)	(N·m)
1	0.831	8.911
2	0.704	8.41
3	0.589	8.032
4	0.451	7.872
5	0.342	7.768
6	0.175	7.934
7	0.113	7.592

Mixture #2: The concrete was not vibrated prior to measurement.

Point	Speed	Torque
n°	(rev/s)	(N·m)
1	0.795	1.763
2	0.694	1.733
3	0.553	1.739
4	0.468	1.65
5	0.319	1.608
6	0.214	1.588
7	0.095	1.447

Mixture #5

Point	Speed	Torque
n°	(rev/s)	(N·m)
1	0.9	9.163
2	0.776	7.784
3	0.601	7.37
4	0.47	6.644
5	0.366	6.568
6	0.229	5.989
7	0.167	6.614

Mixture #3.

Point	Speed	Torque
n°	(rev/s)	(N·m)
1	0.806	5.209
2	0.685	4.922
3	0.568	4.495
4	0.447	4.298
5	0.325	3.783
6	0.207	3.456
7	0.106	3.014

Mixture #6: The concrete was not vibrated prior to measurement.

Point	Speed	Torque
n°	(rev/s)	(N·m)
1	0.803	3.118
2	0.681	2.997
3	0.575	2.933
4	0.45	2.703
5	0.331	2.463
6	0.209	2.232
7	0.095	1.834

Mixture #7: The concrete was not vibrated prior to measurement.

Point	Speed	Torque
n°	(rev/s)	(N·m)
1	0.796	2.875
2	0.684	2.818
3	0.555	2.673
4	0.452	2.621
5	0.332	2.478
6	0.216	2.175
7	0.1	2.045

Mixture #8

Point	Speed	Torque
n°	(rev/s)	(N·m)
1	0.805	7.163
2	0.678	7.045
3	0.57	6.88
4	0.433	6.677
5	0.328	6.471
6	0.217	6.329
7	0.097	6.108

Mixture 9. The concrete was not vibrated prior to measurement.

Point	Speed	Torque
n°	(rev/s)	(N·m)
1	0.807	2.634
2	0.69	2.645
3	0.576	2.594
4	0.462	2.546
5	0.326	2.437
6	0.217	2.441
7	0.095	2.203

Mixture 10

Point	Speed	Torque
n°	(rev/s)	(N·m)
1	0.799	3.487
2	0.684	3.423
3	0.543	3.37
4	0.463	3.224
5	0.33	3.165
6	0.224	2.911
7	0.108	2.671

Mixture #11

Point	Speed	Torque
n°	(rev/s)	(N·m)
1	0.799	4.555
2	0.694	4.519
3	0.578	4.527
4	0.458	4.344
5	0.311	4.332
6	0.219	4.267
7	0.079	4.285

Mixture #12

Point	Speed	Torque
n°	(rev/s)	(N·m)
1	0.8	6.051
2	0.682	6.027
3	0.569	5.921
4	0.48	5.89
5	0.312	5.678
6	0.204	5.524
7	0.088	5.512

Mixture #12: Second measurement (30 min after the first one)

Point n°	Speed (rev/s)	Torque (N·m)
1	0.797	8.648
2	0.678	8.453
3	0.556	8.208
4	0.448	7.916
5	0.331	7.646
6	0.218	7.312
7	0.093	6.876

Concrete parameters calculated from the down curves

Date	Mixture	File	Yield stress (Pa)	Plastic viscosity (Pa·s)
10/24/00	1	LNAC004	1619	181
10/24/00	2	LNAC005	406	18
10/24/00	3	LNAC006	771	136
10/24/00	4	LNAC008	2139	51
10/25/00	5	LNAC009B	1753	94
10/25/00	6	LNAC011	505	78
10/25/00	7	LNAC012	549	54
10/25/00	8	LNAC013	1662	67
10/26/00	9	LNAC014	624	25
10/26/00	10	LNAC016	740	50
10/26/00	11 See note	LNAC018	1189	27
10/26/00	12	LNAC020	1503	38

Note for Mixture #11: the lowest rotation speed was recorded as 0, leading to an error in the data processing. These values were calculated later, from the raw data, with the same equations, without the point at speed zero.

Data and graphs obtained using the CEMAGREF-IMG

List of the various tests and comments.

Mixture #	Text file for the seal	Text file for the concrete	Height of the sheared concrete sample (m)	Comments
1	Mix1a.txt	Seal1a.txt	0.655	
2	Mix2a.txt	Seal2a.txt	0.678	Segregation at the end of the test: width 70 mm, depth of segregation 30 mm to 70 mm
3	Mix3a.txt	Seal3a.txt	0.670	
4	Mix4b.txt	Seal4a.txt	0.655	
5	Mix5b.txt	Seal5a.txt	0.345	Concrete too stiff to start the test. Part of the concrete is removed from the rheometer. Test restarted at T0+33 min
6	Mix6a.txt	Seal6a.txt	0.655	
7	Mix7a.txt	Seal7a.txt	0.635	Light segregation at the end of the test: width=60 mm, depth: 10 mm
8	Mix8a.txt	Seal8a.txt	0.645	
9	Mix9a.txt	Seal9a.txt	0.605	
10	Mix10a.txt	Seal10a.txt	0.675	
11	Mix11a.txt	Seal11a.txt	0.645	
12	Mix12a.txt	Seal12a.txt	0.645	A second test is performed at To+43 min. corresponding to Mix12b.txt and Seal12a.txt. For this test, vibration is needed to re-start the rotation, applied with vibrating poker put in the concrete specimen.

The measurements of the width of the sheared zone are given in Appendix C.

Direct calculation of the shear yield stress

We have $\tau_0 = \frac{C}{2\pi h R_c^2}$ so $|\Delta\tau_0| = \frac{C}{\pi h R_c^3} |\Delta R_c|$ and finally: $|\Delta\tau_0| = 2\tau_0 \frac{|\Delta R_c|}{R_c}$

The mean error on the measurement of the width of the sheared zone is estimated to be equal to the maximum diameter of the aggregate (i.e., 1.25 time diameter 16 mm for mixture #1 to #7, 1.25 time diameter 20 mm for mixture #8 to #11 and 1.25 time diameter 6.3 mm for mixture #12)

The following figures present the values of the shear yield stress calculated for each mixture and for each rotation speed, with their corresponding error bar. In a perfect experiment, all the values of calculated shear yield stress should be equal on each figure. This was not the case so, for each mixture, the shear yield stress was calculated as the mean of the lowest value of the tops of the error bars and the largest value of the bottoms of the error bars. This shear yield stress is considered to be acceptable only if it is included in all error bars. According to this procedure, we can see on the following figures, that the values obtained for mixture #3, mixture #9 and mixture #12 (respectively: 850 Pa, 423 Pa and 1148 Pa) are not acceptable. The decrease of the calculated shear yield stress values with the rotation speed observed with mixture #3 is probably due to the horizontal segregation of coarse aggregate, which tends to occur more and more during the test, because of the increase of the dead zone. Then, the mixture-composition is assumed to change, from the inner cylinder vicinity (where the

mixture is richer in fine elements) to the outer cylinder (where the mixture is leaner). The tendency observed for mixture #9 and mixture #12 is not clear, and it could be due to an error in the measurements.

No measurement was available for mixture #5, owing to the fact that the concrete top surface was hardly visible, and for the second test with mixture #12. Only one measurement was available for each of Mixture #1 and #4.

The sheared zone width observed on mixture #4 was low, as compared to the maximum diameter of aggregate, even at the maximum rotation speed. Therefore, it can be assumed that the part of the sample that was sheared during the test was more a mortar than the concrete in bulk. Finally, the shear yield stress calculated is not an exact value but a minimum bound of the concrete yield stress.

Yield values deduced from the width of the sheared zone and the equation 21 in Section 3.3 (main part of this report).

Mixture #	t_0 (Pa)
1	1832
2	437
3	-
4	> 2138
5	-
6	487
7	410
8	1417
9	-
10	535
11	1034
12	-
12*	-

**second test*

Width of the sheared zone E_c

Mixture 1

W (rad/s)	Experimental E_c (mm)
0.756	35

Mixture 2

W (rad/s)	Experimental E_c (mm)
0.900	50
0.600	30
0.300	20
0.100	10

Mixture 3

W (rad/s)	Experimental E_c (mm)
1.700	80
1.500	80
1.200	70
0.900	60
0.600	50
0.500	50
0.300	40
0.100	30

Mixture 4

W (rad/s)	Experimental E_c (mm)
1.518	10

Mixture 6

W (rad/s)	Experimental E_c (mm)
1.800	130
1.500	110
1.300	110
1.000	100
0.900	100
0.700	80

0.600	80
0.400	70
0.300	50

Mixture 7

W (rad/s)	Experimental E_c (mm)
2.000	140
1.700	140
1.500	130
1.200	130
1.000	120
0.800	90
0.600	60
0.300	60
0.150	20

Mixture 8

W (rad/s)	Experimental E_c (mm)
1.700	40
1.500	30
1.300	20
1.000	20
0.800	20
0.500	20
0.300	5

Mixture 9

W (rad/s)	Experimental E_c (mm)
2.100	110
1.700	90
1.200	50
0.900	30
0.600	25
0.300	20
0.150	15

Mixture 10

W (rad/s)	Experimental Ec (mm)
1.900	150
1.600	150
1.300	140
1.000	120
0.800	90
0.500	40
0.200	30

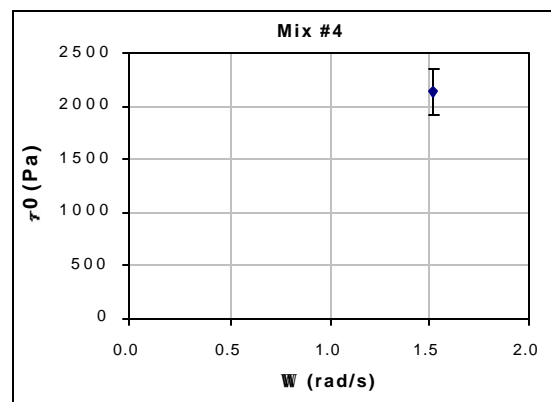
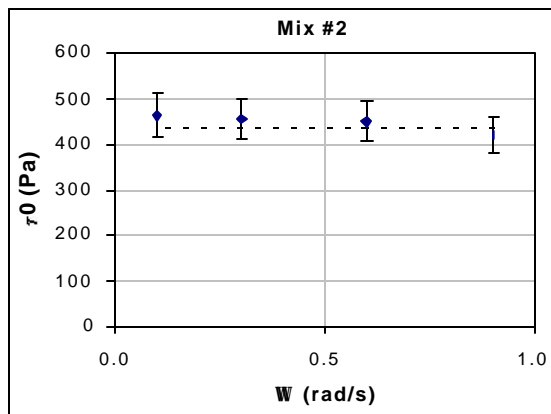
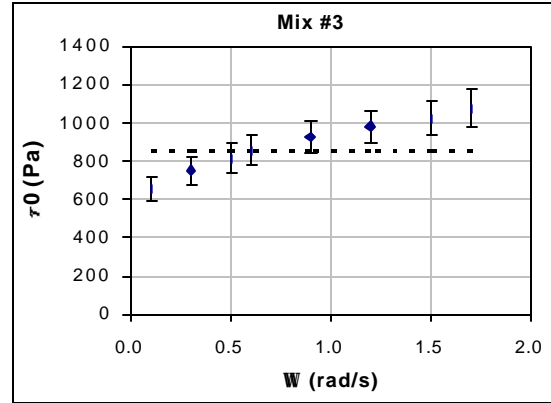
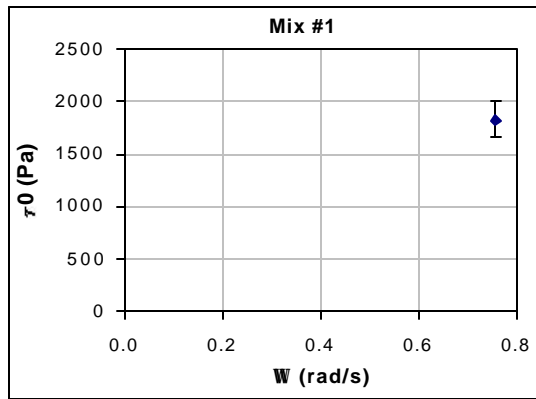
Mixture 11

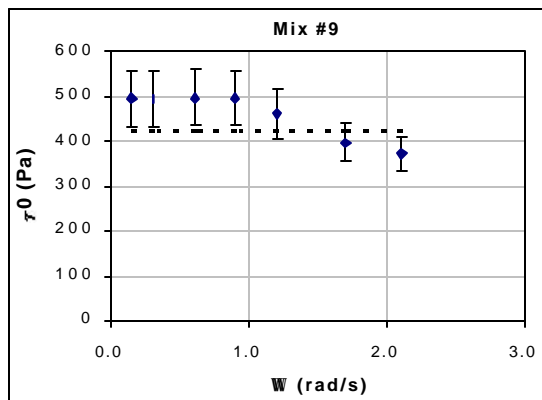
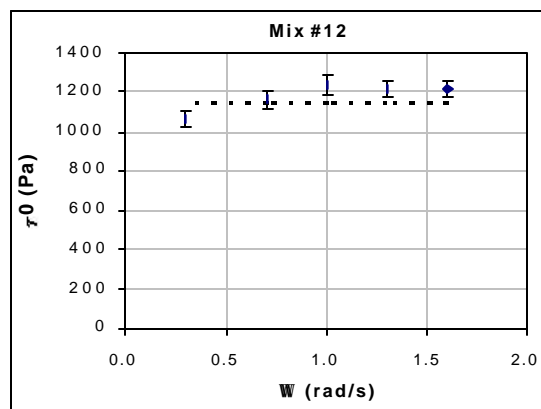
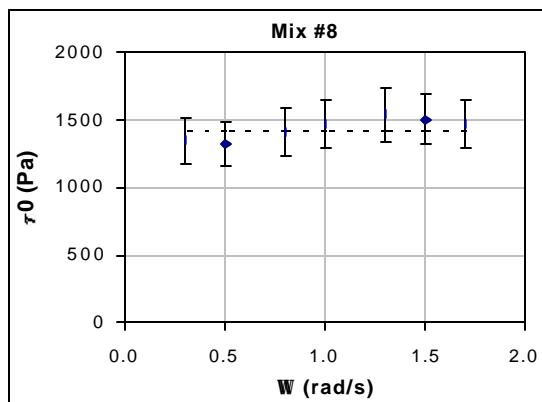
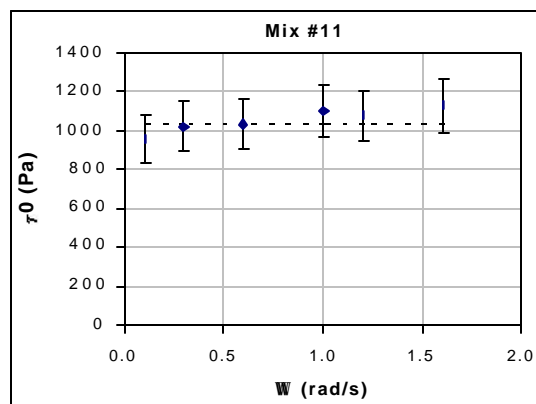
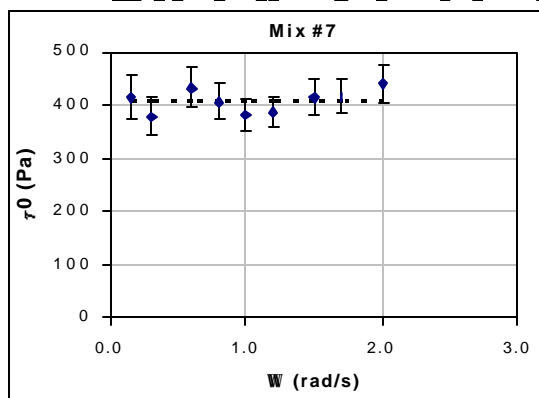
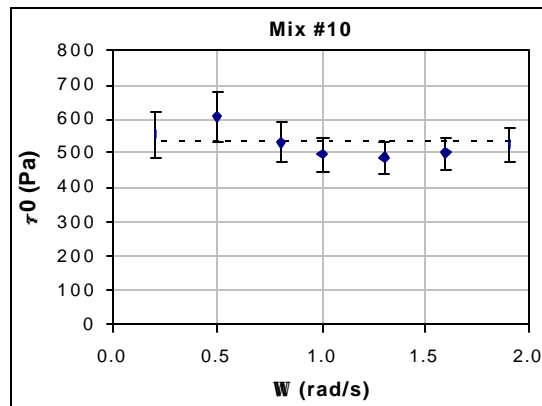
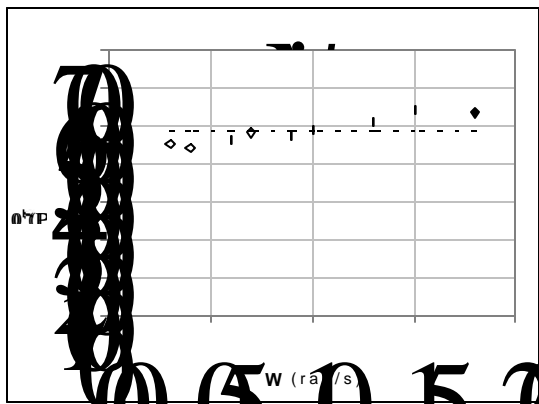
W (rad/s)	Experimental Ec (mm)
1.600	40
1.200	40
1.000	30
0.600	30
0.300	20
0.100	20

Mixture 12

W (rad/s)	Experimental Ec (mm)
1.600	50
1.300	40
1.000	25
0.700	25
0.300	20

Values of the shear yield stress calculated with Equation 21 from Section 3.3 for different rotation speeds. The horizontal dotted lines give the value adopted for each mixture. To be acceptable a dotted line must pass through the error bars.





Fitting of the curves for torque vs. rotation speed obtained for the seals

The following table summarizes the data concerning the fitting of the experimental curves obtained for the seals alone. Figures of these curves can be found below.

Curve fitting for measurements on the seal alone

Mixture #	Equation	Mean error (N·m)	Range of fit	
			W_{max} (rad/s)	W_{min} (rad/s)
1	$C_{\text{seal}}=135.3 + 17.89 \Omega$	8.3	1.889	0.1
2	$C_{\text{seal}}=68.9 + 3.02 \Omega$	11.3	2.017	0.1
3	$C_{\text{seal}}=93.1 + 3.59 \Omega$	8.8	2.129	0.1
4	$C_{\text{seal}}=114.5 + 0.71 \Omega$	7.9	2.052	0.1
5	$C_{\text{seal}}=162.6 - 3.49 \Omega$	18.7	2.300	0.1
6	$C_{\text{seal}}=119.8 + 6.49 \Omega$	5.1	2.039	0.1
7	$C_{\text{seal}}=128 + 4.06 \Omega$	7.7	1.987	0.1
8	$C_{\text{seal}}=133.9 + 4.65 \Omega$	4.6	1.872	0.1
9	$C_{\text{seal}}=143.4 + 3.09 \Omega$	7.3	2.067	0.1
10	$C_{\text{seal}}=140.4 + 7.59 \Omega$	4.5	1.898	0.1
11	$C_{\text{seal}}=131.6 - 2.49 \Omega$	5.4	1.635	0.1
12	$C_{\text{seal}}=151.8 + 5.08 \Omega$	5.7	1.956	0.1
12*	$C_{\text{seal}}=151.8 + 5.08 \Omega$	5.7	1.956	0.1

*second test

Analysis with the Bingham model

The results are summarized in the table below. Figures of these curves can be found below under “Experimental and fitted torque-rotation speed curves”. It can be seen that, for some mixtures, the τ_0 values calculated with the Bingham model are significantly different from the values calculated directly. This means that even if the inner cylinder of the CEMAGREF-IMG rheometer is equipped with a metallic grid, a significant slippage occurs between the cylinder and some concretes. This phenomenon may be related to a horizontal segregation, where coarse particles are expelled from the sheared zone, so that shear tends to be concentrated in a thin annulus around the rotating cylinder, where the material is more fluid than in the rest of the sample.

Results according the Bingham model

Mixture #	τ_0 (Pa)	μ (Pa s)	Mean error	$\dot{\gamma}_{\max}$ (1/s)	Range of fit	
			(N/m)		$\dot{\gamma}_{\max}$ (rad/s)	$\dot{\gamma}_{\min}$ (rad/s)
1	1027	253	23.6	5.4	1.057	0.1
2	463	3	11.6	40.8	1.936	0.1
3	576	124	20.2	9.1	1.817	0.1
4	1282	82	27.0	13.1	1.519	0.1
5	848	125	15.2	10.4	1.677	0.1
6	384	63	14.7	10.3	1.838	0.1
7	356	43	13.9	12.6	2.053	0.1
8	1129	42	8.3	16.8	1.741	0.1
9	504	3	5.8	46.6	2.131	0.1
10	504	43	10.9	13.5	2.021	0.1
11	967	21	8.1	20.7	1.834	0.1
12	929	47	9.4	16.5	1.971	0.1
12*	1252	105	24.5	12.1	1.651	0.1

*second test

Summary

The table below summarizes the values of τ_0 calculated with the Bingham model and from the width of the sheared zone E_c . When the difference is high, slippage has probably occurred between the inner cylinder and the concrete sample. In this case, the rheological parameters calculated with the Bingham model are not valid and should not be considered.

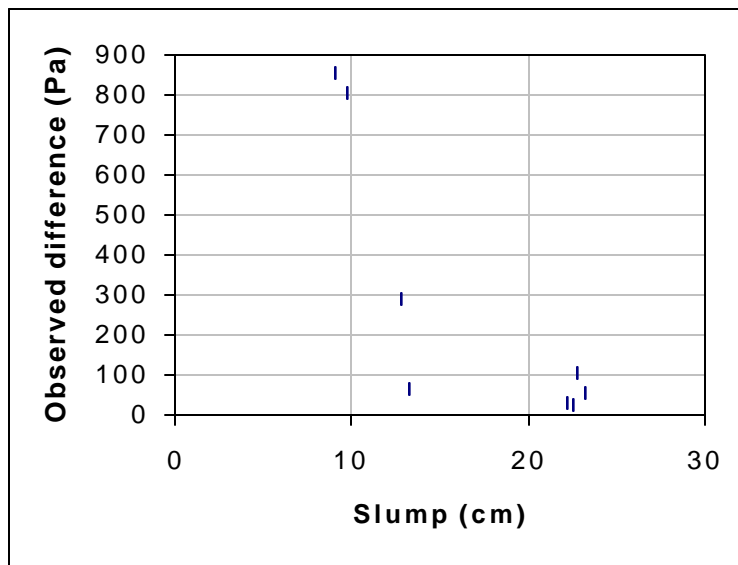
The figure on page A-102 shows the differences observed between the two methods as a function of the slump. It appears that for slump lower than approximately 110 mm, slippage occurs, as in mixture #5 and 12. Again in this case, the rheological parameters evaluated with Bingham model are not valid and cannot be used for these tests.

According to “Direct calculation of the shear yield stress” (page A-94), mixture #3 was certainly subject to segregation and rheological parameters are probably not relevant. Mixture #9 and #12 (for the first test) were probably not subject to slippage because their slumps were respectively 232 mm and 150 mm; moreover, the shear yield stress calculated with the Bingham model is close to the one calculated with E_c . Therefore, even if the direct measurement of the shear yield stress was subject to errors in measurement, the rheological values calculated with Bingham can be accepted.

Comparisons of shear yield stresses calculated directly from E_c and with the Bingham model assuming no slippage

Mixture #	t_0 calculated with Bingham (Pa)	t_0 calculated from E_c (Pa)	Difference (Pa)	Slump (cm)
1	1027	1832	805	9.7
2	463	437	25	22.5
3	576	-	-	18.7
4	1282	>2138	>856	9
5	848	-	-	10.5
6	384	487	103	22.7
7	356	410	55	23.2
8	1129	1417	289	12.8
9	504	-	-	23.2
10	504	535	32	22.2
11	967	1034	67	13.2
12	929	-	-	15
12*	1252	-	-	10.3

* second test



Difference between the shear yield stress calculated with Equation 21 or Equation 28 (see Section 3.3) and the slump

Finally, the only reliable rheological values for use in comparing the different rheometers are summarized in the table below.

Rheological values judged to be reliable

Mixture #	t_0 calculated with E_c (Pa)	t_0 calculated with Bingham (Pa)	μ calculated with Bingham (Pa s)
1	1832	-	-
2	437	-	3
3	-	-	-
4	>2138	-	-
5	-	-	-
6	487	-	63
7	410	-	43
8	1417	-	-
9	-	504	3
10	535	-	43
11	1034	-	21
12	-	929	47
12*	-	-	-

* second test

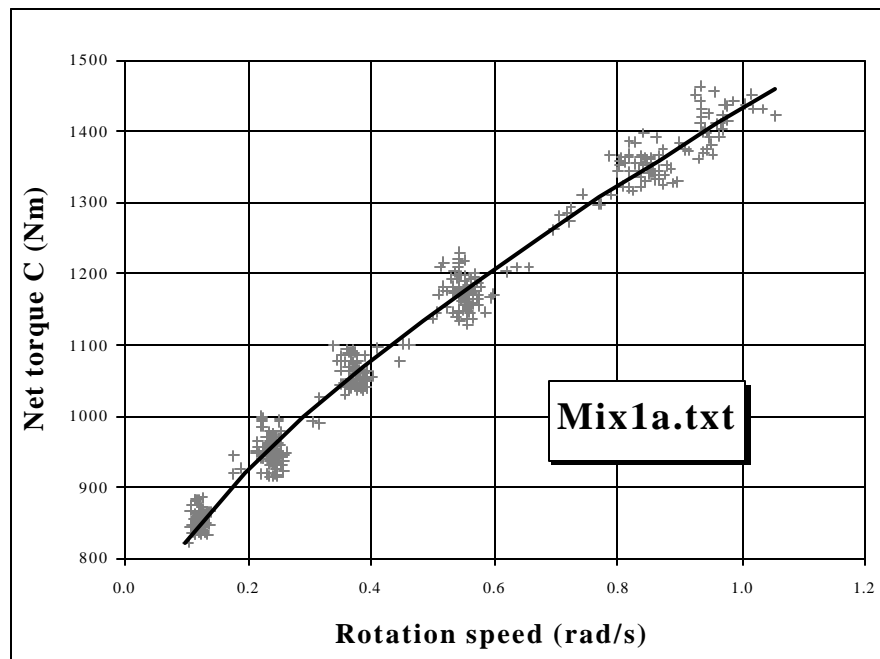
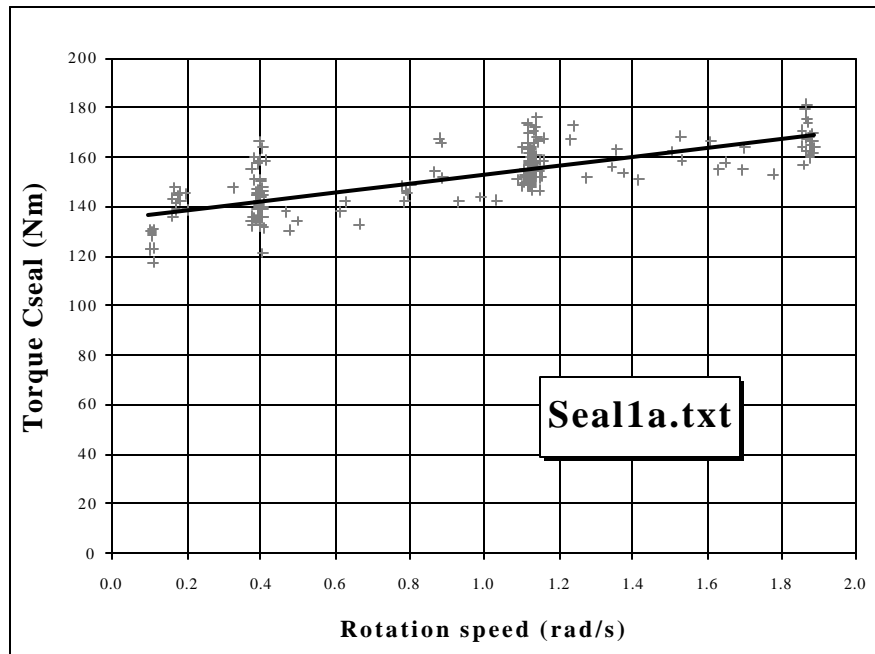
For further investigations with the CEMAGREF-IMG rheometer, it is proposed to fix blades on the surface of the inner cylinder to avoid slippage.

Experimental and fitted torque-rotation speed curves

C seal: torque applied to the seal alone

Net torque: is torque really applied to the concrete sample

MIXTURE 1

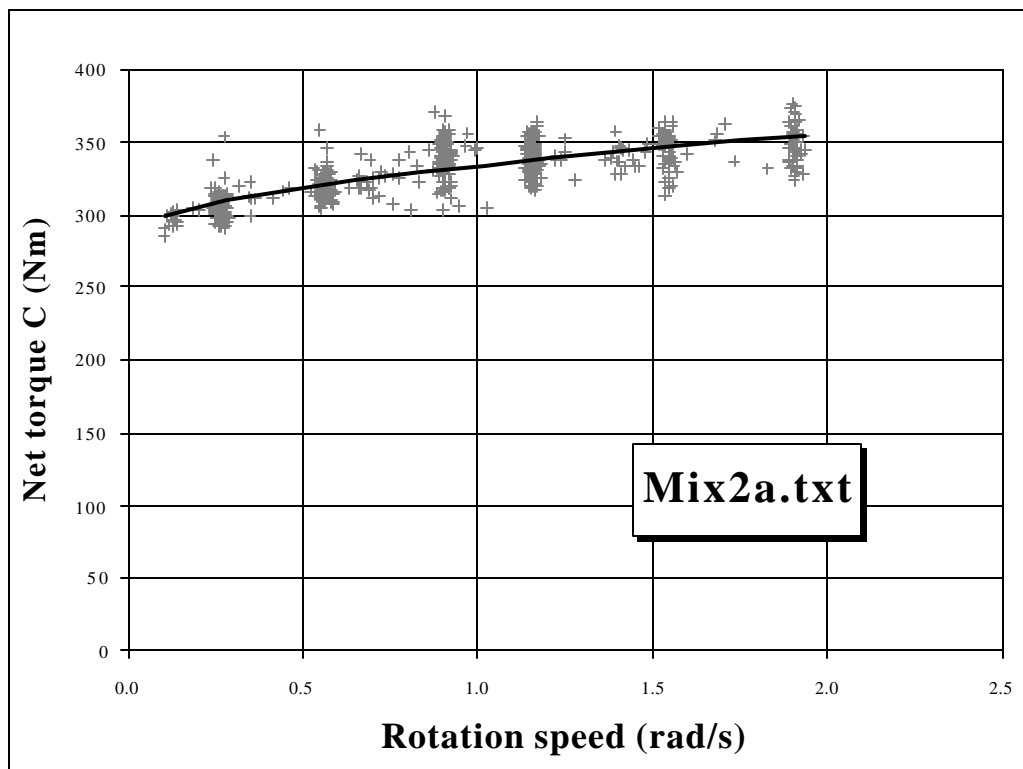
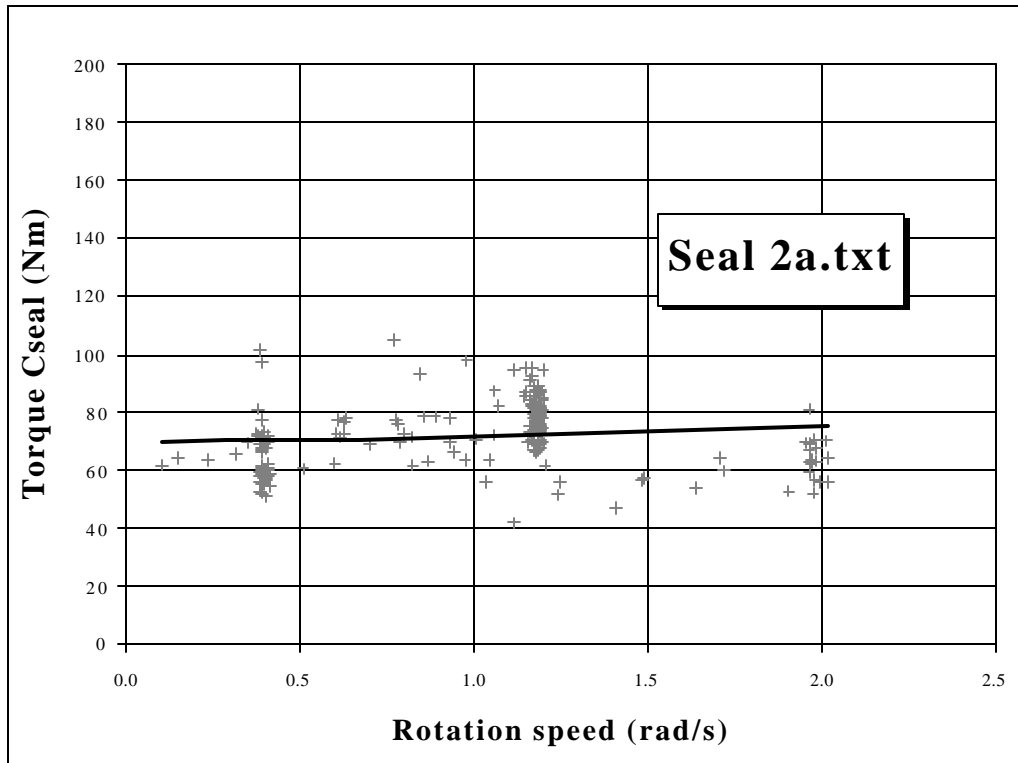


Legend

+ Experimental values
Section 3.3)

- Curve fitting (see Equation 28 and equation 29 in

MIXTURE 2

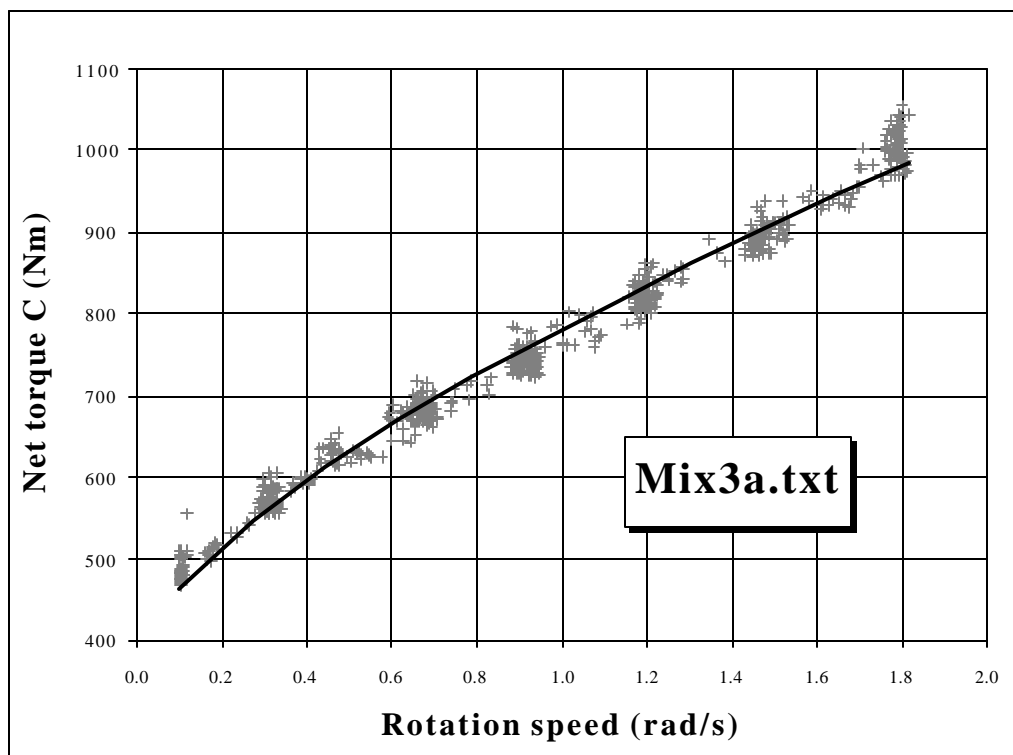
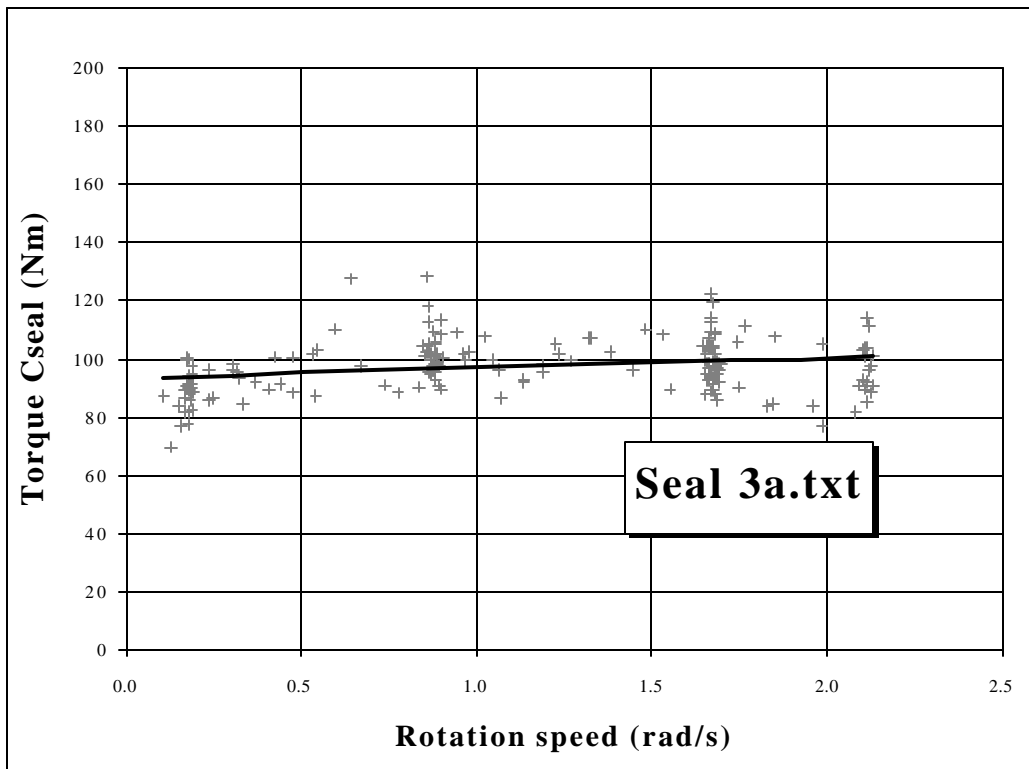


Legend

+ Experimental values

— Curve fitting (see Equation 28 and equation 29 in Section 3.3).

MIXTURE 3

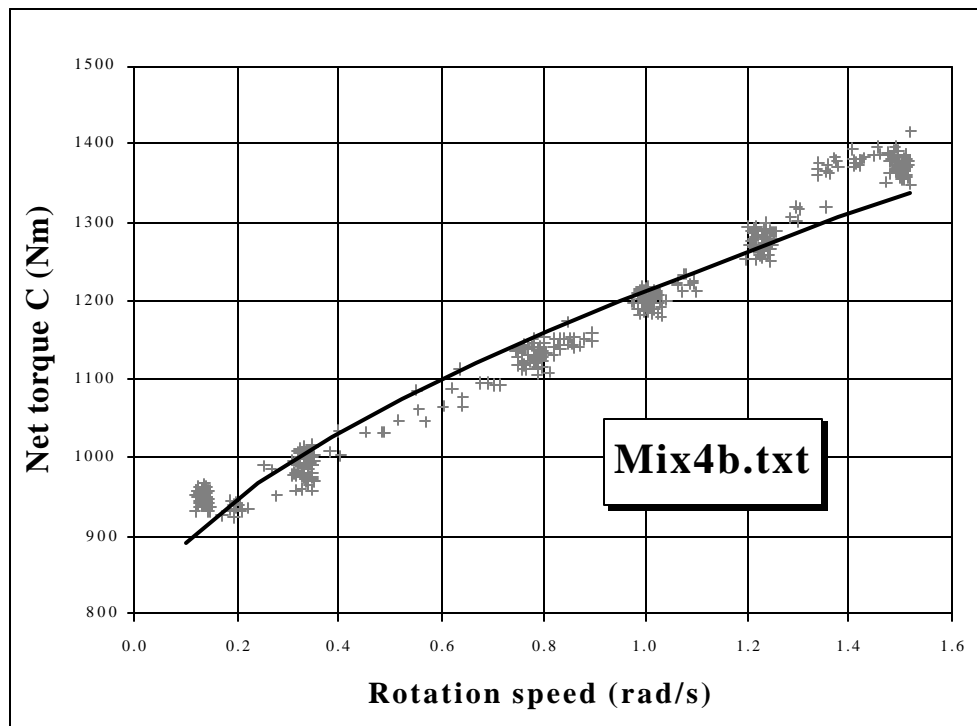
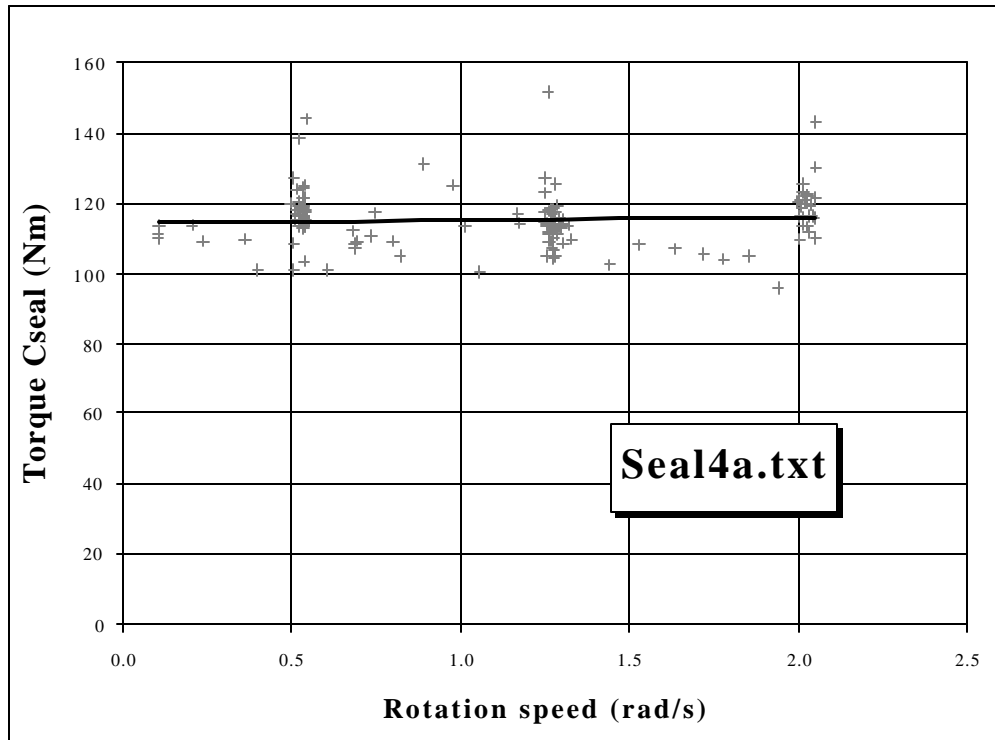


Legend

· + Experimental values

— Curve fitting (see Equation 28 and equation 29 in Section 3.3).

MIXTURE 4

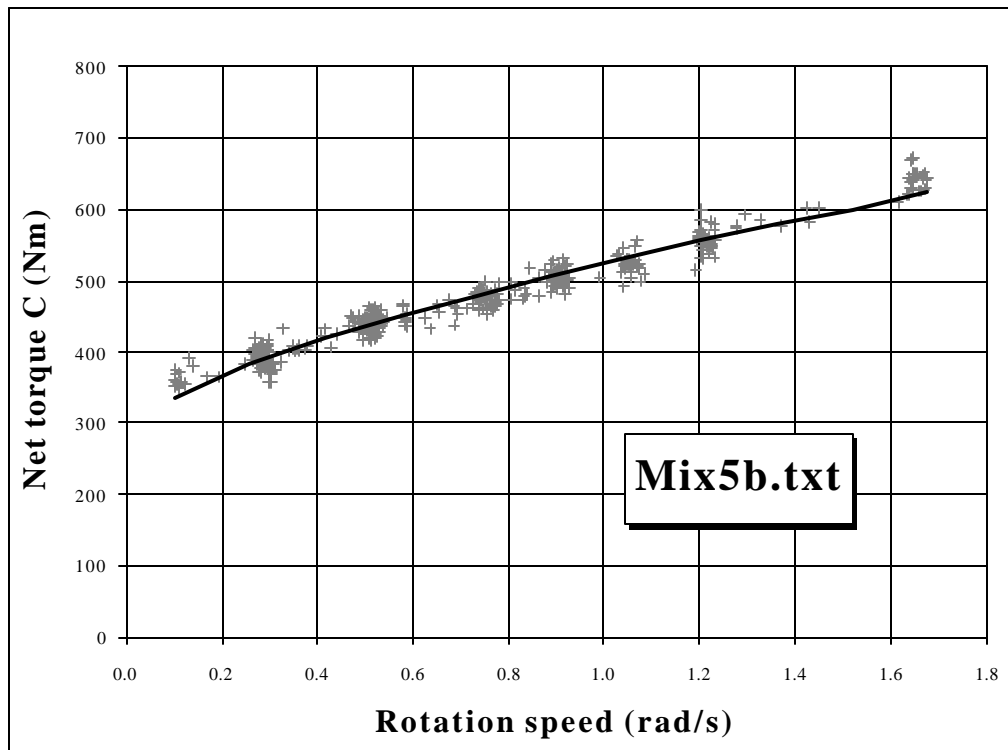
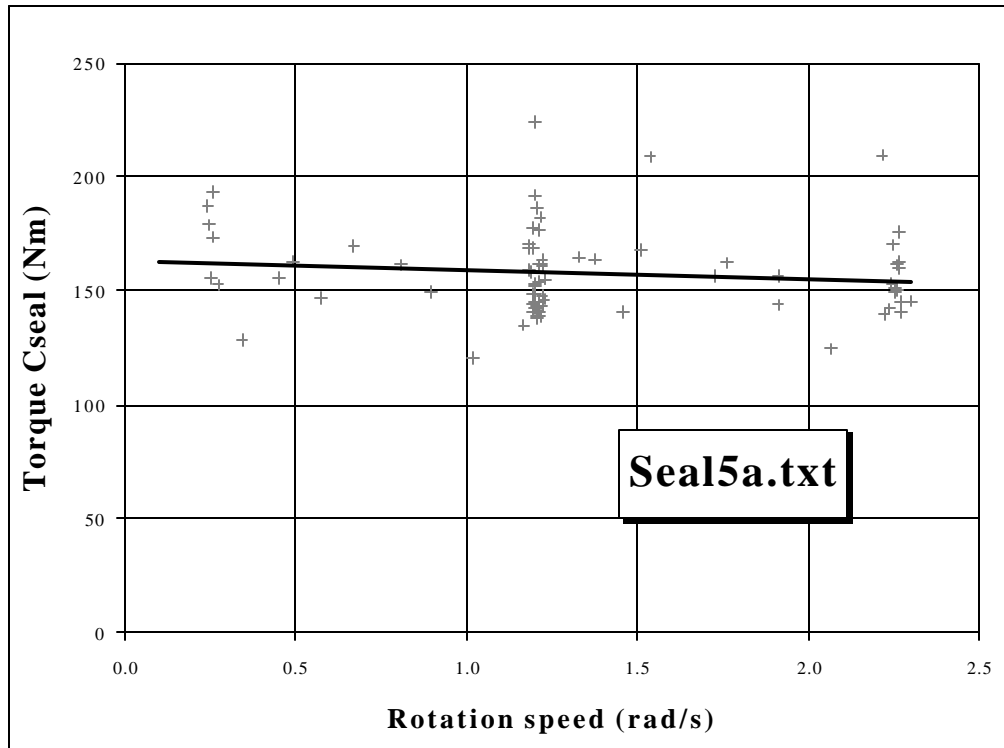


Legend

+ Experimental values
 - Curve fitting (see Equation 28 and equation 29 in Section 3.3).

- Curve fitting (see Equation 28 and equation 29 in Section 3.3).

MIXTURE 5



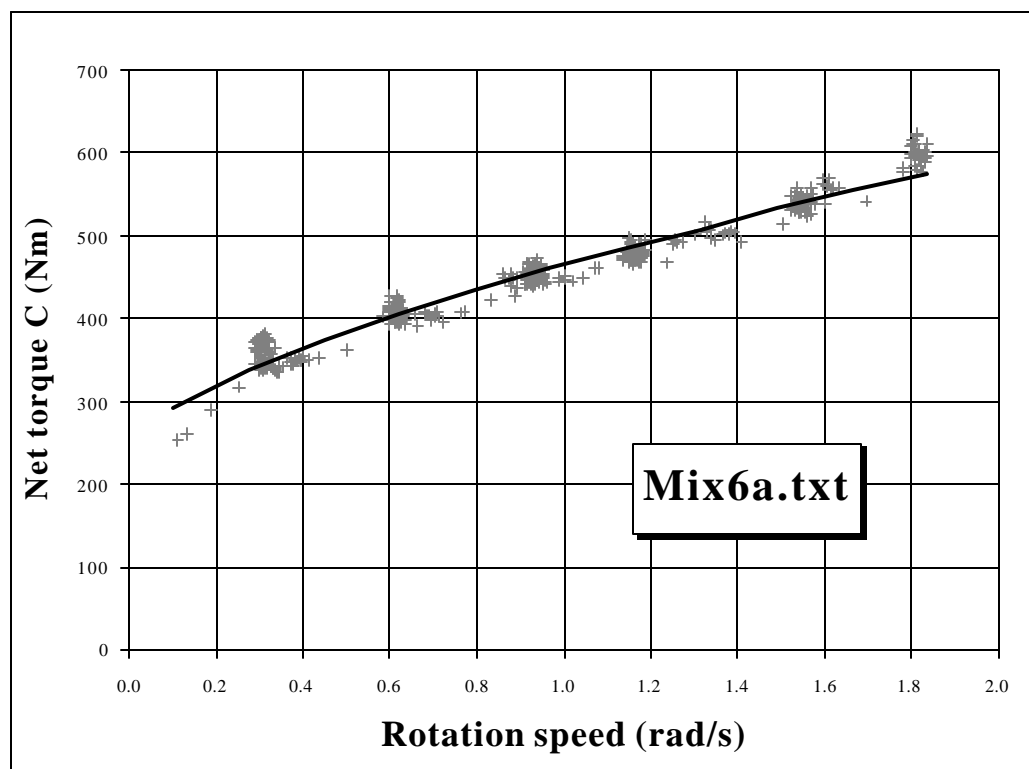
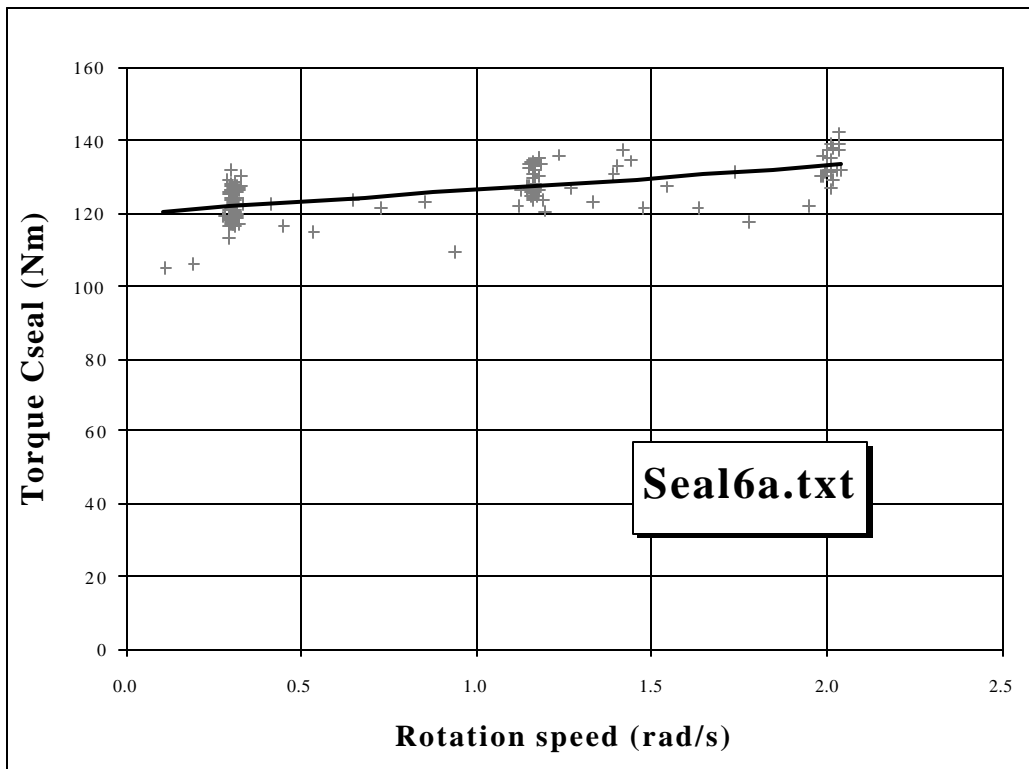
Legend

· + Experimental values

$\frac{3}{4}\frac{3}{4}$ - Curve fitting (see Equation 28 and equation 29 in

Section 3.3).

MIXTURE 6

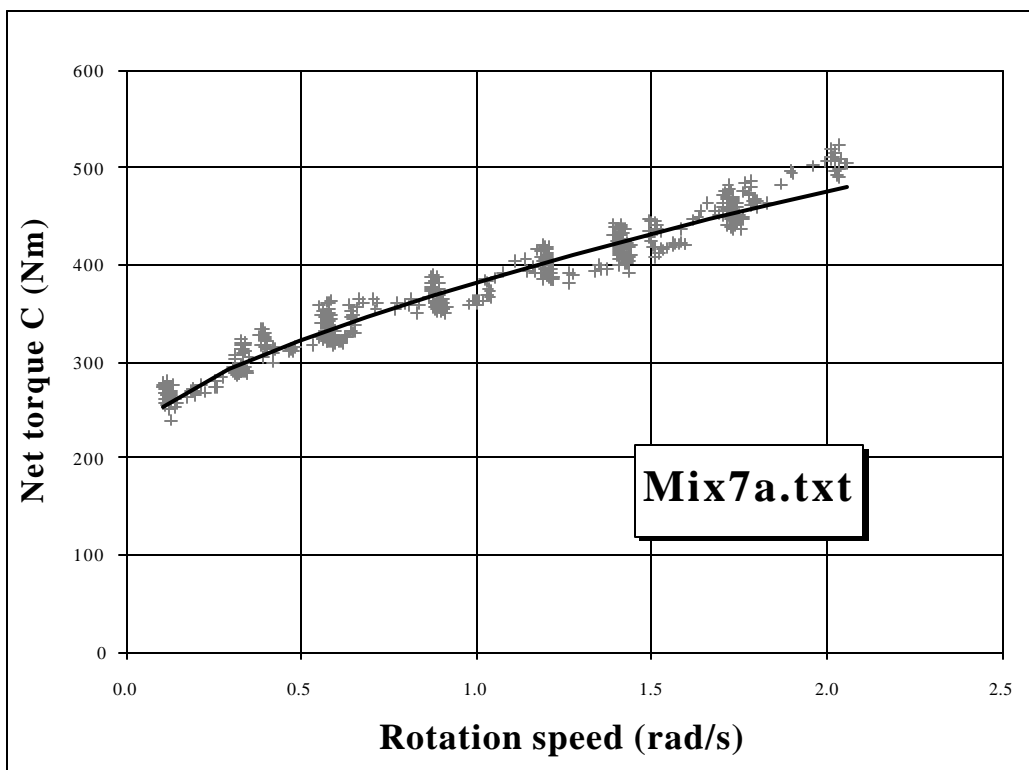
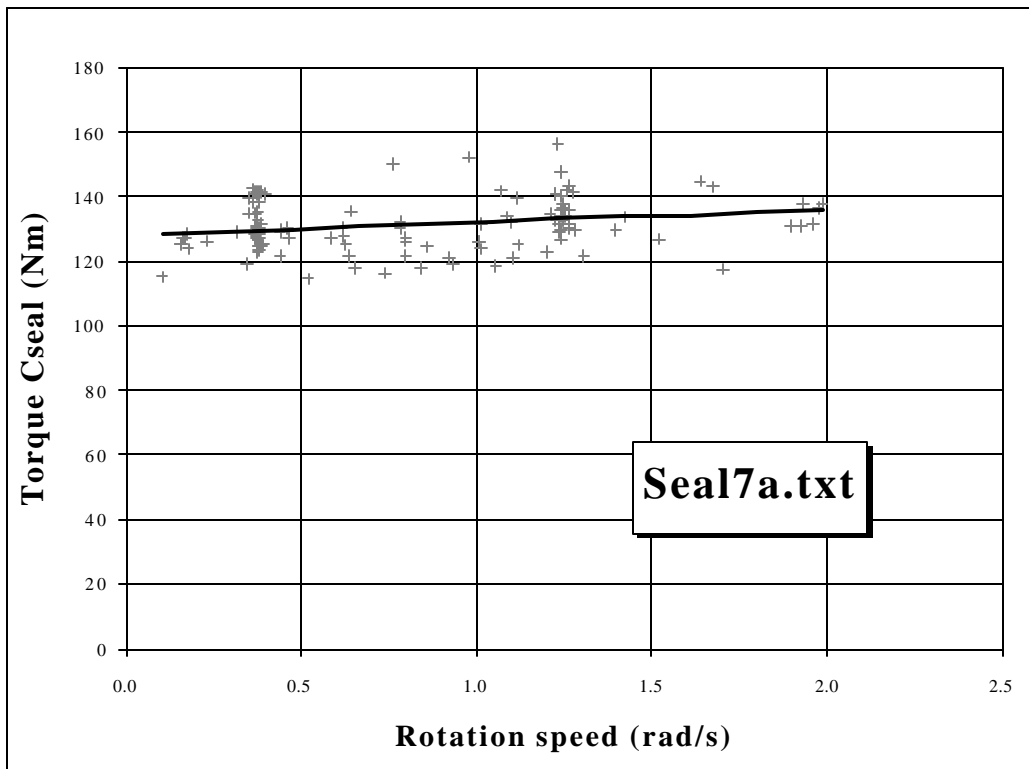


Legend

+ Experimental values

— Curve fitting (see Equation 28 and equation 29 in Section 3.3).

MIXTURE 7

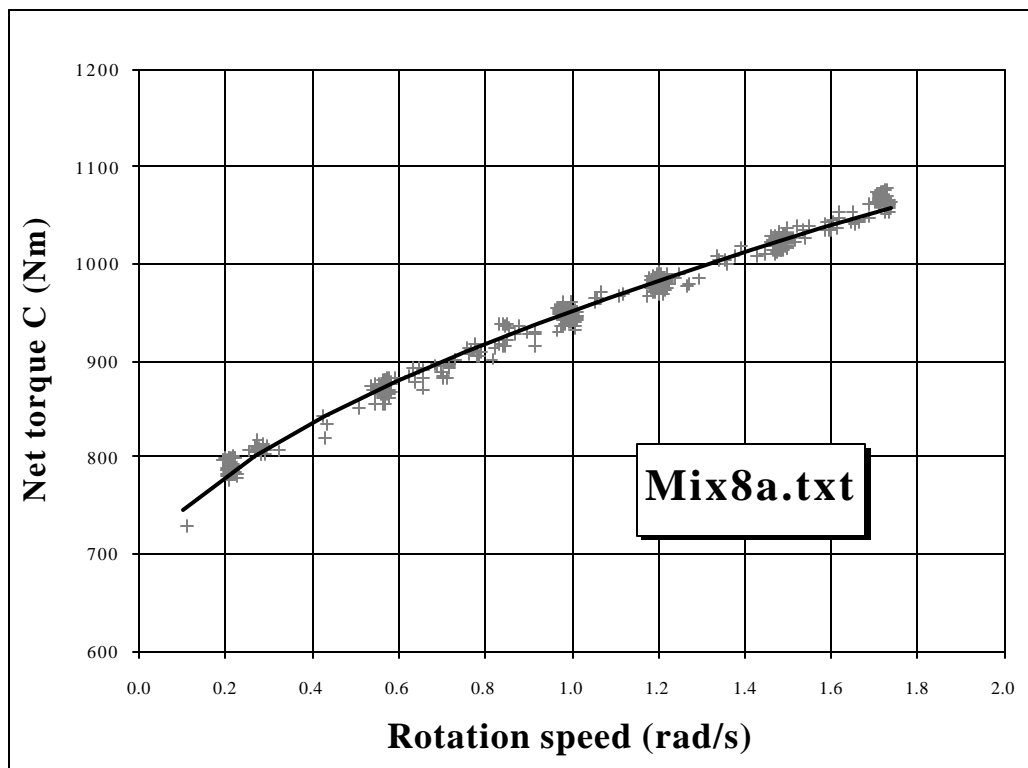
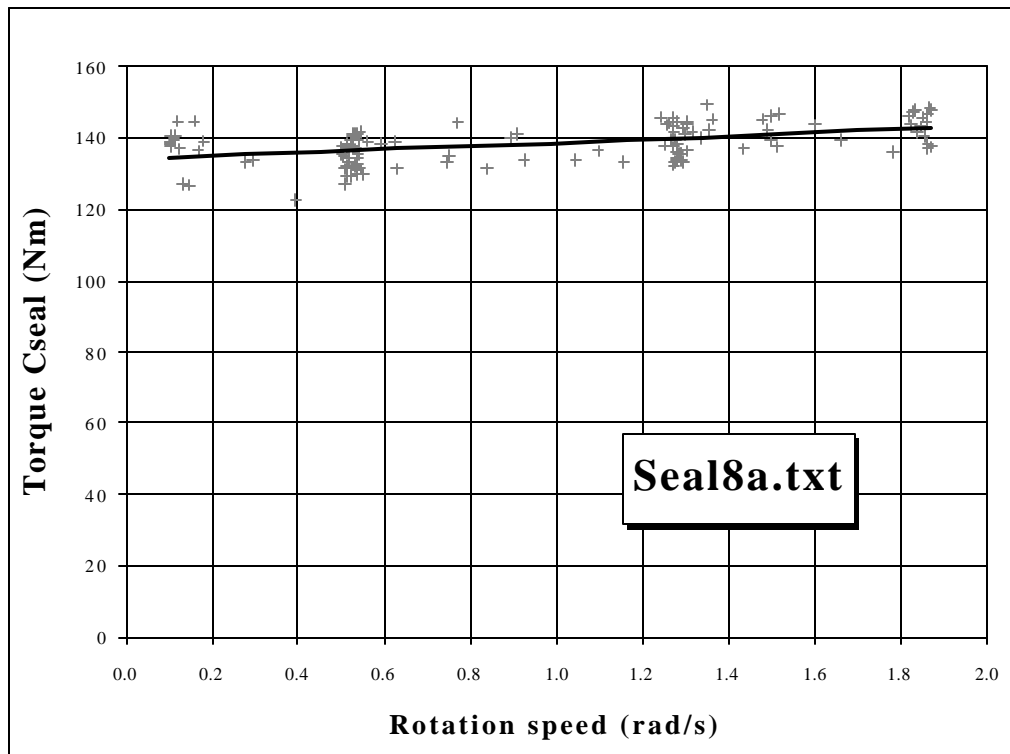


Legend

· + Experimental values
3.3).

$\frac{3}{4}\frac{3}{4}$ - Curve (see Equation 28 and equation 29 in Section

MIXTURE 8

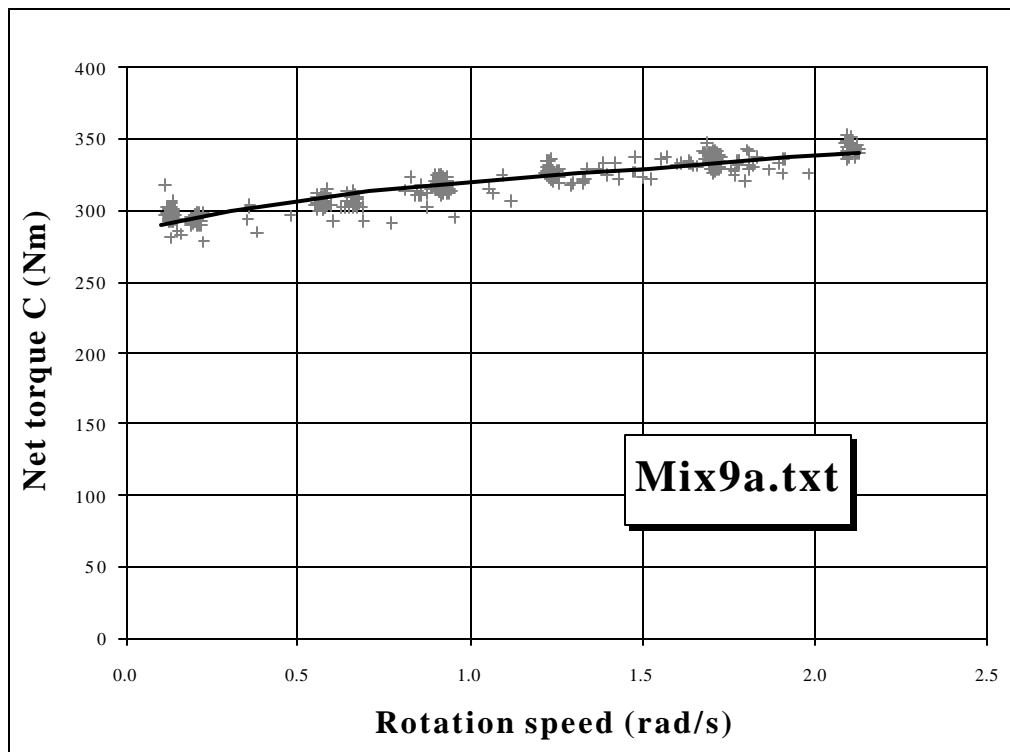
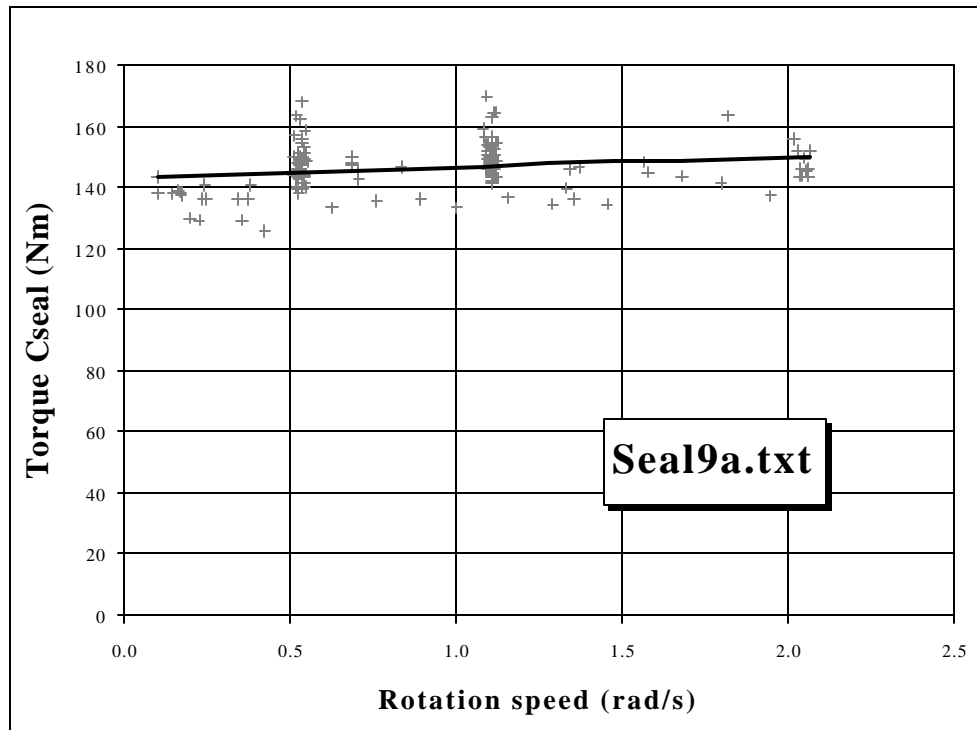


Legend

+ Experimental values

— Curve fitting (see Equation 28 and equation 29 in Section 3.3).

MIXTURE 9

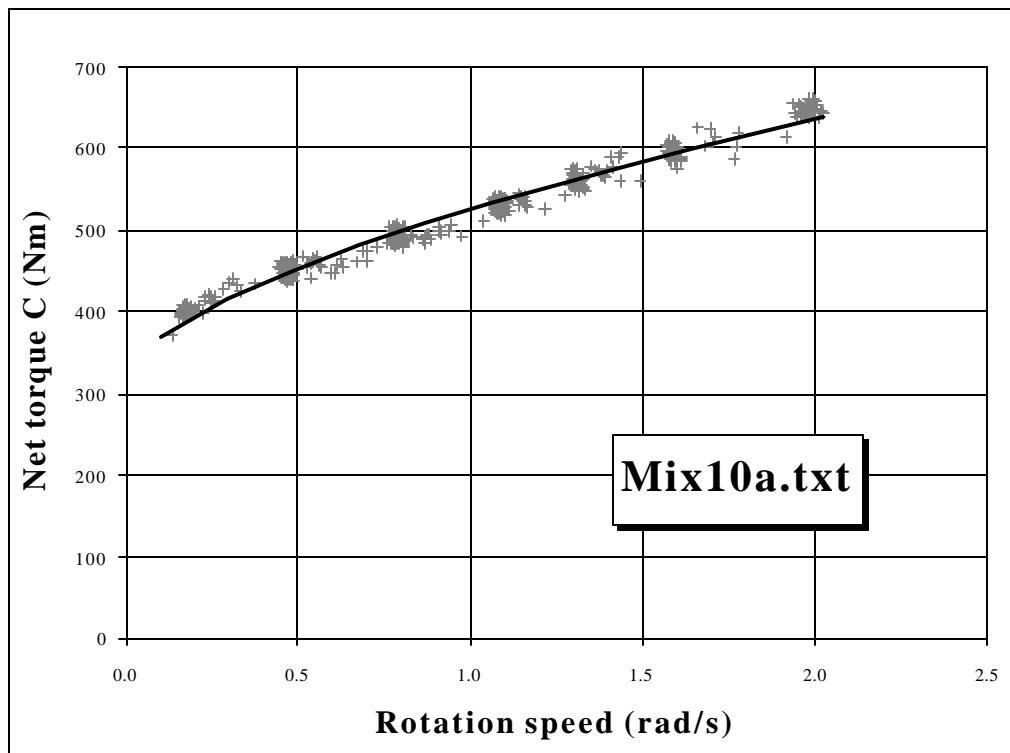
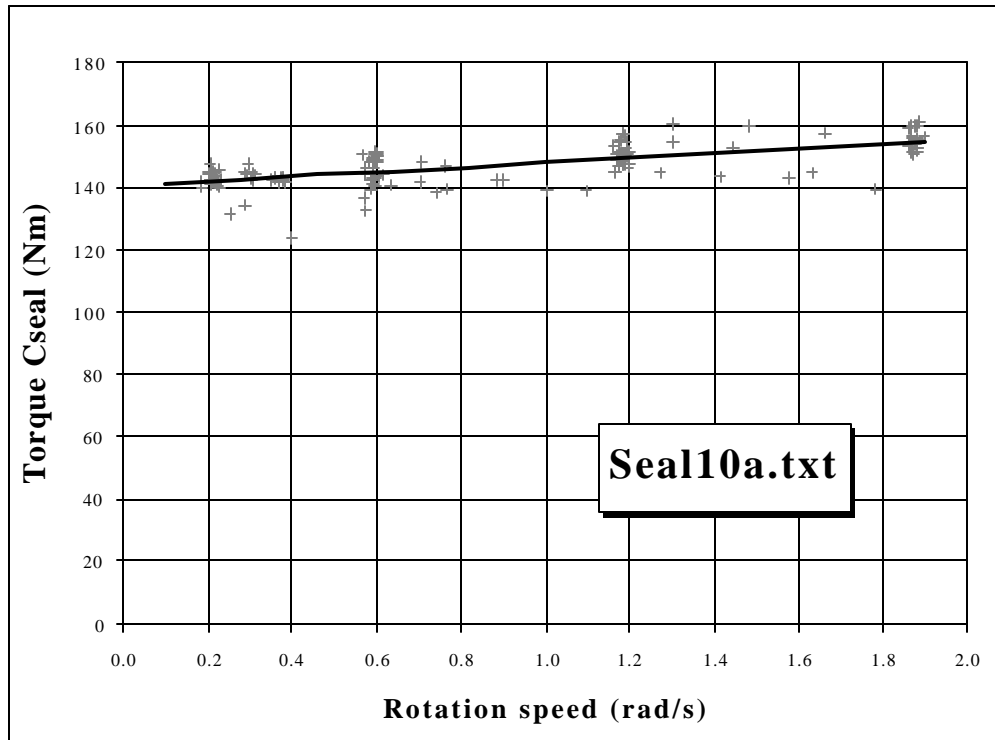


Legend

- + Experimental values

$\frac{3}{4}\frac{3}{4}$ - Curve fitting (see Equation 28 and equation 29 in Section 3.3).

MIXTURE 10



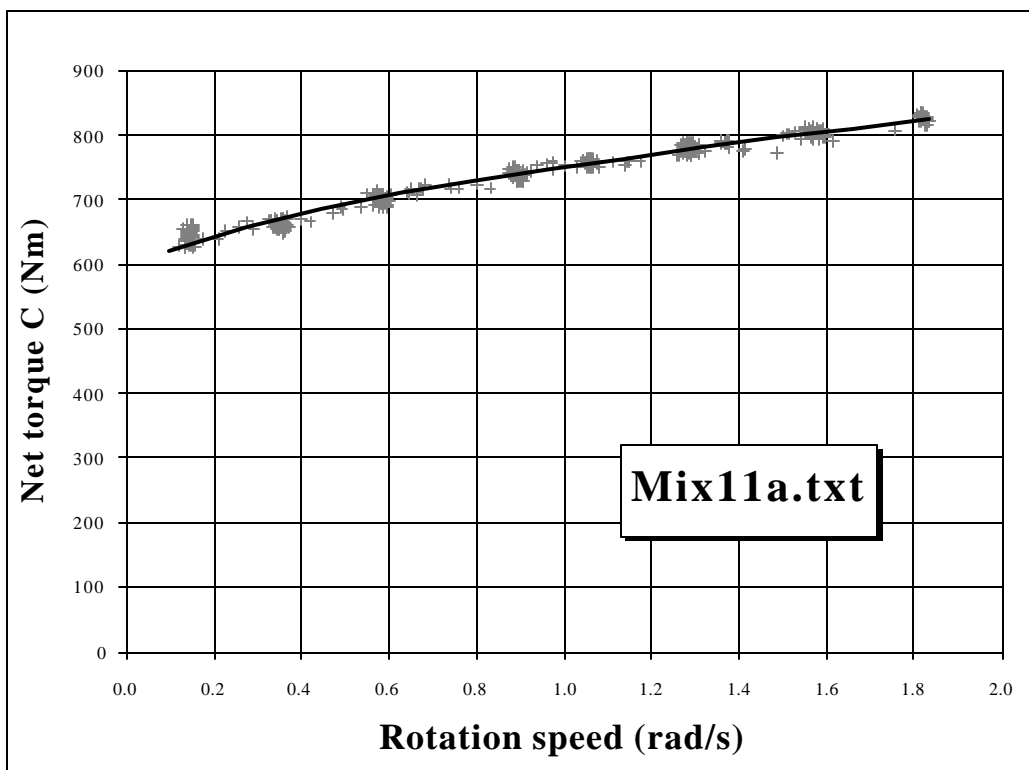
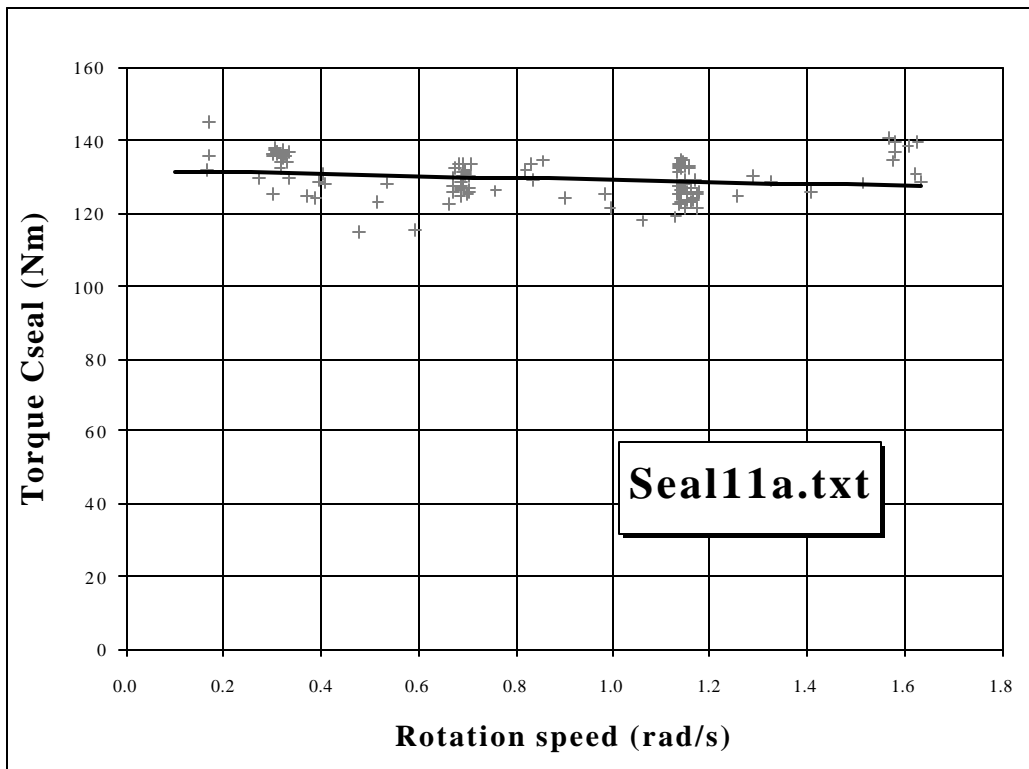
Legend

+ Experimental values

— Curve fitting (see Equation 28 and equation 29 in

Section 3.3).

MIXTURE 11

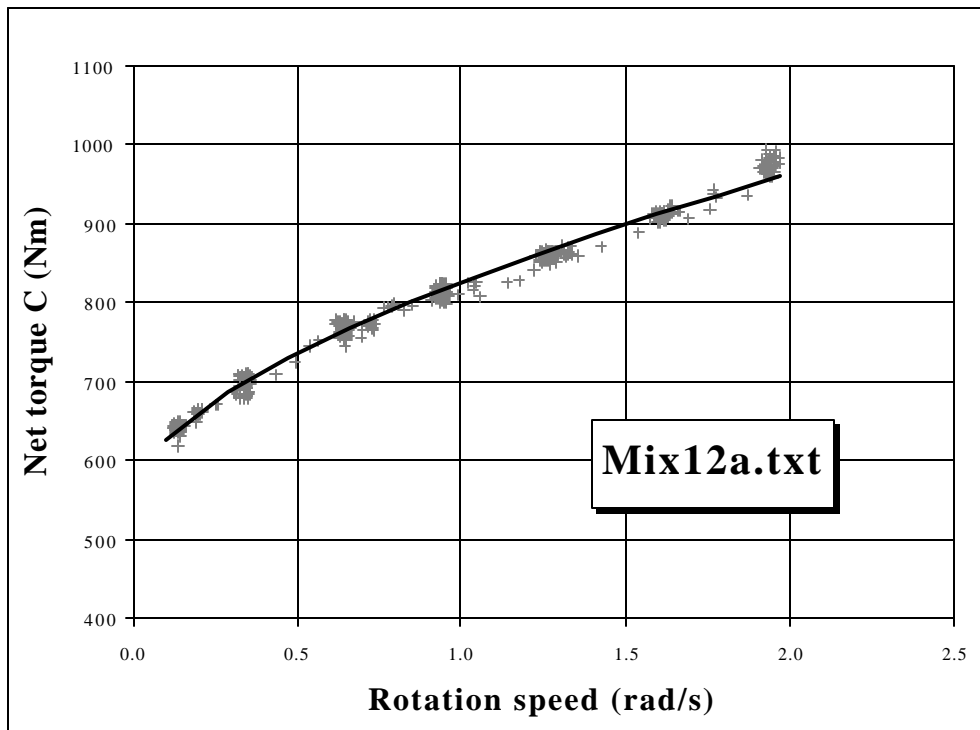
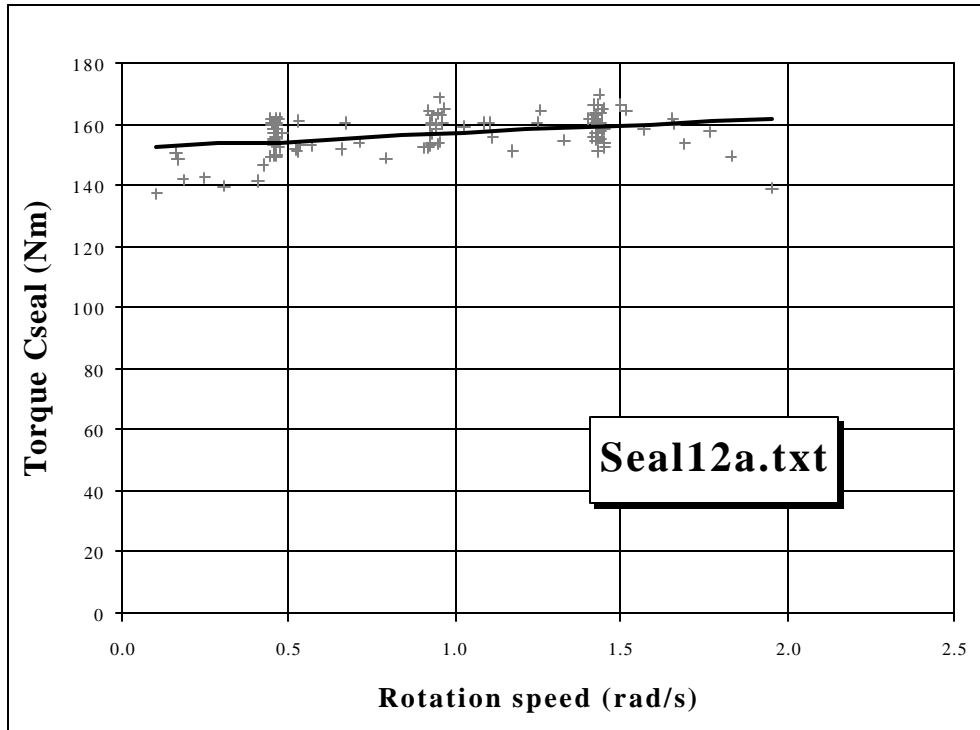


Legend

+ Experimental values

$\frac{3}{4}\frac{3}{4}$ - Curve fitting (see Equation 28 and equation 29 in Section 3.3).

MIXTURE 12

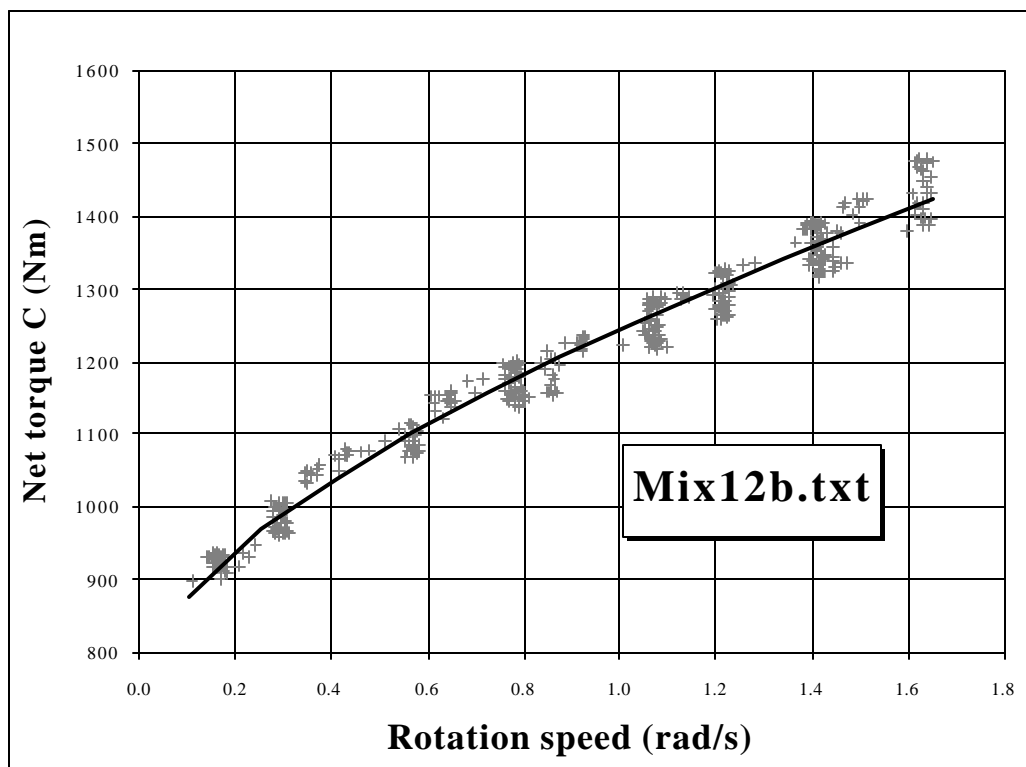
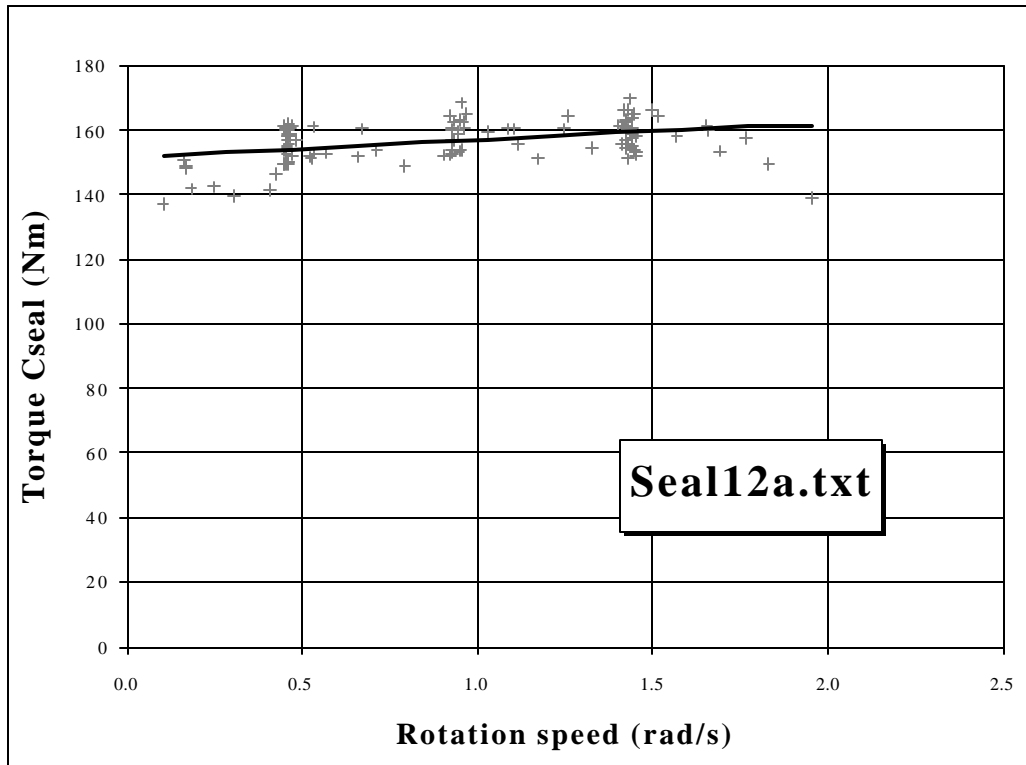


Legend

+ Experimental values

$\frac{3}{4}\frac{3}{4}$ - Curve fitting (see Equation 28 and equation 29 in Section 3.3).

MIXTURE 12 (second test)



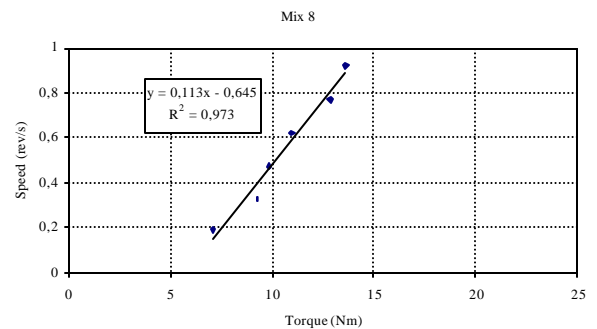
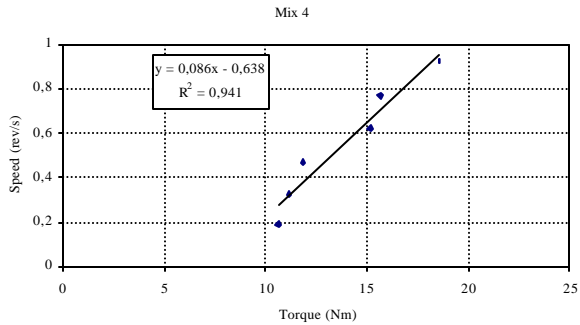
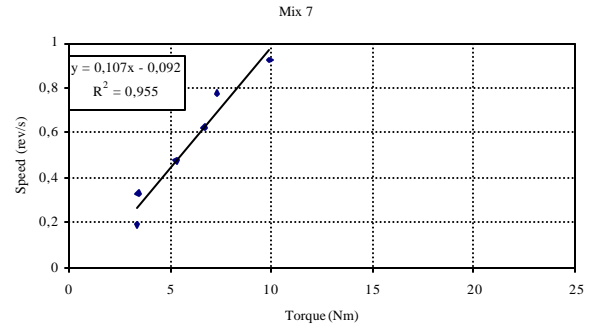
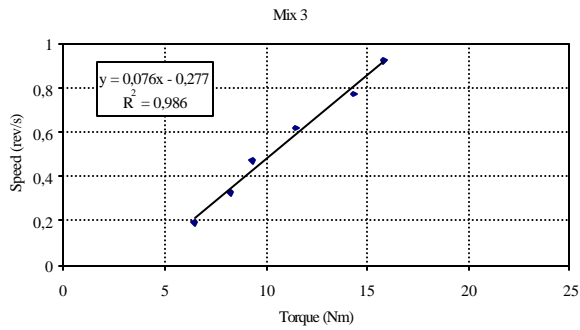
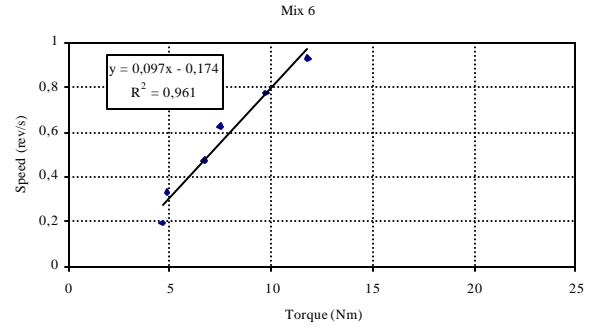
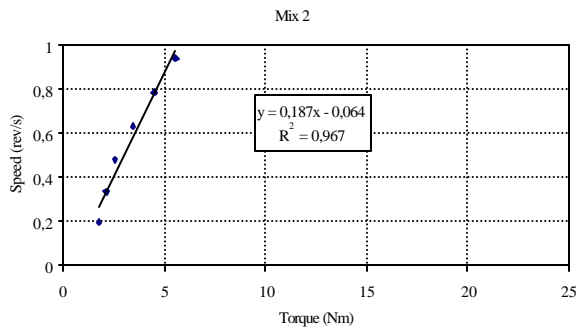
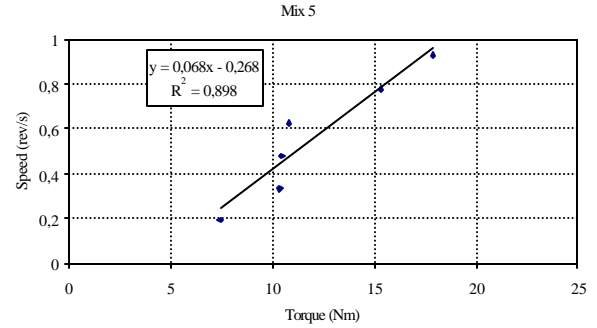
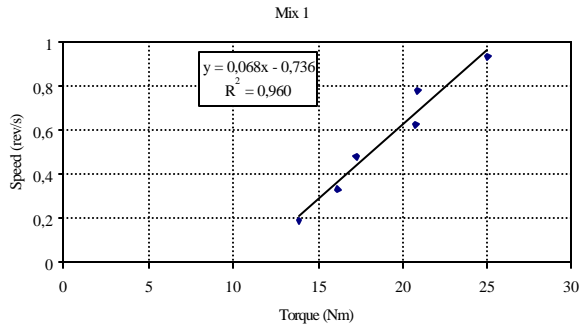
Legend

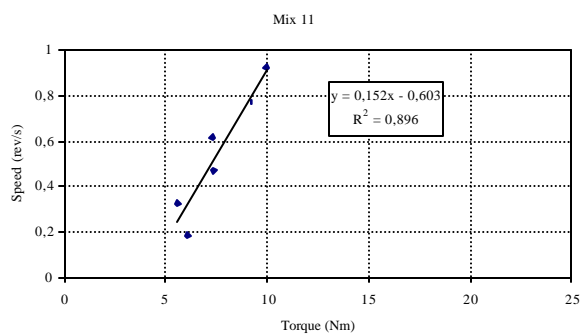
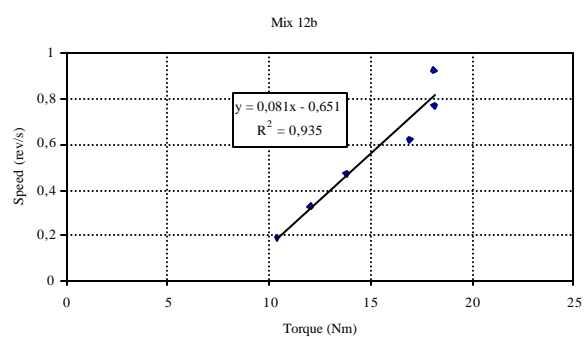
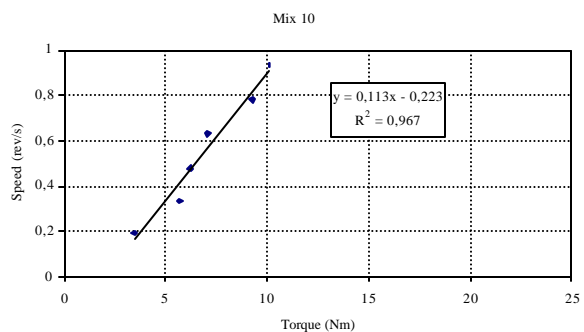
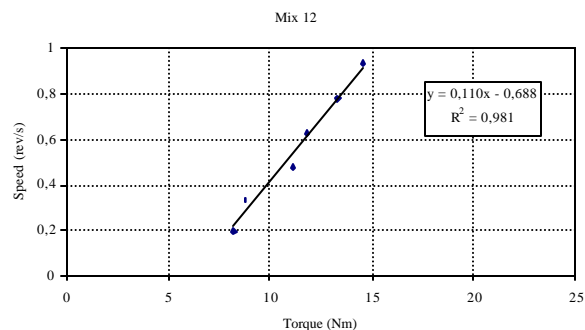
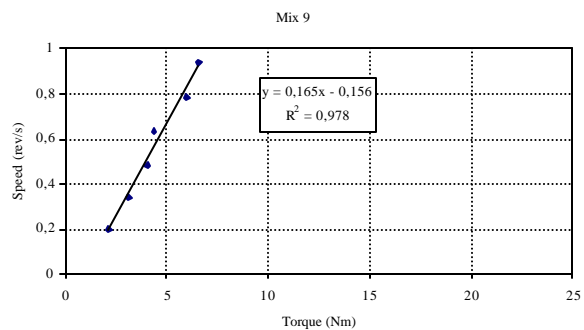
+ Experimental values

— Curve fitting (see Equation 28 and equation 29 in Section 3.3).

Data and graphs obtained using the IBB

The dotted line represents the modified Bingham model fitted to the points.





The following tables show the data points used for the graphs above. The readings were recorded by decreasing rotation speed. The data used for calculations are from Point 1 (Point 0 is excluded) to Point 6 included. The speeds equal to 0 are not taken into account for calculations.

For each mixture the following parameters were used:

H = Yield stress; G = Viscosity; R2 = correlation factor;

M and B are parameters to calculate the yield stress and viscosity

Mixture #1: Parameters values are:

H = 14.722; G = 10.842; R2 = 0.96;

M = 0.068; B = -0.736

Point #	Torque N m	Speed Rev/s
0	26.098	0.979
1	25.02	0.931
2	20.918	0.778
3	20.808	0.626
4	17.3	0.477
5	16.223	0.334
6	13.925	0.193
7	4.222	0
8	4.04	0

Mixture #2: Parameters values are:

H = 5.345; G = 0.341; R2 = 0.966;

M = 0.187; B = -0.064

Point #	Torque N m	Speed Rev/s
0	6.255	0.984
1	5.535	0.937
2	4.514	0.782
3	3.447	0.629
4	2.565	0.479
5	2.15	0.336
6	1.778	0.195
7	0.522	0
8	0.289	0

Mixture #3: Parameters values are:

H = 13.207; G = 3.669; R2 = 0.986;

M = 0.076; B = -0.278

Point #	Torque N m	Speed Rev/s
0	17.777	0.97
1	15.824	0.925
2	14.319	0.77
3	11.447	0.62
4	9.305	0.471
5	8.263	0.328
6	6.487	0.191
7	1.571	0
8	1.058	0

Mixture #4: Parameters values are:

H = 11.656; G = 7.438; R2 = 0.941;

M = 0.086; B = -0.638

Point #	Torque N m	Speed Rev/s
0	19.531	0.969
1	18.547	0.924
2	15.629	0.768
3	15.193	0.62
4	11.867	0.469
5	11.142	0.324
6	10.634	0.189
7	4.464	0
8	4.81	0

Mixture #5: Parameters values are:
H = 14.612; G = 3.915; R2 = 0.898;
M = 0.068; B = -0.268

Point #	Torque N m	Speed Rev/s
0	21.627	0.978
1	17.891	0.93
2	15.334	0.779
3	10.834	0.626
4	10.45	0.479
5	10.354	0.334
6	7.462	0.195
7	4.327	0
8	4.04	0

Mixture #8: Parameters values are:
H = 8.846; G = 5.71; R2 = 0.973;
M = 0.113; B = -0.645

Point #	Torque N m	Speed Rev/s
0	16.26	0.974
1	13.58	0.923
2	12.853	0.772
3	10.917	0.621
4	9.833	0.473
5	9.247	0.326
6	7.064	0.189
7	3.208	0
8	3.559	0

Mixture #6: Parameters values are:
H = 10.314; G = 1.8; R2 = 0.961;
M = 0.097; B = -0.174

Point #	Torque N m	Speed Rev/s
0	14.375	0.977
1	11.748	0.927
2	9.675	0.774
3	7.469	0.622
4	6.686	0.474
5	4.822	0.329
6	4.61	0.191
7	0.763	0
8	0.962	0

Mixture #9: Parameters values are:
H = 6.062; G = 0.948; R2 = 0.978;
M = 0.165; B = -0.156

Point #	Torque N m	Speed Rev/s
0	7.057	0.989
1	6.559	0.94
2	5.951	0.785
3	4.339	0.633
4	4.032	0.484
5	3.142	0.338
6	2.132	0.197
7	0.966	0
8	0.577	0

Mixture #7: Parameters values are:
H = 9.311; G = 0.856; R2 = 0.955;
M = 0.107; B = -0.092

Point #	Torque N m	Speed Rev/s
0	11.378	0.975
1	9.906	0.926
2	7.332	0.774
3	6.684	0.624
4	5.3	0.473
5	3.434	0.329
6	3.348	0.19
7	0.541	0
8	0.192	0

Mixture #10: Parameters values are:
H = 8.883; G = 1.982; R2 = 0.967;
M = 0.113; B = -0.223

Point #	Torque N m	Speed Rev/s
0	11.695	0.984
1	10.053	0.934
2	9.244	0.781
3	7.04	0.629
4	6.208	0.478
5	5.669	0.335
6	3.455	0.195
7	1.019	0
8	1.443	0

Mixture #11: Parameters values are:
H = 6.568; G = 3.959; R2 = 0.896;
M = 0.152; B = -0.603

Point #	Torque N m	Speed Rev/s
0	12.497	0.975
1	9.985	0.926
2	9.168	0.773
3	7.314	0.62
4	7.375	0.472
5	5.555	0.327
6	6.084	0.189
7	3.127	0
8	2.982	0

Mixture #12b: Parameters values are:
H = 12.359; G = 8.049; R2 = 0.935;
M = 0.081; B = -0.651

Point #	Torque N m	Speed Rev/s
0	19.739	0.978
1	18.056	0.928
2	18.141	0.774
3	16.892	0.622
4	13.809	0.473
5	12.019	0.329
6	10.366	0.192
7	4.362	0
8	4.137	0

Mixture #12: Parameters values are:
H = 9.074; G = 6.237; R2 = 0.98;
M = 0.11; B = -0.687

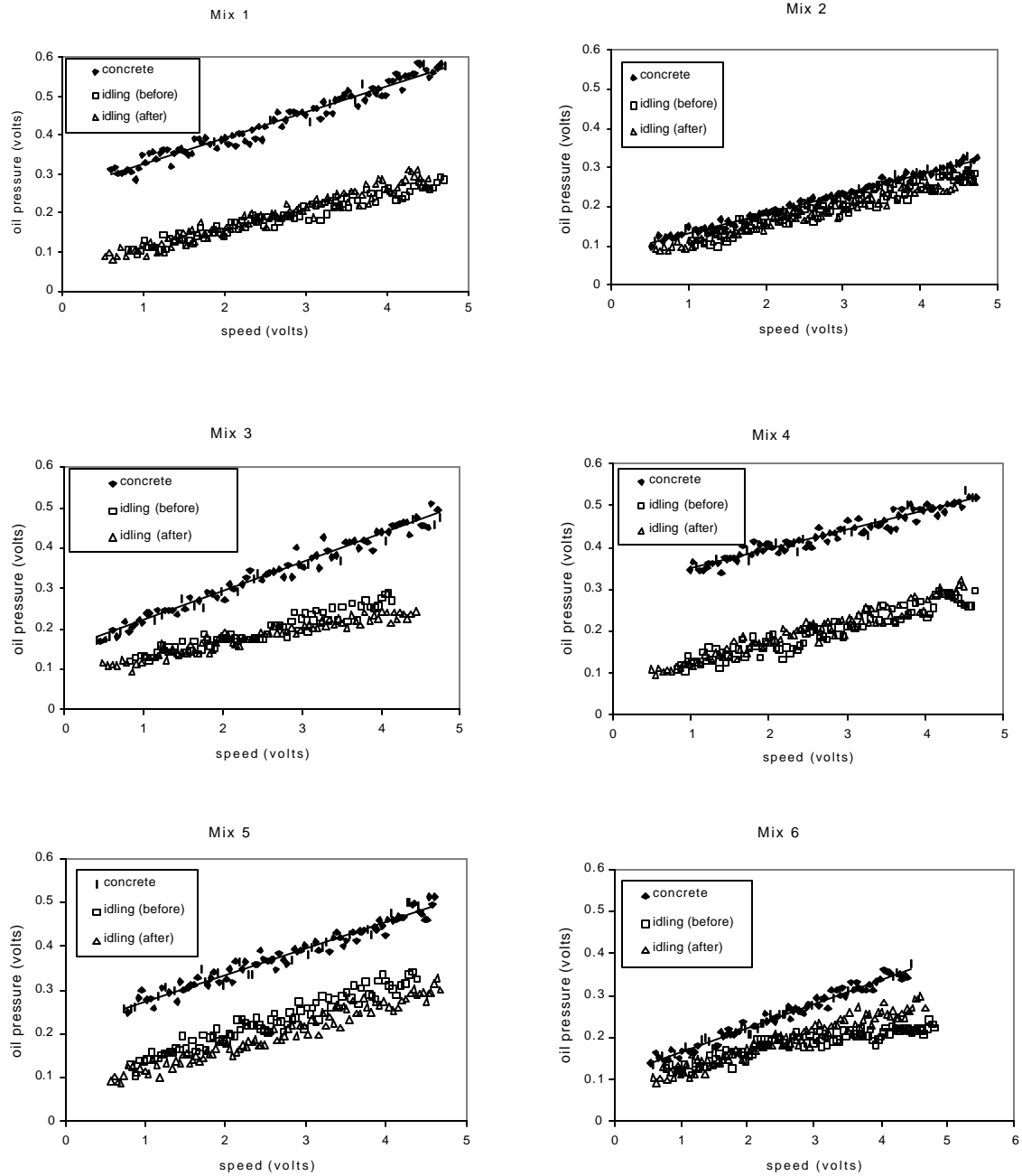
Point #	Torque N m	Speed Rev/s
0	15.703	0.98
1	14.563	0.933
2	13.309	0.779
3	11.814	0.629
4	11.123	0.479
5	8.77	0.333
6	8.206	0.194
7	2.819	0
8	2.694	0

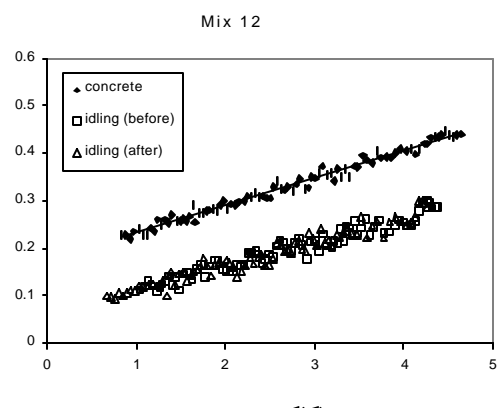
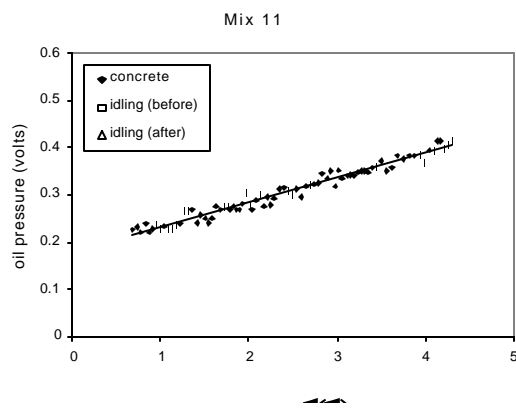
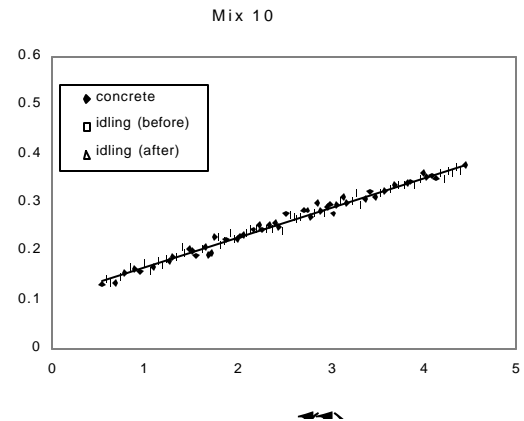
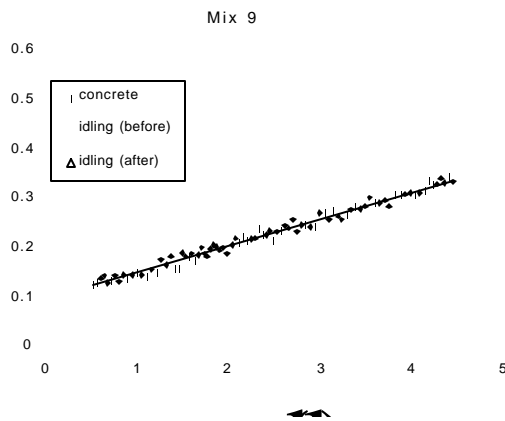
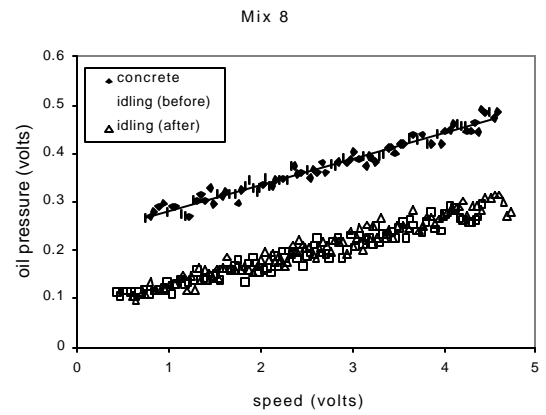
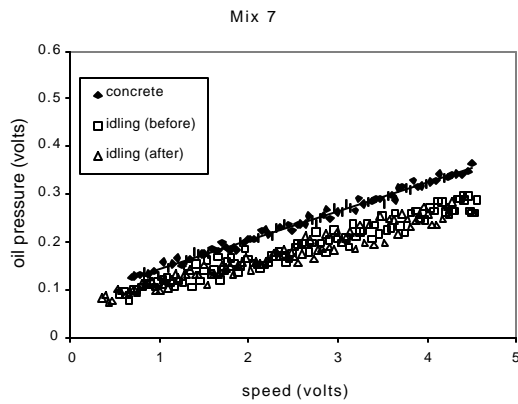
**Summary of the values
calculated from the
measurement with the IBB**

Mixture #	Plastic Viscosity Nms	Yield stress Nm
1	14.722	10.842
2	5.345	0.341
3	13.207	3.669
4	11.656	7.438
5	14.612	3.915
6	10.314	1.8
7	9.311	0.856
8	8.846	5.71
9	6.062	0.948
10	8.883	1.982
11	6.568	3.959
12	9.074	6.237

Data and graphs obtained using the Two-Point test

Details of the analysis are included in Section 3.5 of the main part of this report.





Summary of the results calculated from the figures above. Details of the calculations are given in Section 3.5 of the main part of this report.

test number	regression analysis output: oil pressure vs speed (voltages)						g (Nm)	h (Nms)	Bingham constants	
	idling			concrete (after correction)					yield stress (Pa)	plastic viscosity (Pa.s)
	intercept	slope	R ²	intercept	slope	R ²				
1	0.060	0.049	0.946	0.256	0.068	0.962	7.53	3.51	919	61
2	0.064	0.047	0.934	0.081	0.051	0.985	0.65	0.74	80	13
3	0.082	0.045	0.915	0.149	0.071	0.974	2.57	4.80	314	83
4	0.077	0.047	0.924	0.303	0.046	0.937	8.68	-	1059	-
5	0.066	0.056	0.944	0.215	0.060	0.958	5.73	1.11	698	19
6	0.077	0.044	0.934	0.108	0.057	0.974	1.19	2.40	145	41
7	0.064	0.048	0.940	0.085	0.060	0.990	0.81	2.22	98	38
8	0.081	0.06	0.943	0.228	0.053	0.967	5.65	1.29	689	22
9	0.061	0.048	0.936	0.095	0.054	0.983	1.31	1.11	159	19
10	0.054	0.054	0.940	0.108	0.060	0.985	2.07	1.11	253	19
11	0.070	0.047	0.932	0.180	0.052	0.965	4.23	0.92	516	16
12	0.062	0.050	0.936	0.174	0.057	0.982	4.30	1.29	525	22

Notes:

- Mixture 4 - plastic viscosity not measurable due to low slump, yield value should be treated with caution
- Mixtures 3, 5, 6 - idling data from single test only (others mean of two tests)

Appendix D: Calibration report for the CEMAGREF-IMG


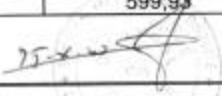
Acquisition system calibration

CONSTAT METROLOGIQUE N°00812-2000				
Instrument concerné: Carte d'acquisition lotek DAQCARD 112B Lecture sur micro ordinateur portable TOSHIBA Modèle PA1224E Appartenant à: LCPC NANTES - section ECR				
Référence utilisée : Multimètre FLUKE 8840A				
Méthode de mesure: L'opération consiste à comparer des valeurs de tension (injectée sur l'entrée de la carte d'acquisition) à celles lues sur le micro-ordinateur. La lecture des valeurs injectée est effectué avec le multimètre FLUKE.				
Description de la constatation: vérification du 10/10/2000 résolution = 0,002volt				
Valeurs lues en volts				
Référence en V	Voie CH0	Voie CH1	Référence en V	Voie CH2
-0,0001	-0,003	-0,003	-0,0002	-0,003
0,249	0,247	0,247	0,499	0,498
0,500	0,498	0,498	1,000	0,998
0,750	0,747	0,747	1,500	1,498
1,000	0,998	0,998	2,000	1,997
1,250	1,248	1,248	2,500	2,498
1,500	1,497	1,498	2,999	2,998
1,750	1,748	1,748	3,499	3,498
2,000	1,997	1,997	3,999	3,998
2,250	2,248	2,248	4,499	4,498
2,500	2,498	2,498	4,999	4,998
2,749	2,747	2,748		
2,999	2,998	2,998		



| **Conclusion:** | | | | |
| **Agent vérificateur : GOURRAUD** | | | **Date du constat : 11/10/2000** | |

Speed-meter calibration

CONSTAT METROLOGIQUE																																																							
N°00891-2000																																																							
																																																							
Instrument concerné: Chronomètre N° 39 ECR Appartenant à LCPC NANTES section Exécution des Chantiers Routiers																																																							
Référence utilisée : Heure officielle "France Inter" mesurée à l'aide de l'horloge mère micro quartz BODET (référence 927202). N° inventaire 2354000 L'horloge est située dans la salle 057 du parc routier.																																																							
Méthode de mesure: L'opération consiste à mesurer des intervalles de temps sur l'horloge mère et à comparer ces valeurs à celles obtenues sur le chronomètre . Le chronomètre est déclenché manuellement.																																																							
Description de la constatation: vérification du 17/10/2000																																																							
<table border="1"><thead><tr><th colspan="3">Valeurs lues en secondes</th></tr><tr><th>Intervalle de temps mesuré sur l'horloge mère</th><th>valeurs chronomètre</th><th>Valeurs chronomètre</th></tr></thead><tbody><tr><td>10</td><td>10,09</td><td>9,96</td></tr><tr><td>20</td><td>20,03</td><td>20,03</td></tr><tr><td>30</td><td>30,00</td><td>29,96</td></tr><tr><td>40</td><td>39,90</td><td>39,90</td></tr><tr><td>50</td><td>49,93</td><td>49,90</td></tr><tr><td>60</td><td>60,06</td><td>60,07</td></tr><tr><td>90</td><td>90,06</td><td>90,00</td></tr><tr><td>120</td><td>119,96</td><td>119,90</td></tr><tr><td>180</td><td>180,06</td><td>179,87</td></tr><tr><td>240</td><td>240,12</td><td>239,93</td></tr><tr><td>300</td><td>300,06</td><td>299,84</td></tr><tr><td>360</td><td>360,03</td><td>359,84</td></tr><tr><td>420</td><td>420,03</td><td>419,96</td></tr><tr><td>480</td><td>480,15</td><td>479,87</td></tr><tr><td>540</td><td>540,00</td><td>539,87</td></tr><tr><td>600</td><td>600,00</td><td>599,93</td></tr></tbody></table>		Valeurs lues en secondes			Intervalle de temps mesuré sur l'horloge mère	valeurs chronomètre	Valeurs chronomètre	10	10,09	9,96	20	20,03	20,03	30	30,00	29,96	40	39,90	39,90	50	49,93	49,90	60	60,06	60,07	90	90,06	90,00	120	119,96	119,90	180	180,06	179,87	240	240,12	239,93	300	300,06	299,84	360	360,03	359,84	420	420,03	419,96	480	480,15	479,87	540	540,00	539,87	600	600,00	599,93
Valeurs lues en secondes																																																							
Intervalle de temps mesuré sur l'horloge mère	valeurs chronomètre	Valeurs chronomètre																																																					
10	10,09	9,96																																																					
20	20,03	20,03																																																					
30	30,00	29,96																																																					
40	39,90	39,90																																																					
50	49,93	49,90																																																					
60	60,06	60,07																																																					
90	90,06	90,00																																																					
120	119,96	119,90																																																					
180	180,06	179,87																																																					
240	240,12	239,93																																																					
300	300,06	299,84																																																					
360	360,03	359,84																																																					
420	420,03	419,96																																																					
480	480,15	479,87																																																					
540	540,00	539,87																																																					
600	600,00	599,93																																																					
Conclusion: 																																																							
Agent vérificateur : sedran	Date du constat : 24/10/2000																																																						

CONSTAT METROLOGIQUE

N°00892-2000



Instrument concerné:

Capteur de vitesse de rotation (dynamo tachymétrique)
Radio Energie Type RN14, n°1122504
Appartenant à LCPC NANTES section Exécution des Chantiers Routiers

Référence utilisée :

Chronomètre n°39 ECR
Carte d'acquisition IOTEK DAQCARD 112B micro ordinateur TOSHIBA PA122E

Méthode de mesure:

L'opération consiste à mesurer le temps nécessaire à un repère effectué sur le couvercle du cylindre intérieur du rhéomètre pour qu'il fasse un nombre de tours défini. On enregistre en même temps le voltage généré par la dynamo, à l'aide du système d'acquisition à une fréquence de 5Hz. On compare alors la vitesse de rotation mesurée, à la moyenne du voltage enregistrée.(voir schémas page 2)

Description de la constatation:

Première série			
Nombre de tours du cylindre	Temps (s) De rotation	Ω (rad/s)vitesse de rotation du cylindre	Tension moyenne U (v) générée par la dynamo
10	28,16	2,23	-3,591
10	39,16	1,60	-2,552
10	62,22	1,01	-1,557
5	47,66	0,66	-1,001
2	43,29	0,29	-0,41
1	60,56	0,10	-0,135
		0,00	-0,002
Deuxième série			
10	28,06	2,24	-3,544
10	35,75	1,76	-2,749
10	52,37	1,20	-1,818
5	48,47	0,65	-0,923
2	43,38	0,29	-0,37
1	64,65	0,10	-0,109
		0,00	-0,002

Conclusion:

Equation d'exploitation (moindre carrés)
 $\Omega = -0,6225 \cdot U + 0,0322$
 Ω (en rad/s) vitesse de rotation du cylindre. U(en volts) voltage fournie par la dynamo

Agent vérificateur : sedran

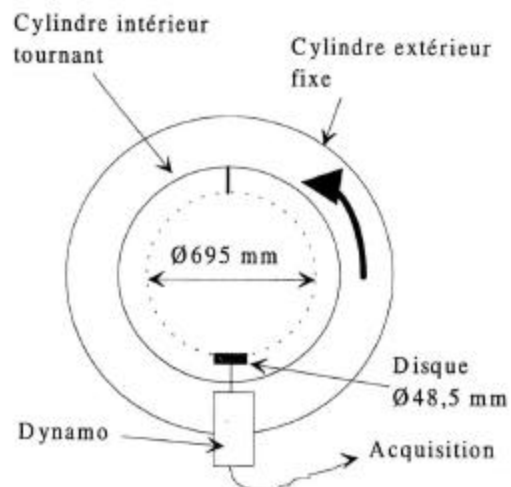
Date du constat : 24/10/2000

CONSTAT METROLOGIQUE

N°00892-2000




Schémas de montage



Torque cells calibration

CONSTAT METROLOGIQUE

N° 00776-2000



Instrument Concerné :

Deux capteurs du couplemètre du rhéomètre du CEMAGREF.
 Ponts d'extensométrie TS 205 SEDEME.
 Calibration shunt avec un $\Delta R/R$ de $1 \cdot 10^{-3}$:

- 3,117 V pour le capteur n° 1.
- 3,163 V pour le capteur n° 2.

Température : 18 °C
 Temps de préchauffage des ponts d'extensométrie : 1h

Référence utilisée (Désignation + Incertitude) :

Peson de la presse MFL 100. Certificat d'étalonnage n° 00025-2000.
 Échelle 50 %.

Méthode de mesure :

La pratique a consisté à étalonner en statique, et en traction, sur la presse MFL 100, les deux capteurs montés en série entre deux rotules.

Description de la constatation:


Force de référence	Premier cycle		Deuxième cycle		Troisième cycle		Couple * correspondant
	Capteur 1	Capteur 2	Capteur 1	Capteur 2	Capteur 1	Capteur 2	
kN	V	V	V	V	V	V	N m
0	0	0	0	0	0	0	0
5	0,581	0,582	0,582	0,584	0,582	0,585	580
10	1,16	1,161	1,161	1,163	1,162	1,166	1160
15	1,741	1,738	1,742	1,74	1,742	1,744	1740
20	2,32	2,317	2,322	2,32	2,322	2,323	2320
25	2,907	2,902	2,908	2,904	2,906	2,908	2900
20	2,319	2,313	2,32	2,315	2,323	2,32	2320
15	1,74	1,732	1,741	1,734	1,741	1,736	1740
10	1,161	1,151	1,16	1,153	1,16	1,156	1160
5	0,576	0,58	0,58	0,576	0,582	0,579	580
0	-0,005	0	0	-0,005	0	0,001	0

* Couple indiqué = Effort de référence multiplié par 0,116 m (bras de levier du couplemètre).

CONCLUSION:

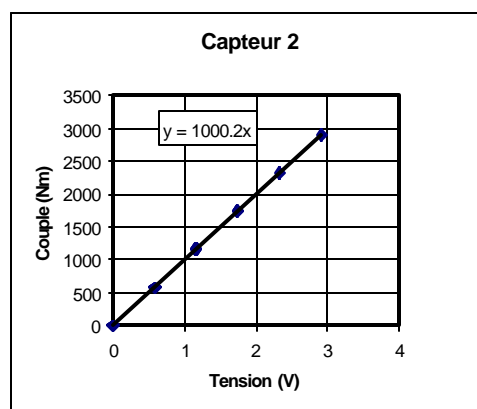
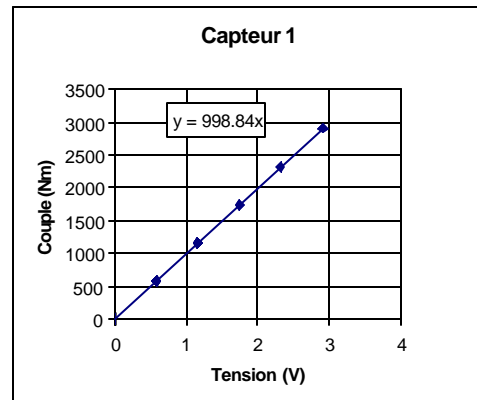
Agent vérificateur: Claude BOULAY

Date du constat : 03 / 10 / 2000



Calibration des capteur de couple du rhéomètre CEMAGREF
Constat métrologique n° 00776-2000

Capteur 1		Capteur 1	
C(Nm)	Tension (V)	C(Nm)	V
0	0	0	0
580	0.581	580	0.582
1160	1.16	1160	1.161
1740	1.741	1740	1.738
2320	2.32	2320	2.317
2900	2.907	2900	2.902
2320	2.319	2320	2.313
1740	1.74	1740	1.732
1160	1.161	1160	1.151
580	0.576	580	0.58
0	-0.005	0	0
0	0	0	0
580	0.582	580	0.584
1160	1.161	1160	1.163
1740	1.742	1740	1.74
2320	2.322	2320	2.32
2900	2.908	2900	2.904
2320	2.32	2320	2.315
1740	1.741	1740	1.734
1160	1.16	1160	1.153
580	0.58	580	0.576
0	0	0	-0.005
0	0	0	0
580	0.582	580	0.585
1160	1.162	1160	1.166
1740	1.742	1740	1.744
2320	2.322	2320	2.323
2900	2.908	2900	2.908
2320	2.323	2320	2.32
1740	1.741	1740	1.738
1160	1.16	1160	1.156
580	0.582	580	0.579
0	0	0	0.001



Appendix E: Calculation of the Kendall coefficient of concordance

Outline of the procedure for calculating Kendall's coefficient of concordance, W (summarized from Ref. [1]).

n objects have been ordered according to p criteria :

Criterion	Object	1	2		n
1		r_{11}	r_{21}		r_{n1}
2		r_{12}	r_{22}		r_{n2}
p		r_{1p}	r_{2p}		r_{np}
sum		$r_{1.}$	$r_{2.}$		$r_{n.}$
					$r_{..}$

r_{ij} is the rank of an object i according to criterion (apparatus) j . In our case, the objects are the mixtures and the criteria the rheometers.

For each line of the table, the sum of the terms is $\frac{n(n+1)}{2}$. Then $r_{ij} = p \frac{n(n+1)}{2}$.

If all the rankings are identical, all the terms in a given column are equal, and the $r_{i.}$ are equal to $p, 2p, 3p, \dots$

The following parameter is used : $S = \sum_{i=1}^n (r_{i.} - \frac{r_{ij}}{n})^2$. If all the rankings are identical, S is

maximum, and $S = S_{\max} = \frac{p^2(n^3 - n)}{12}$. Kendall's W parameter is $W = \frac{12S}{p^2(n^3 - n)}$, and

$0 \leq W \leq 1$.

The hypothesis tested here is that the p rankings are independent. The critical value of W (at 95% confidence level) are given in a reference table (not given here) for different n and p . If the calculated value of W is higher than the reference value, the hypothesis is rejected, i.e., the rankings are not independent.

Appendix F: Artifacts in Rheological Measurements

This appendix deals with some problems related to the granular nature of fresh concrete. They are not addressed in classical fluid rheology, and they may aid in interpretation of rheometric measurements dealing with concrete.

Size of tested specimen

Concrete is a heterogeneous material. For making significant measurements of any of its material properties, it is essential:

- to minimize the risk of spatial segregation; This has been done in the present program by designing mixtures with continuous grading size and sufficient fine particle proportions, and by taking precautions such as careful transport and re-mixing before sampling. The absence of segregation has been checked by a number of fresh concrete analyses (see Chapter 2);
- to test specimens, the sizes of which are large compared to the largest dimension of heterogeneity. Here, this dimension is taken as the maximum size of aggregate (MSA).

Assuming that a ratio of 10 between test specimen and MSA is acceptable, and taking a MSA of 20 mm, this would lead to a cube having a 200 mm length, which makes a volume of 8 L. However, there is not any clear threshold in this respect: the bigger the specimen, the closer the measurement is to the 'real' value. On the contrary, the smaller the specimen, the lower the correlation between the apparent and real properties.

Let us also note that it is the volume of *sheared* concrete that matters, not the total volume of concrete contained in the apparatus.

Slip at the boundaries of the specimen

All methods used to deduce 'basic' rheological parameters from bulk measurements in rheometers implicitly assume that the velocity gradient in the tested specimen is continuous up to the interface. This means that the velocity between two parallel, plane surfaces is supposed to vary linearly with distance between the surfaces. This assumption is correct for a Newtonian liquid like some oil and water, at least for low Reynolds numbers.

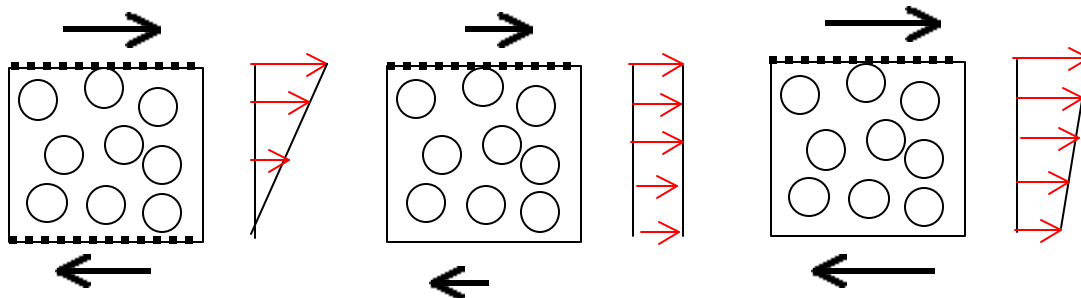


Figure F-1: Velocity gradient in a sheared layer. A) without slip; B) with slip, at low rate; C) with slip, at high rate.

However, with granular suspensions like fresh concrete, a interfacial layer forms spontaneously in the vicinity of the wall, owing to the exclusion of coarse particles, which makes the material locally more fluid than the bulk of the suspension. From a macroscopic viewpoint, everything happens as if the strain rate was concentrated in this limit layer, creating a sliding motion. This phenomenon is well known in concrete pumping technology [2]. Various authors [2, 3, 4, 5] have proposed the following model to describe this phenomenon:

$$\boldsymbol{t} = \boldsymbol{t}_{0,i} + \boldsymbol{h} \cdot \boldsymbol{v}_g \quad (\text{F- 1})$$

where τ is the shear stress, $\boldsymbol{t}_{0,i}$ is the *interfacial* yield stress, \boldsymbol{h} is the interfacial viscous constant and \boldsymbol{v}_g the sliding velocity. Of course, $\boldsymbol{t}_{0,i}$ is always smaller than the *concrete* yield stress \boldsymbol{t}_0 . This means that when a shear force is applied to the material by the wall, there is first a sliding motion (with no shear in the bulk of the concrete specimen). Concrete starts to shear only when the shear stress \boldsymbol{t} attains the yield stress, which means that the sliding velocity is high enough (see Figure F-1).

Applying this concept to the basic rheometric problem, let us assume that an ideal ‘Couette’ coaxial viscometer is used, with e being the gap between the cylinders, and R the mean radius and the ratio $e/R \ll 1$. With a conventional Bingham material, and *no slip* at the interface, the analysis of the test is performed as follows:

$$\boldsymbol{t} = \boldsymbol{t}_0 + \mu \dot{\boldsymbol{g}} \quad (\text{F- 2})$$

$$\dot{\boldsymbol{g}} = \frac{\Omega R}{e} \quad (\text{F- 3})$$

$$\Gamma = 2\boldsymbol{p} R^2 h \boldsymbol{t} \quad (\text{F- 4})$$

$$\frac{\Gamma}{2\boldsymbol{p} R^2 h} = \boldsymbol{t}_0 + \mu \left(\frac{R}{e} \Omega \right) \quad (\text{F- 5})$$

where

- \boldsymbol{G} is the torque (in N·m);
- h is the height of the specimen (in m);
- μ is the concrete plastic viscosity (in Pa·s); and
- \boldsymbol{W} the relative angular speed (in rad/s) between the two cylinders.

To deduce the basic parameters \mathbf{t}_0 and μ from the macroscopic measurements, the strategy is to plot the ratio $\frac{\Gamma}{2\mathbf{p}R^2 h}$ as a function of $\frac{R}{e} \Omega$, then to identify the yield stress with the intercept and the plastic viscosity with the slope of the obtained straight line.

Now, let suppose that a slip, described by Equation F-1, to take place at the exterior interface. When the slip velocity is high enough, the relationship between the torque and the angular speed is still linear, and we have:

$$\dot{\mathbf{g}} = \frac{\Omega R - v_g}{e} \quad (\text{F- 6})$$

$$\mathbf{t} = \mathbf{t}_0 + \mu \frac{\Omega R - v_g}{e} = \mathbf{t}_{0,i} + \mathbf{h} v_g \quad (\text{F- 7})$$

which gives finally, when the concrete specimen is sheared:

$$\frac{\Gamma}{2\mathbf{p}R^2 h} = \mathbf{t}_0^{ap.} + \mu^{ap.} \left(\frac{R}{e} \Omega \right) \quad (\text{F-8})$$

where

$$\mathbf{t}_0^{ap.} = \frac{\mathbf{h}}{\mu/e + \mathbf{h}} \mathbf{t}_0 + \frac{\mu/e}{\mu/e + \mathbf{h}} \mathbf{t}_{0,i} \quad \text{is the apparent yield stress, and}$$

$$\mu^{ap.} = \frac{\mathbf{h}}{\mu/e + \mathbf{h}} \mu \quad \text{is the apparent plastic viscosity.}$$

To assess the significance of this artifact, we will refer to the thesis of Kaplan [2], who measured the four needed parameters \mathbf{t}_0 , μ , $\mathbf{t}_{0,i}$ and \mathbf{h} for a variety of 37 mixtures. Taking arbitrarily a value of 100 mm for e , mean values of 0.47 and 0.39 are found for the ratios $\mathbf{t}_0^{ap.}/\mathbf{t}_0$ and $\mu^{ap.}/\mu$, respectively. It means that for a coaxial viscometer having a mean distance of 100 mm between inner and outer cylinder, and no roughness to avoid slippage on the external wall, an error of more than 50 % can occur in the experimental assessment of Bingham parameters.

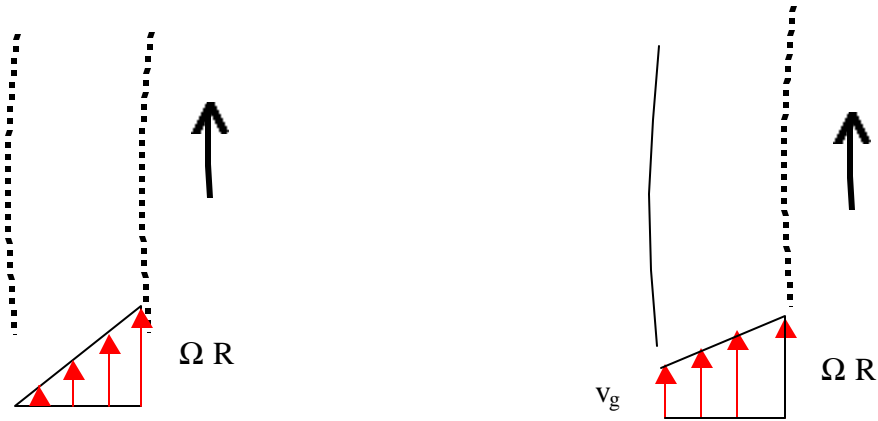


Figure F-2: Rate field in the gap of the viscometer. A) with no slip; B) with slip at the outer wall.

Wall effect

In a dry packing of particles, it is well known that the porosity tends to increase when the distance between walls decreases. This is due to the supplementary porosity appearing at the interface between grains and walls. Since the wall has no curvature, the volume of individual voids is greater when a border surface of these voids is constituted by the wall of the container (see Figure F-3). In other words, the porosity is higher near a wall.

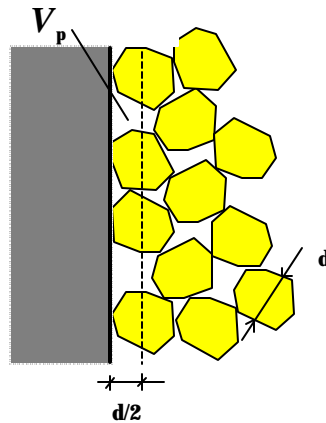


Figure F-3: Wall effect in a dry packing of particles. In the perturbed interfacial volume V_p , porosity is higher than in the bulk of the specimen [6].

Such an effect also takes place in granular suspensions. During the research devoted to self-compacting concrete rheometry [7], tests were carried out where the height of the sheared specimen was changed (see Figure F-4). In this set-up, a supplementary blade system was added to the original ones, the height of which could be adjusted.

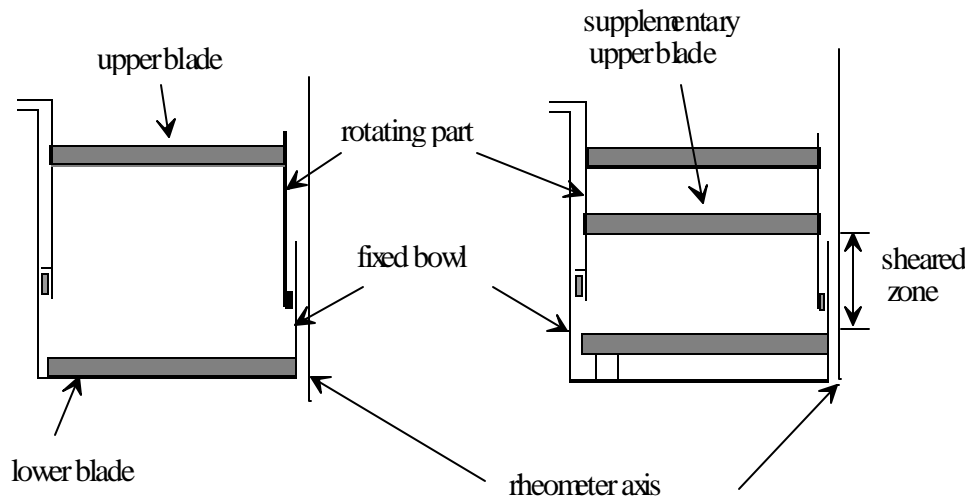


Figure F-4: Modification of BTRHEOM rheometer, to display wall effect in rheometric measurements.

A grid was fixed on the top of intermediate blades (see Figure F-5) and a piece of plastic was added to fill the space under the bottom blades to limit the dead zones to the interstices of the blades. So the tests could be considered as *confined* tests.

In the first series of tests, confined tests were performed on mixtures having a maximum aggregate size of 16 mm. The effect of interblade distance and coarse/fine aggregate ratio (G/S) on the apparent Bingham constants was investigated. Test results are displayed in Figure F-6. It can be seen that strong perturbations take place as soon as the ratio between interblade distance and maximum size of aggregate is less than four. As a general trend, apparent rheological parameters tend to increase with the wall effect. This could be anticipated, since the porosity of the mixture tends to grow, while the water dosage remains constant. The higher the aggregate content in the mixture, the more pronounced the wall effect.

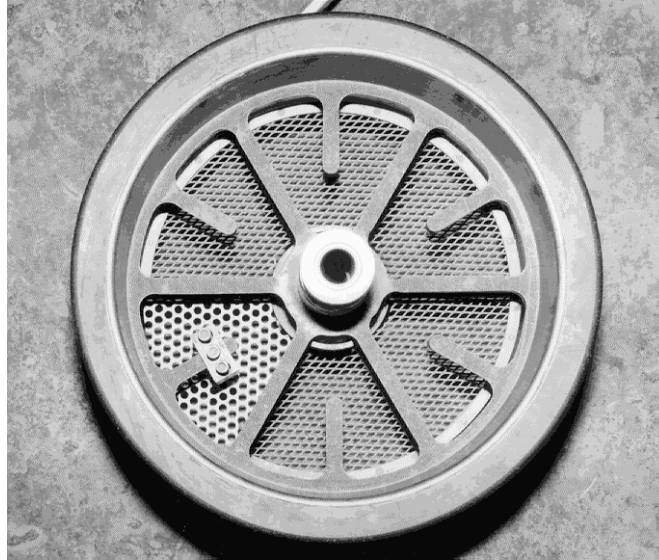


Figure F-5: Confining grid. A door can be seen on the “south-west” part of the wheel, through which concrete could be poured into the test zone [6].

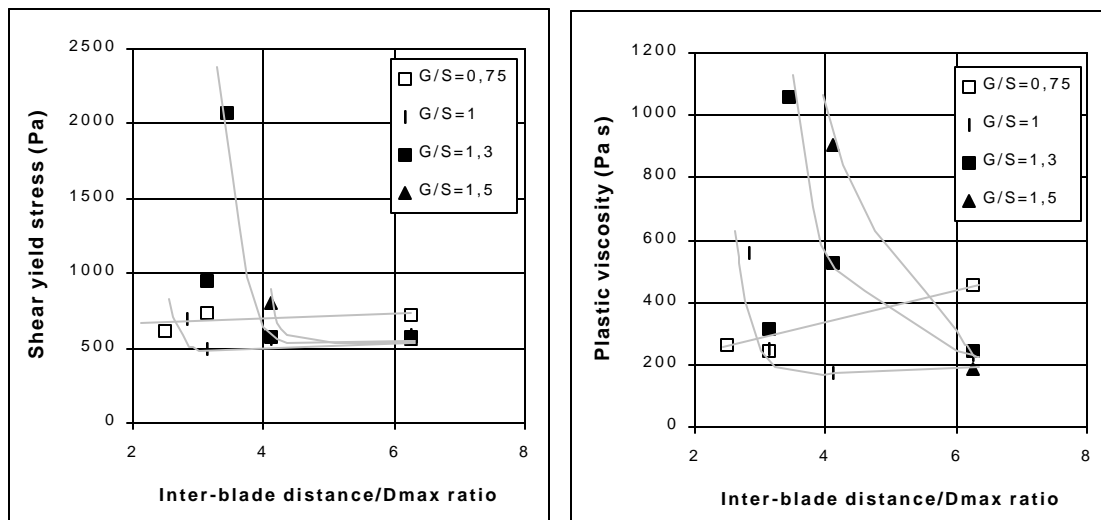


Figure F-6: Confined tests performed on a series of mixtures, with various interblade distances and coarse/fine aggregate ratios [6].

In a second series [7] of confined tests, a self-compacting mixture with a maximum size of 12.5 mm was tested in this set-up. The yield stress still tended to increase while the plastic viscosity decreased with the wall effect (see Figure F-7). This could be attributed to the ease of accumulation of coarse aggregates in the voids of the blades (since the mixture was not originally saturated in coarse aggregate).

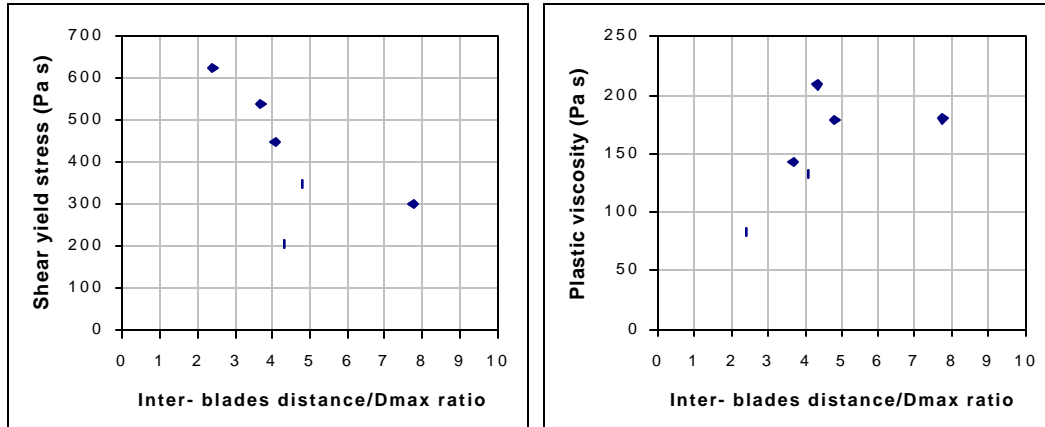


Figure F-7: Confined tests performed on a self-compacting mixture.

This assumption was confirmed by a third test series [7] shown in Figure F-8. Here a concrete having an maximum aggregate size of 25 mm is tested. Black dots deal with confined tests, while white dots deal with *unconfined* tests. For *unconfined* tests, the plastic piece under the bottom blades was removed in order to increase the dead zone volume and consequently to facilitate the coarse aggregate segregation. The confined tests were difficult to perform; sometimes, blockage occurred since the interblade distance/MSA was between 2 and 3 (“bridging effect” due to coarse aggregates). On the other hand, unconfined tests went smoothly, but a significant *decrease* in apparent Bingham parameters (especially yield stress) took place when the interblade distance decreased. This could be due to the migration of coarse aggregate into the dead zone, so that the material in the sheared zone became a kind of mortar.

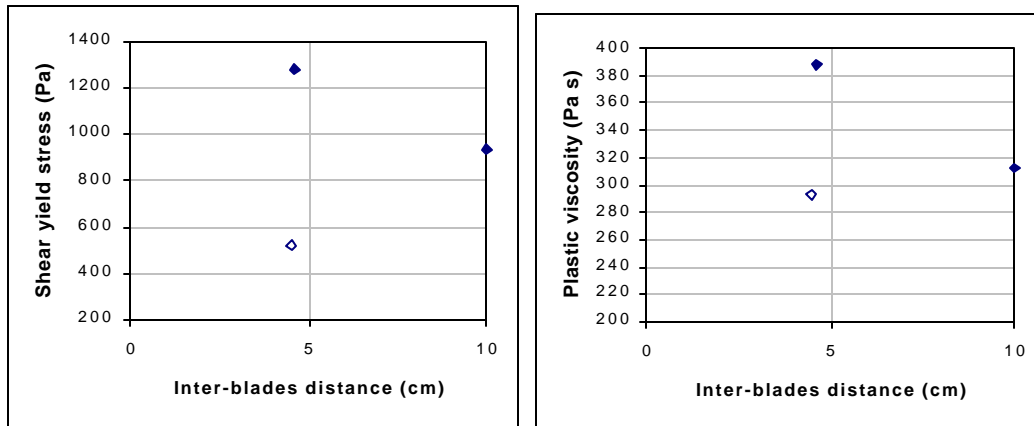


Figure 8: Effect of confinement on apparent Bingham constants. Black dots: confined tests; white dots: unconfined tests.

As a tentative conclusion, we may state that:

- as soon as the distance between blades is less than four to five times the maximum size of aggregate, perturbations of the apparent Bingham parameters take place in the rheometer;
- if concrete is confined in the sheared zone, both apparent yield stress and the apparent plastic viscosity tend to be higher than the true values. Difficulties are encountered in running the tests, owing to bridging effects;
- if coarse particles can migrate from the sheared zone to the dead zone, a significant decrease of apparent rheological parameters may occur.

Artifacts and rheometers – A critical review

In order to judge to which extent the previous artifacts may affect the various rheometers, some pertinent characteristics are recalled in Table F-1. In the light of the previous considerations, the following statements are proposed:

Table F-1: Comparison between rheometers.

Rheometer	Tested volume of <i>sheared</i> concrete [L]	Slip risk	Minimum distance between moving parts [mm]
BML	5.2	Minimum	45
BTRHEOM	4.4	Minimum	100
CEMAGREF-IMG	500	Medium	220
IBB	21	High	50
Two-point	10	High	50

- The BML has a limited volume of sheared concrete. This may give a certain standard deviation in measurements. The slip risk is minimal, owing to the fact that all limits of sheared specimen are equipped with blades. The main critical issue lies in the distance between blades, which is only two to three times the maximum size of aggregate for most commercial concretes. Wall effect almost certainly plays a major role in BML data, affecting all the sheared concrete zone. As the ratio of sheared concrete over the total volume of specimen is low ($5.2/17 = 0.31$), tests can be considered as *unconfined*. Therefore, some coarse aggregate migrations in dead zones can be anticipated, giving a significant decrease in apparent Bingham constants;
- The BTRHEOM has an even more limited volume of sheared specimen, providing a significant standard deviation of measurements. On the other hand, artifacts dealing with slip risk and wall effect are minimal. As for the latter, the ratio between interblade distance and maximum size of aggregate is about five. Therefore, no significant systematic error in the determination of ‘true’ Bingham constants is expected;
- The CEMAGREF-IMG tests a very large volume of concrete. This is the advantage of having a ‘gigantic’ rheometer. Also, the distance between blades is more than ten times the MSA, so that no wall effect is anticipated. Unfortunately, the roughness of

the inner cylinder is not high enough to avoid any slippage. This fact led us to eliminate a number of data. For the rest of the data, where the yield stress was the same regardless of the calculation method (see Section 3.3), it can be reasonably considered that the true rheological parameters have been quite well evaluated.

- In the IBB, the volume of concrete tested is quite high for a laboratory device. Some wall effect may take place, although a very small volume of concrete is concerned. On the other hand, nothing is done to prevent slippage between concrete and the smooth inner wall. Therefore, an underestimation of Bingham constants could be expected, if a calibration process similar to the one used for Two-Point (see Section 3.5) would be carried out. Moreover, the cross section of the impeller is lower than the MSA. For very fluid mixtures, the impeller may shear cement paste instead of the whole particle size range. This is why, in the fluid range of tested mixtures, IBB tends to see Newtonian materials, instead of Bingham ones;
- For the Two-Point test, it is unlikely that the wall effect will significantly affect the measurements, given the small volume concerned. The total volume of sheared concrete is satisfactory with regard to statistical variability of rheological properties. The lack of blades on the inner wall is probably the main problem. It would be interesting to compare the results of this test with and without blades. Both horizontal and vertical slippage would have to be prevented, given the complicated flow pattern in this test.

Appendix G: Seal friction in CEMAGREF-IMG test: Effect of concrete height

Introduction

The aim of this calculation is to find a maximum bound of the potential effect of concrete height on the seal friction in the CEMAGREF-IMG rheometer. In the standard calculation, and for a given rotation speed, the torque obtained with the rheometer (almost) empty is deduced from the gross torque to calculate the torque attributable to concrete shear. Does concrete pressure significantly affect the seal friction? If the answer is yes, then the yield stress obtained by the standard calculation will be higher than the ‘true’ one.

Quantitative analysis

The torque generated by the seal may be written as follows:

$$C_{\text{seal}} = C_{0,\text{seal}} + K_1 \Omega + K_2 \sigma_v \quad (\text{G-1})$$

where σ_v is the vertical stress applied on the seal, Ω the rotation speed, and $C_{0,\text{seal}}$, K_1 and K_2 are constants depending on the lubrication given by the mortar included in the concrete. In practice, the seal friction is evaluated with a thin layer of concrete in the bottom of the rheometer to account for this lubrication. K_1 corresponds to the ‘fluid friction’ term, while K_2 stands for the ‘solid friction’ one.

For a given concrete, the mean value of the seal friction, within the range of rotation speeds applied during a test, can be written as following:

$$\overline{C_{\text{seal}}} = \overline{C_{0,\text{seal}}} + K_2 \sigma_v \quad (\text{G-2})$$

When the rheometer is almost empty (the practical case for seal evaluation) we have:

$$\overline{C_{\text{seal,e}}} = \overline{C_{0,\text{seal}}} + K_2 \sigma_{v,e} \quad (\text{G-3})$$

with

$$\sigma_{v,e} = \frac{Mg}{S}$$

where

- M is the mass of the inner cylinder. Due to the high rigidity of the seal, this mass is not supported by the motor axis but by the seal itself.
- g is the acceleration due to gravity
- S is the area of the seal in contact with the bottom of the rheometer

When the rheometer is almost full we have:

$$\overline{C_{seal,f}} = \overline{C_{0,seal}} + K_2 \sigma_{v,f} \quad (G-4)$$

with

$$\sigma_{v,e} = \frac{Mg}{S} + \rho_c gh$$

where

– ρ_c is the concrete density

- h is the height of the concrete sample.

We now have

$$\overline{C_{seal,f}} - \overline{C_{seal,e}} \leq \left(\frac{\sigma_{v,f}}{\sigma_{v,e}} - 1 \right) \overline{C_{seal,e}} \quad (G-5)$$

and

$$\overline{C_{seal,f}} - \overline{C_{seal,e}} \leq \frac{\rho_c h S}{M} \overline{C_{seal,e}} \quad (G-6)$$

Numerical example:

$$\rho_c = 2300 \text{ kg/m}^3$$

$$h = 0.7 \text{ m}$$

$$S = (\pi \cdot 0.076^2) \cdot 0.01 \text{ m}^2 = 0.0239 \text{ m}^2$$

$$M = 180 \text{ kg}$$

The mean value of $\overline{C_{seal,e}}$ for all the tests made during the lab week was 133 N·m

Then

$$\overline{C_{seal,f}} - \overline{C_{seal,e}} \leq 29 \text{ N} \cdot \text{m}$$

So the maximum offset that may occur on the shear yield stress is:

$$\Delta \tau_0 \leq \frac{29}{2 \rho h R_{int}^2}$$

where R_{int} is the inner cylinder radius

$$R_{int} = 0.38 \text{ m}$$

Finally, the maximum error in the evaluation of the shear yield stress is

$$\Delta \tau_0 \leq 45 \text{ Pa}$$

Conclusion

This is the order of magnitude of the typical standard deviation for the yield stress as measured with BTRHEOM [8]. On the other hand, the difference in absolute value between yield stress given by CEMAGREF-IMG and BML ranges from 287 Pa to 1094 Pa. For the CEMAGREF-IMG vs. Two-Point test, the difference ranges from 312 Pa to 1079 Pa. Therefore, it is concluded that a errors in evaluating the seal friction in the CEMAGREF-IMG test cannot explain all the discrepancy between this rheometer and the other devices.

References for the Appendixes

- 1 G.Saporta, « Probabilités, analyse des données et statistiques ». Editions TECHNIP, 1990 (in French)
- 2 KAPLAN D., “Pompage des bétons “ (Pumping of concrete), Etudes et recherches des Laboratoires des Ponts et Chaussées, OA 36, November, available at LCPC, 2000 (in French)
- 3 WEBER R., “The transport of concrete by pipeline” (translated by C. Van Amerongen), Cement and Concrete Association Translation No. 129, 1968
- 4 MORINAGA M., “Pumpability of concrete and pumping pressure in pipelines”, Fresh Concrete: Important Properties and Their Measurement, Proceedings of a RILEM Seminar, Leeds, Vol. 7, pp. 1-39, 1973
- 5 BROWNE R., BAMFORTH P., “Tests to Establish Concrete Pumpability”, ACI Journal, No. 74-19, May, 1977
- 6 DE LARRARD F., “Concrete Mixture-Proportioning”, Modern Concrete Technology, No. 9, E & FN SPON, London, 421 p., 1999
- 7 BARBILLON C., “Influence du confinement sur les bétons autonivelants” (Influence of the confinement on Self Compacting Concrete), Master thesis from Ecole Normale Supérieure de Cachan, June, 1997
- 8 HU C., “Rhéologie des bétons fluides (Fluid concrete rheology)”, Etudes et recherches des LPC, OA 16, published by LCPC, September, 1995